RESEARCH ON CONCENTRATED PHOTOVOLTAIC THERMAL AND DAYLIGHTING (CPVTD) SYSTEMS USING ROUND AND FLAT OPTICAL FIBERS

AFSHIN ASLIAN

FACULTY OF ENGINEERING
UNIVERSITY OF MALAYA
KUALA LUMPUR

2021

AFSHIN ASLIAN

[THESIS/DESSERTATION] SUBMITTED IN FULFILMENT OF THE REQUIREMENTS FOR THE DEGREE OF DOCTOR OF PHILOSOPHY

**FACULTY OF ENGINEERING
UNIVERSITY OF MALAYA
KUALA LUMPUR**

2021

UNIVERSITY OF MALAYA

ORIGINAL LITERARY WORK DECLARATION

Name of Candidate: Afshin Aslian

Registration/Matric No: KHA130092

Name of Degree: PhD

Title of Thesis: Development of Concentrated Photovoltaic-Thermal and Lighting (CPVTD) Solar Energy System for Residential Buildings

Field of Study: Engineering Design (Solar Energy Systems)

 I do solemnly and sincerely declare that:

(1) I am the sole author/writer of this Work;
(2) This Work is original;
(3) Any use of any work in which copyright exists was done by way of fair dealing and for permitted purposes and any excerpt or extract from, or reference to or reproduction of any copyright work has been disclosed expressly and sufficiently and the title of the Work and its authorship have been acknowledged in this Work;
(4) I do not have any actual knowledge nor do I ought reasonably to know that the making of this work constitutes an infringement of any copyright work;
(5) I hereby assign all and every rights in the copyright to this Work to the University of Malaya ("UM"), who henceforth shall be owner of the copyright in this Work and that any reproduction or use in any form or by any means whatsoever is prohibited without the written consent of UM having been first had and obtained;
(6) I am fully aware that if in the course of making this Work I have infringed any copyright whether intentionally or otherwise, I may be subject to legal action or any other action as may be determined by UM.

Candidate's Signature   Date: 19/8/2021

Subscribed and solemnly declared before,

Witness's Signature   Date: 20/8/2021

Name:

Designation:

ABSTRACT

Concentrated photovoltaic and thermal (CPVT) system is proposed. The system concentrates the sunlight and implements solar cells in focal point of a concentrator. Heat collector is located behind the cells and transmits the heat to a heat exchanger. The system has high efficiency in direct sunlight. So, a sun tracker is required as a subsystem. By integrating the function of daylighting to the CPVT system, the functionality of system improves, and the developed system can be deployed in residential buildings. In this research substance-field (Su-Field) and functional analysis of Teoriya Resheniya Izobretatelskikh Zadach (TRIZ) are applied to develop a comprehensive model of problem in integrating three functions i.e. electricity, heat and light into a developed system. The model of concentrated photovoltaic-thermal and daylighting (CPVTD) solar energy system for residential buildings is presented through integrating light function to a CPVT system.

Developing a CPVTD system for residential building is a fine process that requires satisfying several design considerations such as total efficiency, thermal, electrical and daylighting performance with significant innovations and improvements. Since a CPVTD is a complex system that consists of combination of different components, the design considerations are interconnected and often conflicting. As a result, multi-variable optimization is often required for increasing the total efficiency, reducing bulk of system, improving reliability and durability and minimizing the total cost.

In this research we focused on optical components and heat sink of a CPVTD system. These components are imaging dish, secondary concentrator, optical fiber and heat sink. These components are the main components that convert sunlight to electricity, hot water and daylight.

A novel secondary concentrator, a new rectangular optical fiber, and a compact energy conversion device "that we name hear" a receiver is designed and fabricated. In a compact energy conversion device, we can split the bulk of transmitted light for different purposes, i.e. electrical power conversion, heat and daylighting. A glass rectangular optical fiber designed for transmitting sunlight. The fiber simulated, fabricated and tested as a medium for transmitting sunlight from focal point to photovoltaic cells in the compact energy conversion device. A receiver of CPVTD with round optical fiber is fabricated and tested. The results show that using optical fiber as a medium in receiver reduced the temperature of multi-junction cells and increased the distance between the cells. Therefore, the surface of heatsink increased, and heat exchange between fluid and heat sink enhanced.

Keywords: fiber optics, concentrator, photovoltaic, coupler, daylighting

ABSTRAK

Dengan menyepadukan fungsi cahaya siang kepada sistem CPVT, aplikasi dan kefungsian boleh digunakan dalam bangunan kediaman. Dalam kajian bidang bahan ini (Su-Field) analisis dan fungsi analisis Teoriya Resheniya Izobretatelskikh Zadach (TRIZ) diaplikasikan untuk membangunkan model yang komprehensif dalam masalah untuk mengintegrasikan tiga fungsi iaitu elektrik, haba dan cahaya ke dalam sistem yang dibangunkan. Model kekuatan haba dan cahaya siang fotovoltaik (CPVTD) sistem tenaga solar untuk bangunan kediaman adalah dicadangkan dan dibentangkan melalui pengintegrasian fungsi cahaya kepada sistem CPVT.

Pembangunan sistem CPVTD untuk bangunan kediaman adalah satu proses yang halus dan memerlukan kepuasan untuk beberapa pertimbangan reka bentuk seperti jumlah kecekapan, haba, prestasi elektrik dan cahaya pada waktu siang dengan inovasi dan peningkatan. Disebabkan CPVTD adalah sistem yang kompleks yang terdiri daripada gabungan komponen yang berbeza, pertimbangan reka bentuk adalah saling berkaitan dan sering bercanggah. Akibatnya, pengoptimuman pelbagai pembolehubah sering diperlukan untuk meningkatkan jumlah kecekapan, pengurangan sebahagian besar sistem, meningkatkan kebolehpercayaan, ketahanan dan meminimumkan jumlah kos.

Piring parabolik telah digunakan sebagai penumpu asas dan pengesan solar dwipaksi sebagai sistem pengesanan sel solar pelbagai simpang untuk menjana elektrik. Gentian optik polimer multimode dan silika dengan lapisan keras polimer digunakan sebagai gentian optik. Penyambung yang baru untuk CPVTL sebagai pengumpul dan penumpu kedua direka sebagai penumpu dan pencapah input cahaya. Keputusan simulasi menunjukkan bahawa kecekapan penghantaran cahaya daripada dua penyambung adalah sangat tinggi. Peranti penukaran tenaga yang padat direka untuk menjana tiga jenis tenaga dalam bidang fotovoltaik dan fotonik. Dalam peranti penukaran tenaga yang padat,

v

cahaya yang dipancarkan melalui gentian optik pemisah dan menukarkan cahaya tenaga elektrik, haba dan cahaya sejuk. Buat kali pertama, gentian optik rata direka, simulasi, direka dan diuji sebagai medium untuk memancarkan cahaya solar.

CPVTD ini direka dan diuji untuk mengukur prestasi dan kecekapan peranti tenaga padat. Satu reka bentuk pengumpul yang baru dapat meningkat kecekapan gandingan cahaya matahari untuk gentian optik sehingga 92% dan fluks cahaya ditambah yang dipancarkan oleh gentian optik rata adalah 105% lebih daripada gentian optik bulat konvensional. Kami juga telah membangunkan satu kaedah fabrikasi baru untuk gentian rata dengan ketepatan dimensi yang lebih tinggi dan tidak memerlukan proses tambahan pemesinan untuk mendapatkan kerataan yang baik yang berpatutan dan kos pembuatan yang lebih rendah.

ACKNOWLEDGEMENTS

In the Name of God, the Most Gracious, the Most Merciful

To my wife, Shafagh, for her unending support and to my father, Javad and my mother, Farah and my daughters Atena and Saba for their encouragement. I would like to express my sincere gratitude to my advisors Prof. Dr. Kok Keong Chong and Dr. Tan Chin Joo for the continuous support of my PhD study and related research, their guidance helped me writing of this thesis.

TABLE OF CONTENTS

LIST OF FIGURES

LIST OF TABLES

LIST OF SYMBOLS AND ABBREVIATIONS

a   :   Length of rectangle.

α   :   zenith angle

B   :   attenuation coefficient of solar radiation in the Earth atmosphere

b   :   width of rectangle.

CPV   :   Concentrated photovoltaic

CPVT   :   Concentrated photovoltaic-thermal

CPVTD   :   Concentrated photovoltaic-thermal and daylighting

CTPC   :   compound truncated pyramid and cone

D   :   Diameter of dish

d   :   Diameter of concentrated light

dL   :   Distance between two sequential reflections

h   :   hour angle

I0   :   intensity of extraterrestrial radiation

L   :   Length of optical fiber

La   :   Attenuation

Li   :   Local latitude

n1   :   index of core

n2   :   index of cladding

NA   :   Numerical Aperture

Nav   :   Average number of reflections

ni   :   a day in year

Ni   :   Number of reflections

Nt   :   Total number of reflections

P1   :   Input power

P2	:	Output power
PV	:	Photovoltaic
R	:	Radius of round optical fiber
r	:	polar coordinate of interface of fiber
Rav	:	Arithmetic average of reflectivity
RGOF	:	Glass flat optical fiber
TRIZ	:	Teoriya Resheniya Izobretatelskikh Zadach
α	:	critical angle
αR	:	Attenuation coefficient due to Rayleigh scattering
δ	:	Declination
θ	:	Angle between dL and trajectory onto the plane through the dL including to 2x
θ_1	:	Reflected angle
θd	:	Angle of incident relative to axis of optical fiber
λ	:	Wavelength
τ0	:	Transmission of optical fiber at angle 0 degree
ω	:	polar coordinate of interface of fiber

LIST OF APPENDICES

CHAPTER 1: BACKGROUND

1.1 General background

Sunlight is an electromagnetic wave. 52-55 percent of energy is transmitted through infrared wavelength of the spectrum (above 700nm) and 42-45 percent is transmitted through visible wavelength of the spectrum (400-700 nm (Makarova & Kharitonov, 1972). A high-efficiency solar system could absorb the most spectral band of sunlight. Concentrating sunlight is promised method that increases efficiency. Multi-junction III-V photovoltaic cells have reached the highest efficiency among other cells up to 41% (Tyagi, Rahimb, Rahimb, & Selvaraj, 2013). The concentrator thermal systems using a parabolic mirror could absorb up to 60% of inlet energy. Figure 1.1 shows a CPV system using a dish, a secondary concentrator, heatsink, and multi-junction cell.
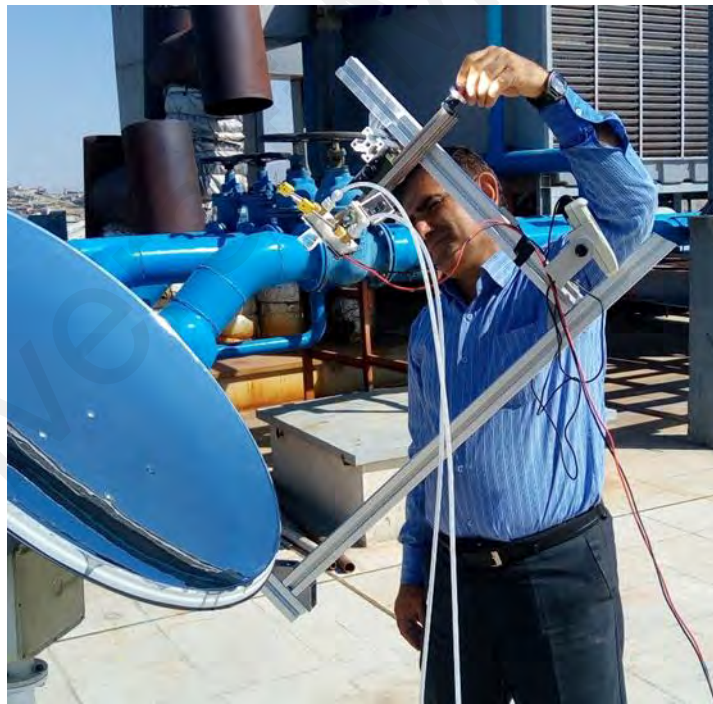
Figure1- 1: A CPV system using a parabolic dish, a compound parabolic concentrator as secondary concentrator and a heatsink.

In a CPV system, the heat is wasted simply by environmental factors. So the obtained energy is less than 30% of the total inlet to the systems (Dan & Arvizu, 2013).

Photovoltaic modules manufacturers are being faced a decline in efficiency due to shading, bird excrement, increasing temperature, dust, and high humidity (Santhakumari & Sagar, 2019).

One of the ways for improving the efficiency of solar systems is concentrating sunlight, and converting concentrated light simultaneously to hot water and electricity. The wasted heat of CPV could also be collected and transferred for heating or cooling. Concentrator photovoltaic thermal (CPVT) systems reached the high efficiency of 60% in 2015 and 71% in 2019 (Burhan, Shahzad, & Ng, 2019; Xu, Ji, Sun, Huang, & Jin, 2015). However, the share of CPVT in electrical production by PV modules in the world is not considerable. The most important reason is the cost of CPVT systems, the complexity of the system, reliability, and limited applications of the system (Burhan et al., 2019).

Commercial and residential buildings are the main sector of electricity consumers in Malaysia that consume 54% of total electricity (Tenaga, 2014). 7.5% of total electricity in the world is consumed for lighting (IEA, 2012). It means that around 8700 GWh of electricity was consumed for lighting in 2013 and 8739.7 GWh in 2018 in Malaysia (Tenaga, 2019). This amount of electrical energy is approximately equal to RM 160,000,000 (Tenaga, 2019). Daylighting is an important segment of lighting, especially for residential and commercial usage. Many buildings suffer from a lack of access to sunlight. Many customers use curtains on a sunny day to prevent the heat of sunlight. Cold daylighting is a solution for natural lighting without transferring heat.

Concentrated photovoltaic and thermal systems for generating electricity and heat simultaneously exist in the market. In addition, concentrated sunlight systems are designed and built to transmit sunlight by fiber optics. Both systems use light concentrators. The research done so far has been based on different systems. To the best

of our knowledge, a single system for generating electricity, hot water, and cold light simultaneously has not been studied.

Generating multiple concept designs is the first step in designing a system or device. Then, from these conceptual designs, the best design is selected based on criteria such as price, durability, technology, and customer needs. TRIZ is systematic creative thinking that applies a wide range of methods, tools, and strategies available to designers in an advanced creative integrated design system philosophy. In this research, the method of substance-field is used and developed in order to generate several conceptual designs of CPVTD systems.

1.2   Daylighting through optical fibers

Initially, a group of French researchers raised the idea of carrying concentrated solar energy in 1980 (Cariou, Dugas, & Martin, 1982). The idea was soon considered by other researchers. A flexible optical fiber bundle transmits high intensity of solar radiation with less loss of energy.

Gradually, daylighting by passive solar lighting attracted many researchers as a result of carrying concentrated solar energy efficiently. Fused – silica- core showed less attenuation of the solar radiation spectrum.

Using PMMA as the core of optical fibers indicated high potential capability in indoor daylighting for large amount application in buildings. Hard polymer cladding silica (HPCS) demonstrated that can transmit about 94% of the solar radiation in ten meters distance (Rahou, Andrews, & Rosengarten, 2013).

In our best information, different round optical fibers were studied for transmitting sunlight and there is no literature on using rectangular optical fiber for transmitting sunlight. Square core optical fiber developed for matching with laser diode output beam.

Rectangular core fibers in the market have round clad. The core is made of fused silica for its Broadband UV to NIR Transmittance while clad maybe glass or low refractive polymer.

1.3 CPVTD

Stand-alone or net-zero energy buildings are defined as residential or commercial buildings with greatly reduced energy needs (Pless & Torcellini, 2010). The consumed energy in a residential building can be in various forms, including light, heat, and electricity. Electric power generation from sunlight and converting electricity to heat or light has low efficiency. In a concentrated photovoltaic system, the temperature of the photovoltaic module increases; therefore, a cooling system is required. Moreover, concentrated photovoltaic and thermal (CPVT) systems demonstrated higher efficiency versus conventional thermal solar systems (Mittelman, Kribus, & Dayan, 2007)

In this research integration of CPVT and solar lighting system is presented that will cause more efficiency and functionality but is more complicated. Carrying concentrated solar energy for daylighting by fiber optics is a promising method that has been improved during the early decades. This method is used in CPVTD system. Figure 1.2 shows a block diagram of a CPVTD system. Sunlight is concentrated on the primary and secondary concentrators. The concentrated light transmits into an energy conversion system and converts to heat, cold light, and electricity.
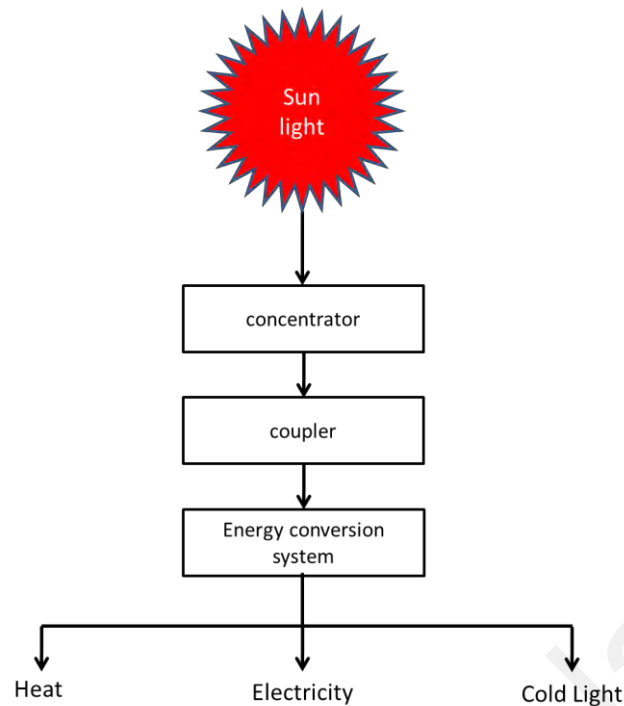
Figure 1- 2: block diagram of CPVTD system

1.4 Problem Statement

- The rooftop surface of a residential building is a major available surface for generating electricity, hot water, and cold light simultaneously, and the solar system requires the highest efficiency due to the lack of available surface.

- A residential building needs all kinds of energy including electricity, heat and light.

- The efficiency of stationary silicon photovoltaic modules for residential buildings with limited spaces is not high while it is reduced in converting electricity to hot water and light.

- Many residential buildings suffer from a lack of access to direct sunlight and use artificial light for daylighting.

- Sunlight in hot climate causes more energy consumption for cooling buildings and people usually use artificial light to prevent heat transfer by sunlight through windows.

- Converting sunlight to electricity in a concentrated photovoltaic and thermal (CPVT) system and converting electricity to light waste a portion of inlet energy.

- The spectrum of artificial light is less compatible with the human eye than sunlight.

- Light dissipation in concentrated sunlight transmission is very high, and sunlight transmission with less loss can dramatically increase the efficiency of the whole system.

- A compact improved CPVTD system for residential application is not presented by other researchers.

1.5   Research Objectives

The specific objectives of this research project are:

- To develop a compact energy conversion device using in CPVTD system with a minimum of 60% total efficiency.

- To develop a new method for coupling light to the receiver of a compact energy conversion device for generating electricity, hot water, and cold daylighting

- Comparison of flat and round fiber optics in the relative transmission of sunlight.

- Design and fabrication of a flat fiber optic sample to transmit sunlight.

1.6   Research Scope

This research is limited to:

- Concentrated photovoltaic - thermal and solar lighting system using fiber optics.

- Designing a compact energy conversion device for converting sunlight to electricity, hot water, and daylighting.

- Application of substance-field and functional analysis of TRIZ methodologies to define problems in designing CPVTD and generating concepts.

- Choosing the best methods for heating water and generating electricity in the receiver of CPVTD.

A CPVTD system has as many components as a CPVT system. The system has components such as a cold-water tank, a hot-water tank, a water pump, a thermometer, water flow control valves, a barometer, a thermometer, water pipes, a heat exchanger, a centralized structure, a primary light, and a solar tracker. The heart of the CPVT system is located in the focus, which includes the light coupler to the solar cells and the heat exchanger cooling the solar cells. The focus of this research is on converting sunlight into cold light at the same time as generating electricity and hot water. Therefore, other sections are not included in this research. In addition, heat exchangers and solar cells are selected and used according to the design of this new device.

1.7   Research Methodology

- TRIZ methodology for problem definition and concepts generation.

- Mathematical analysis

- Simulation for analysis of the CPVTD system.

- Experimental study for evaluating the efficiency of components and the system.

In this thesis, several conceptual designs are created using the Su -field method. Then one of these conceptual designs is selected as the main design. In the next step, the main parts within the scope of this dissertation will be examined. The study of each part

consists of three steps. First, mathematical analysis, then simulation, and finally laboratory testing are performed. In cases where laboratory testing is not possible, just the simulation results are considered.

CHAPTER 2: LITERATURE REVIEW

2.1   Introduction

A CPVTD system generates electricity, heat, and light from direct concentrated sunlight. Before designing this system, it is necessary to review some basic and general information. This information includes direct sunlight in different areas, the primary sunlight concentrator, sun tracker, optical fibers, light coupler, and TRIZ. The above information gives us a better understanding of the operating conditions of this system. A schematic of a CPVTD system is shown in Appendix A. Both CPVT and daylighting systems use direct sunlight. Therefore, first, we will have an overview of the intensity of direct sunlight in different areas and at different times.

2.2   Sun direct irradiation

The power that is transmitted from the sun to each part of the world is dependent on the geometrical position of the place, the day of the year, the hour, and climate condition. For direct irradiation, we assume that there is no cloud in the sky.

There are some equations with different levels of error. An equation with reasonable accuracy is (Radosavljević & Đorđević, 2001) :

$$I_0 = 1367 \left[1 + 0.0333 \cos \frac{360n}{365} \right] (\sin L \sin \delta + \cos L \cos \delta \cos h) \qquad (2.1)$$

In the above equation, I_0 is the intensity of extraterrestrial radiation on a horizontal surface for a particular day in a year in (w/m²) and n_i is a day from January 1st. δ is declination, L is local latitude and h is hour angle, and h=0 at noon.

$$\delta = 23.45 \sin[\frac{360}{365}(284 + n_i)] \qquad (2.2)$$

Where maximum δ is 23.45º that comes up with 21st June the longest day in summer and minimum δ is -23.45º that comes up with 20th December the shortest daylight in the northern hemisphere.

$$h = \pm \frac{1}{4} \ (number \ of \ minutes \ from \ local \ solar \ time) \qquad [°] \qquad (2.3)$$

The positive sign accounts for the afternoon and the negative sign accounts for morning hours. For designing dish and connector and fiber, we need a maximum of intensity during the year. We also need to know the annual intensity of the place. This information is found by both measuring and calculating methods.

For maximum irradiation in Kuala Lumpur (Kuala Lumpur's coordinates: 3°08′28″ N, 101°41′11″ E) at noon we have:

$$h = 0, \ L = 3.1390, \ n_i = 80 \qquad (2.4)$$

$$\delta_{max} = -0.4039 \qquad (2.5)$$

$$I_{max} = 1373 \ (w/m²) \qquad (2.6)$$

For minimum irradiation in Kuala Lumpur at noon we have:

$$h = 0, \ L = 3.1390, \ n_i = 180 \qquad (2.7)$$

$$\delta_{min} = 23.241 \qquad (2.8)$$

$$I_{min} = 1241 \qquad (2.9)$$

These results are due to the city of Kuala Lumpur being located near the equator. If we want to get the maximum amount of intensity of extraterrestrial radiation at noon local time for the city of Tehran with a latitude of 35.715298, the following values are:

h= 0, L= 35.715298, n_i=166

δ_{max}=23.3

I_{max}=1292 (w/m²)

For minimum irradiation in Tehran at noon we have:

h=0, L=35.715298, n_i = 354   (2.10)

δ_{min}= -23.4   (2.11)

I_{min} =723   (2.12)

There is a low change in the intensity of sunlight during the year in Kuala Lumpur. However, the atmosphere, high humidity climate, and enormous cloudy days during the year reduce the intensity and total of received energy by the concentrator. On the other hand, direct sunlight comprises infrared, ultraviolet, and visible light. Approximately 45% of direct sunlight is visible light. If we don't use the energy of infrared radiation, we will lose huge energy radiated by the sun.

The effect of the atmosphere on direct radiation is calculated by Bouquer –Lambert law.

$$I = I_0 \, e^{-Bm}$$ (2.13)

$$m = \frac{1}{\cos\alpha}$$ (2.14)

$$\cos a = \sin L_i \sin\delta + \cos L_i \cos\delta \cos h$$ (2.15)

(B) is attenuation coefficient of solar radiation in the Earth's atmosphere and is shown in table 2-1 for the 21st day of each month (Mousavi Maleki, Hizam, & Gomes, 2017). a is zenith angle, δ is declination, Li is local latitude and h is hour angle.

Table 2- 1:Attenuation coefficient of solar radiation considering atmosphere

month	B
January	0,142
February	0,144
March	0,156
April	0,180
May	0,196
June	0,205
July	0,207
August	0,201
September	0,177
October	0,160
November	0,149
December	0,142

$$I_{atm} = 1373(e^{-0.1565}) \quad\quad\quad (2.16)$$

$$I_{atm} = 1173 \text{ W/m}^2 \quad\quad\quad (2.17)$$

I_0 is the maximum intensity of direct sunlight at noon on 21st March with considering the effect of the atmosphere.

If the share of visible sunlight with respect to the total radiation of the sun is to be considered, the maximum visible light will be 527 w/m2 in Kuala Lumpur and 473 w/m2 in Tehran. These equations can be used to calculate the maximum and minimum intensity of sun direct light for different places during the year. From the values obtained in the

above two examples, it can be concluded that the amount of direct sunlight in the visible light spectrum is much less than the total amount of sunlight on the ground. Therefore, using the maximum range of solar spectrum increases the efficiency of an energy conversion device.

2.3   Primary concentrators of solar energy systems

The idea of concentrating sunlight by a lens or other optical concentrators for increasing the intensity of illumination and using the extended heat in focal point was implemented thousands of years ago (Africa, 1975).

Concentrators in CPV and concentrated solar heating (CSH) systems are generally grouped by optical characteristics including low (below 100×), medium (100×-300×), and high concentration (above 300×). However, all systems increase the intensity of light hence fewer amounts of PV cells or heating surface is required for generating electrical power or heat. This strategy will reduce the cost of the total system and reduces land utilization (Luque & Andreev, 2007).

Fresnel lens is one of the concentrators that widely are used in CPV modules and CSH systems. Fresnel lens is made of prism chains. Each prism characterizes a slop surface of a conventional lens (Xie, Dai, Wang, & Sumathy, 2011).

Both image and non-image Fresnel lenses are manufactured. They are widely implemented in solar systems because of their low weight and less cost of production. Fresnel lenses are made from glass and plastics. Polymethyl Methacrylate (PMMA) has shown better results among other polymers with higher durability and mass producibility. Matsuzaki, Abe, and Fujita (2013) introduced a PMMA resin that is significantly more resistant to UV and sand storm tests.

Non-imaging Fresnel lens has more capability to concentrate sunlight with highly uniform flux in a low accurate tracking system. They are usually convex shape with a high concentration ratio and short focal length (Leutz, Suzuki, Akisawa, & Kashiwagi, 1999)

Improving design methodology of dome non-imaging Fresnel lens concluded a new bowl shape Fresnel lens that improved optical efficiency. This much deeper dome shape doesn't capture infrared raise properly. The drawback is condensation of water on the dome. Condensed water fills valleys of Fresnel prisms and lost the concentration function. (Akisawa, Hiramatsu, & Ozaki, 2012).

Other devices for concentrating sunlight are parabolic mirrors that consist of dish and trough. A parabolic dish is an important subsystem that offers the highest thermal and optic efficiency among other options (Lovegrove, Burgess, & Pye, 2011). The cost of this component has a noticeable effect on the total cost of the system. Huge researches are conducted to improve the design of this component for higher efficiency and lower cost of production that is introduced in the chapter. Bigger dish has advantages of using one tracker, stand, control system, and less cabling. Hence, less investment is needed per unit power output. However, the bigger dish is costly and requires high-tech in the production line. As a solution, a 500 m² dish is designed and produced by flat mirrors (Li & Dubowsky, 2011).

Some researchers chose a mini-dish as a primary concentrator. Two reasons presented for this decision. First, making mini-dish is simpler, and second, higher concentration could be achieved. On the other hand, other researchers noticed the cost issue and offered bigger dishes for power plant systems based on cost-effective analysis (Xia, Dai, & Shuai, 2012).

Trough concentrators are highly used in macro power plants. A comparison of linear Fresnel lens and parabolic trough in Italy also showed that for medium-size of concentrating, parabolic trough produces more energy per unit area of solar collector (about 180-190 kwh/m² vs. 130-140 kwh/m²) (Cau & Cocco, 2014). Similar to parabolic dishes, reduction of costs for producing trough is possible by increasing the mirror surface and improving frame stiffness (Marcotte & Manning, 2013). Bending of absorber tube due to non-zero angle of incidence may occur that must be considered in designing supports of absorber tube (Khanna, Singh, & Kedare, 2013). Another problem is increasing the loss of energy while the absorber tube becomes longer. Canavarro, Chaves, and Pereira (2013) reported that increasing aperture size and simultaneously implementing a non-imaging optic reduced the cost and loss of energy.

Dust and wind may affect the durability and performance of parabolic dishes and trough concentrators. A numerical study assessed the deposition rate and disorientation where the amplitude of dust is high. This study also assessed the effectiveness of various windbreaks (Christo, 2012).

Micro optic solar concentrators use a lens array mounted above a planar waveguide. Micro prisms are fabricated at an angle 120º are formed on SU8 photoresist by wavefront technology then coated by aluminum. This pattern is installed on the waveguide planar and reflects light from the surface of the planar to the edge the photovoltaic cell is mounted. This type of concentrator has a unique geometry that allows for more flexibility (less precision) for conventional trackers. By moving the lens array in two directions with respect to the waveguide it is possible to transfer the light toward the PV cell (Hallas, 2011).

A three-dimensional Cross Compound parabolic concentrator (3DCCPC) made from clear polyurethane material can be used for concentrating sunlight with ±40º angle of the

incident without a tracking system. An experimental study of this concentrator showed 70% optical efficiency for this range angle of the incident (Baig, Sellami, Chemisana, Rosell, & Mallick, 2014).

Luminescent solar concentrator concentrates solar light from the surface of a plate by transferring the light to the edge of the plate. The concentration depends on the ratio of side surface to edge surface. Luminescent particles absorb the light and emit at a higher wavelength that is guided in Si plate by total internal reflection. This system has 7% efficiency and research on this concept is ongoing by researchers (Slooff et al., 2008).

2.4   Trackers

For concentrating solar light, providing the lens or mirror is essential and a tracking system is needed to track the sun during the day. Two angles are adjusted during tracking that keeps the face of the concentrator perpendicular to the light that is solar altitude and zenith angle. Each point on the earth is also determined by geographical latitude and longitude. For a person on specific latitude and longitude, the sun's rays make an angle with a line perpendicular to the horizontal plane. This angle is named zenith angle. Another angle is named azimuth or elevation angle. This angle is measured on the horizontal plane clockwise from the north coordinate pointing axis to the projection of the sun's central ray (Stine & Geyer, 2001).

A solar tracker system has a structure that a solar panel or concentrator, gearbox, electrical motors, sensors, and shafts are placed on it. This structure should be strong enough and stable to carry the weight of parts and resists to wind flow. As concentrating solar light increases, the precision of the tracker becomes more important. Dish parabolic concentrator usually has one pole, but Trough and flat modules may use several poles as their length increases.

Trackers can be classified into single-axis and dual-axis trackers or according to motive method into passive and active trackers. Single-axis trackers rotate only around one axis and dual-axis trackers rotate around two axes perpendicular to each other for high accuracy sun tracking. Passive trackers use a gas or liquid for moving and active trackers implement electrical motors. The Passive method is less accurate compare with the active method. However, in some cases such as flat plate PV array, accuracy is less important. Flat plate PV panels account for the most installed capacity globally (smith, 2014).

Single-axis trackers can be divided into three subcategories including horizontal, vertical, and tilted according to the axis angle of the rotation to the ground. In horizontal, a small motor is connected to a long central drive arm. As the drive arm is pushed or pulled, panels slowly rotate east to west. Vertical trackers are more suitable in northern latitudes between 40º-55º and for small commercial scale.

Dual-axis tracking is a design requirement for concentrated photovoltaic systems that relay to direct light especially with a high concentration ratio (more than 300×). Some systems need high accuracy of within 0.05º for consistent power output.

The most important reason for implementing trackers is the ratio of performance to the cost of trackers. A single-axis tracker can raise the performance of fixed-tilt mounting by 24% while the cost increases merely 5%. A dual-axis tracker can improve performance by 38% while costs increase 15% (smith, 2014) and (Engin & Engin, 2012).

Many parameters should be considered when different methods of tracking are compared for choosing a tracking system. For an instant, fixed-tilt systems require the least land and follow by a single axis and dual axis systems typically require the most

land in medium and large-size projects. It seems that the rate of total investment per 1kw electricity may lead to a better criterion for choosing the solar system.

Accordingly, research on tracker components is ongoing for progress in the design of trackers. Some researchers have studied improving sensor-based control systems or programming controllers for less power consumption by the tracking system and gaining higher accuracy. Although these researches improve our knowledge and contribute to clarify the problem represented solutions come to market only if they improve the ratio of performance to cost.

Ahmad, Shafie, and Kadir (2012) studied a computerized control system for a mini tracker and claimed that their system consumes only 5.89% of electricity generated by two very small panels of 1293×329 mm in size. It was found that on sunny days tracker improves performance significantly but in rainy and severe overcast conditions must be off because it consumes energy without increasing the performance of the system.

Another method for tracking the sun position is Sun Spot Center Orientation Method. At the end of every minute spot image of the sun is captured in several frames and is used for calculation and analysis(Xiaofang & Wencheng, 2010).

Tracking by the light-dependent resistor (LDR) and microcontroller for small single axis modules could be a cost-effective and practical method (Kulkarni, Kshirsagar, Laturia, & Ghare, 2013). Outputs of photosensitive sensors are used to evaluate the intensity of sunlight and to realize the position of the sun. These sensors as well as a step motor and microcontroller may be used in a small concentrated photovoltaic system (Hu & Yachi, 2012) and (Ataei, Afshari, Pourmina, & Karimian, 2011). The photodiode is also used as a sensor in small trackers and researchers reported increasing the efficiency of the system in clear days (Jeong, Park, Kim, & Kang, 2013).

In a high precision small tracker for tracking the sun based on an open-loop programming system, the following components may be used: a GPS, a 32-Bit Stellaris microprocessor, a LM3S811 pyranometer, an anemometer, tilt switches, a Micro-Electro-Mechanical inclinometer or solid-state electronic inclinometer, and limit switches (Engin & Engin, 2012).

This system implements GPS for realizing the location and accurate time. It doesn't work in the high-speed wind for protecting the system and consider day and night for start and stop of the system. However, this system should be costly, and a cost-effective analysis is needed for determining the ratio of performance to cost.

2.5   Fiber optics

Fiber has a core and a cladding to transmit the light through the core by total internal reflection. There are many reasons for the loss of fiber. Among them, angle of light, acceptance angle, and threshold of intensity are more important while white light is propagated to the fiber. The angle of acceptance is calculated by:

$$\text{NA} = \sin \alpha = \sqrt[2]{n_1^2 - n_2^2} \tag{2.18}$$

In this equation α is the maximum angle of acceptance that is named critical angle, n_1 is index of core, and n_2 is the index of cladding. Figure 2-1 shows how light propagate inside of fiber and critical angle. A higher index of the core with respect to the index of the cladding means larger NA. However, a higher angle of propagated light causes a higher loss in fiber.
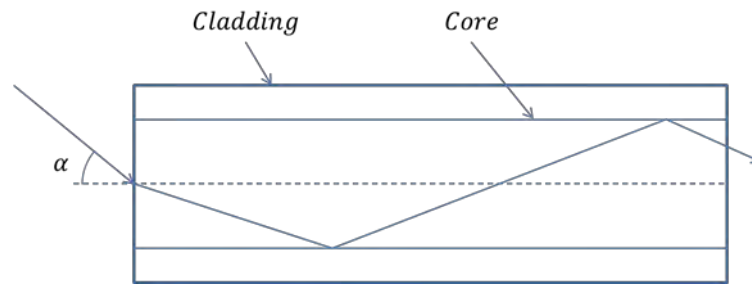
Figure 2-1: Propagation of light in a fiber with core, cladding and critical angle

The Main reasons for the optical loss in the fiber are shown via a fishbone diagram in figure 2.2. Because of these factors, the light has lost during transmission. The total loss in a fiber is proportional to the length of the fiber. The ratio of input power to output in dB is:

$$L_a = 10 log_{10} \frac{p_1}{p_2}$$ (2.19)

L_a is the attenuation in decibel, P1 is input power and P2 is output power both are in watt.

Rayleigh scattering is an intrinsic loss of fiber and is considered a fundamental loss in fiber. It depends on the constituent of the core in fiber. Fluctuation in the density of fiber results in local fluctuation in the refractive index and scattering in all directions. Rayleigh for silica fiber can be estimated by:

$$\alpha_R = \frac{C_R}{\lambda^4}$$ (2.20)

In this equation α_R is in dB/Km and the constant C_R is in (($dB \times \mu m^4$)/Km) and λ is the wavelength of light in μm. It is apparent that with the reduction in wavelength of light the Rayleigh scattering increases significantly with the exponent of four.
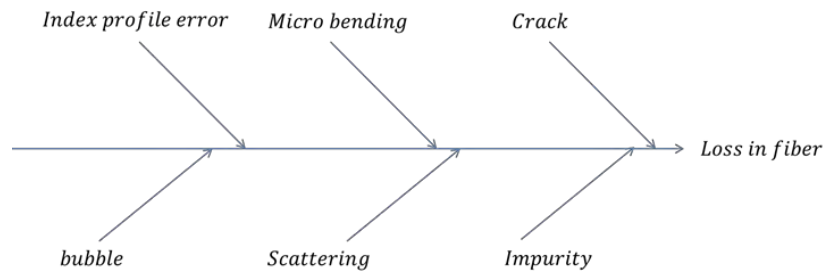
Figure 2-2: Main reasons for loss in a fiber optic

For a low loss in fiber, we ought to decrease the angle of propagated light and perpendicular line to the cross-section of fiber, absorption of light in the core, and length of the fiber.

In the early 1970s, with the advent of fiber optics that relatively had low-loss in long distances, it becomes feasible to transmit the light through fiber optics. Nowadays fiber optics is used widely in all areas of communications in the world. Immunity to electromagnetic, high information transmission capacity, small size, and lightweight are some advantages of fiber optics vs. copper cables (N.L.Christian & Passauer, 1989).

Glass optical fibers are made from glass. The fiber includes core and cladding from glass that have a different refractive index (core's index is higher than cladding). Fibers are categorized into two types of single mode and multimode. Multimode fiber, itself, is divided to step and graded multimode fiber that is related to uniform refractive index and non-uniform refractive index of core respectively. Multimode fiber has a core diameter between 50-1000μm and is usually used in a short distance.

In graded multimode fiber, all modes arrive at the destination at the same time. Single mode fibers have a core diameter between 2-10μm and are available with step-index. Because of the low attenuation of single mode fiber, they can be used in long distances for transmitting the light in one mode. (N.L.Christian & Passauer, 1989).

Although the primary application of fiber optics is transmitting the light for communication, optical fiber can also transmit the light for other purposes. Multimode fibers are capable to transmit high power sunlight in a short distance (below two kilometers). This idea was started in early 1980 by a group of French researchers and followed and improved for various applications by many other researchers.

One of these applications is transmitting concentrated sunlight for heating. Sunlight is concentrated via a parabolic reflector or Fresnel lens and the concentrated light is transmitted by fibers toward a heat exchanger. Amara (2011) used 2 meters length multimode fiber with average 6.2×10^{-3} dB/m attenuation and 20 º numerical apertures.

Passive solar lighting is an attractive application of fiber. A multimode plastic optical fiber with 17.8mm diameter plastic core, 23m length and 0.25dB/m attenuation was used in an experiment for passive solar lighting. This fiber as well as the truncated pyramid concentrator (intensification 2.5× and incident angle below10º) transmitted 25%-30% of incident solar light. This experiment also demonstrated that for a radius 0.45-0.75m, the number of circular bending of fiber didn't affect considerably the transmission intensity (William & Patrick, 2003).

Optical fiber is capable to transmit sunlight for use in thermal solar power generation. In this case, a bundle of multimode silica fiber is needed for their resistance to heat in spot incident points of fiber. A bundle of fused silica core and cladding made of doped silica shows robust performance. Core diameter 1mm, cladding diameter 1.25mm, silicone coating diameter 1.45mm, and NA=(0.44-0.48) is available in the market (Nakamura, Comaskey, & Bell, 2002). The average attenuation per unit depends on the length of the fiber and reduces with adding the length. This fact makes fibers more feasible for transmitting solar energy from the concentrator site to the place of consumption (Kribus, Zik, & Karni, 2000b) and (Feuermann & Gordon, 1999).

Canan Kandilli, Ulgen, and Hepbasli (2008) studied daylighting via the bundle of large core flexible polymethyl methacrylate (PMMA) optical fibers. The length of fiber was 3.12 m. The energy efficiency of the whole system was 0.42 while the exergy efficiency of the system reached 0.17 at a global solar radiation of 582.6 W/m^2. Glass optical fibers have been used for transmitting sunlight in Daylighting systems. Glass optical fibers have advantages of higher transmission relative to polymer fibers. Considering the limitation of core diameter in glass optical fiber, the leakage of fiber at a specific angle of propagation increases with the length of glass optical fibers. The high loss of fiber leads to a limitation in the number of floors that may use glass optical fiber for daylighting. A brief review of round and flat optical fiber and the discussion of leakage in transmitting sunlight through optical fibers.

2.6 Limitations in using optical fiber in transmitting sunlight

2.6.1 Conventional round optical fiber

The initial idea of using conventional round optical fiber for transmitting sunlight can be dated back to forty years ago(Cariou et al., 1982). Recently, significant advances in the technology of the optical fiber have extended its application to transmit the sunlight that involves a wide band of electromagnetic waves with reasonable low loss for a distance of fewer than 20 meters(Feuermann & Gordon, 1999; Firat & Beyene, 2012; Canan Kandilli et al., 2008; Kribus, Zik, & Karni, 2000a; Ullah & Shin, 2012). However, the optical loss of light in optical fiber becomes noticeable in long distances. Considering the said limitation, there are still many applications, especially transmitting daylight via fiber optics for residential and commercial buildings that are regarded as a promising method(Han, Riffat, Lim, & Oh, 2013; Núñez, Antón, & Sala, 2013; Sapia, 2013). The material, diameter, length, and type of optical fibers can affect the efficiency and cost of the whole system(Saleh & Teich, 1991). The material of core and cladding of optical fiber are the major factors to determine the acceptance angle of optical fiber. For transmitting

a high flux of concentrated sunlight, the larger core diameter is usually preferable. One-millimeter core diameter of fused silica with a low refractive index of hard polymer resin as cladding transmits reasonable flux of sunlight with lower loss than polymer optical fibers (Feuermann et al., 2002).

Transmitting sunlight with a wide spectrum of wavelengths via optical fibers encounter several challenges as compared to the application of optical fiber in telecommunication. First, the large core diameter of the optical fiber usually transmits light in multimode, and the optical loss of the multimode fiber is higher as compared to that of single mode fiber provided that both fibers are made of the same material and transmitting the same wavelength of light. Attenuation of power transmission in optical fiber with fused silica as core and hard polymer with a low refractive index as cladding was studied and was found to be independent of the shape of the optical fiber (C. Kandilli & Ulgen, 2009; Senior & Jamro, 2009). However, it was found that there was a leakage of light power caused by transmitting a wide spectrum of sunlight with angles near to the numerical aperture of the optical fiber (Dugas, Sotom, Martin, & Cariou, 1987). According to Dugas et al., the non-zero imaginary component of the refractive index of the cladding will become a significant source of light power leakage if the incident light undergoes many reflections at the interface of core-cladding. To minimize the light leakage, the incident angle of sunlight relative to the numerical aperture of optical fiber should be significantly less than the maximum acceptance angle of the optical fiber. Feuermann et al. studied the dependence of light leakage within their nominal numerical aperture of solar fiber optic on several parameters including incidence angle, optical properties of the core and cladding, and fiber length (Feuermann et al., 2002). Moreover, optical loss can occur when coupling the sunlight to a bundle of optical fibers in which how a bundle of optical fibers being joined together will determine this kind of coupling loss. If a bundle of optical fibers is fabricated by fusing all the optical fibers together, the

loss is lesser than that of the bundle of optical fibers being joined by epoxy adhesive. In the fusing process, the gaps among the optical fibers are diminished by forming one whole solid block, which has improved the coupling efficiency of light to the bundle of optical fibers.

2.6.2   Flat fiber

Flat fibers or rectangular fibers were studied firstly for transmitting neutron, x rays, and light wave circuit. Macatili studied on rectangular waveguide for integrated optics in 1969 (Marcatili, 1969). Square core optical fiber developed for matching with laser diode output beam. Blomster and blomqvist studied on square fiber for high power laser application in 2007 (Blomster & Blomqvist, 2007). Kazuhisa et al. developed rectangular core optical fiber for high power laser in 2010 (Konishi et al., 2010). Ambran et al. demonstrated a physical micro-machining technique to fabricate a multimode interference device in a low-cost flat fiber substrate (Ambran et al., 2012). The width of the flat fiber was 1612 μm and the thickness of the core was about 10 μm.

Rectangular core fibers in market have round clad. Core is made of fused silica for its Broad band UV to NIR Transmittance while clad may be glass or low refractive polymer. Fig. 2-3 shows the attenuation of a square core in the market in different wavelengths. Core of the fiber is fused silica and clad is a hard polymer. These flat fibers are developed for applications in transmitting laser, neutron beam, and x ray. All published data same as round optical fibers are extracted of propagating a beam of laser with specific bandgap and collecting data. Fig. 2-3 reveals that attenuation is as low as 20dB/km at 600nm while the loss of fiber is much more than mentioned loss in transmitting of sunlight.
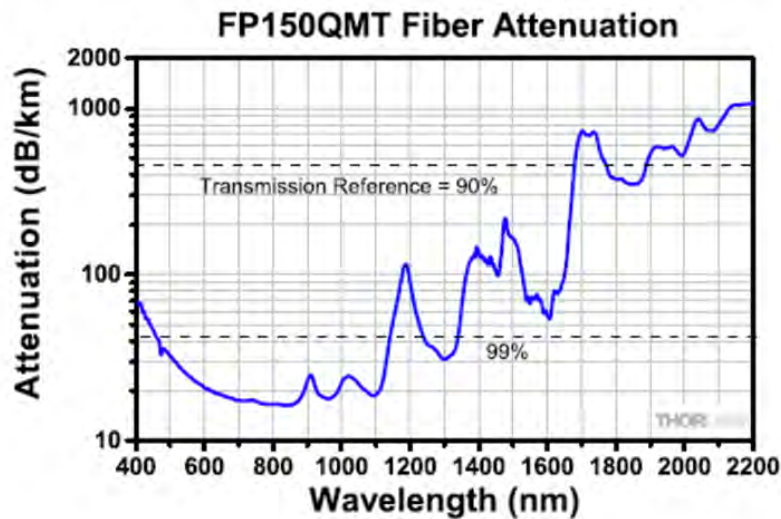
Figure 2-3: attenuation of a square core fiber of a typical square core optical fiber in the market (derived from Thorlabs website)

2.7   Couplers

A coupler transmits the sunlight to fiber optics and may work as a secondary concentrator. The light is also more uniform while exiting the coupler. In fact, we may consider concentrator and coupler as a set of light energizers. Also, fiber optics implemented in light power networks may be considered high-intensity light cables.

Georgios E. Arnaoutakis, Jose Marques-Hueso, Tapas K. Mallick, and Bryce S. Richards (2013) studied on a spherical lens and three coupler taper shape and a Step index low-OH multimode fiber, consisting of silica core 600μm ± 2%, hard polymer cladding 630μm ± 2% and Tefzel coating 1040μm ± 2%. The efficiency of coupling as a function of focal to the diameter of the lens (f/D) and the angle of taper (α) was studied. Measuring coupling efficiency and simulation data demonstrated that the highest efficiency is obtained when 6º<f/D<11º and α<5º.

Fiber optics may be installed directly in the focal point of concentrators and coupler to be placed in contact with fiber at the other end of the fiber. This method will keep the

coupler on site and protect it from outdoor effects (Feuermann & Gordon, 1999) and (Feuermann, Gordon, & Huleihil, 2002).

In 1996, Winston and Ning (1996) introduced a coupler, called a non-imaging radiant energy device, that included a convex lens at the inlet, a non-imaging hyperbolically shaped device, and a concave lens at the outlet.

Feuermann and Gordon (1999) worked on the usage of solar fiber optics in mini-dishes, and they presented a coupling with a single compound parabolic concentrator (CPC) that was placed in the dish and received the light reflected from a small flat mirror. The CPC collected sunlight and was coupled with the fiber optic cable.

Ullah and Shin (2014) studied highly concentrated optical fiber-based daylighting systems that used CPCs for coupling fibers with the generation of concentrated light by a primary concentrator.

The dielectric compound parabolic concentrator (DCPC) is an alternative for compound parabolic concentrator (CPC). Unlike CPC that outer walls are coated by high reflective material, DCPC is made of dielectric material and the light is transmitted via total internal reflection low. This kind of concentrator could be used as a coupler. Measuring the transmittance of an acrylic DCPC showed that it changes with the angle of incident. So that, below 25º angle of incident, its transmittance is 50% and for more than 25º it increases up to 85%. Transmittance fell down again when the angle of the incident is more than 65º(Yu, Su, Zheng, & Riffat, 2014).

In another study, a bundle of fibers transmitted sunlight while a parabolic dish was applied as the main concentrator. The coupler consisted of a secondary mirror and an aspheric lens (Liang, Monteiro, Teixeira, Monteiro, & M.Collares-Pereira, 1998).

Kaiyan, Hongfei, Zhengliang, Taotao, and Jing (2009) studied a novel concentrator used in solar fiber lamp. The concentrator was a curved surface that concentrated sunlight. The coupler consisted of a cylinder mirror reflection surface a deflector and a parabolic mirror that concentrated the light and coupled the light with a fiber optic. It was reported that the connector has a big role in the brightness of the output light. It was also reported that using truncated cone mirror instead of parabolic reduced the brightness and with increasing the angle of cone brightness decreased.

2.8   TRIZ

A clever man in Russia "Altshuller "who worked in a patent office studied more than one million patents and found that all inventors use the same methods and principles for solving problems creatively(Webb, 2002). He worked with his team for many years and discovered more about the same methodologies followed by inventors, discoverers, and founders for solving contradictions in science, industry, economy, education, and so on.

These studies established a type of systematic thinking that helps us to define problems properly, find contradictions, and solve them systematically. Therefore, we may categorize TRIZ with its components as a set of methodologies, principles, and techniques for solving problems and compare it with other solving problem methodologies.

As a problem-solving system TRIZ is capable to be integrated into other techniques or methodologies in various fields. For instant, integration of TRIZ with QFD (Yamashina, Ito, & Kawada, 2002), TRIZ with DFMA (Hipple, 2005) TRIZ, and Six Sigma have been studied in the last decade(Mann, 2002). This problem-solving methodology and other problem-solving methodologies may be considered as parts of a comprehensive problem-solving system.

TRIZ process begins with the definition of the problem in an abstract format. Then the problem reduces to its basic constituents and examines for contradictions. A contradiction matrix and forty principles of TRIZ as well as seventy-nine standard solutions help to find the solution and new concept generation (Altshuller, Fedoseev, & Shulyak, 1998).

After arising a new concept, a maturity study gives a vision for future study of implemented technology. In these processes, some tools such as patent research, facilitate the new concept generation in a short time. The most feature of TRIZ is that it addresses solving contradictions instead of making a tread off in the system.

Figure 2-3 shows the processes of TRIZ methodology. One of the problems in implementing TRIZ is its complexity. Therefore, only experts can use it properly. Even introduced software couldn't compensate the need for experts (Wang, Li, & Yu, 2010).
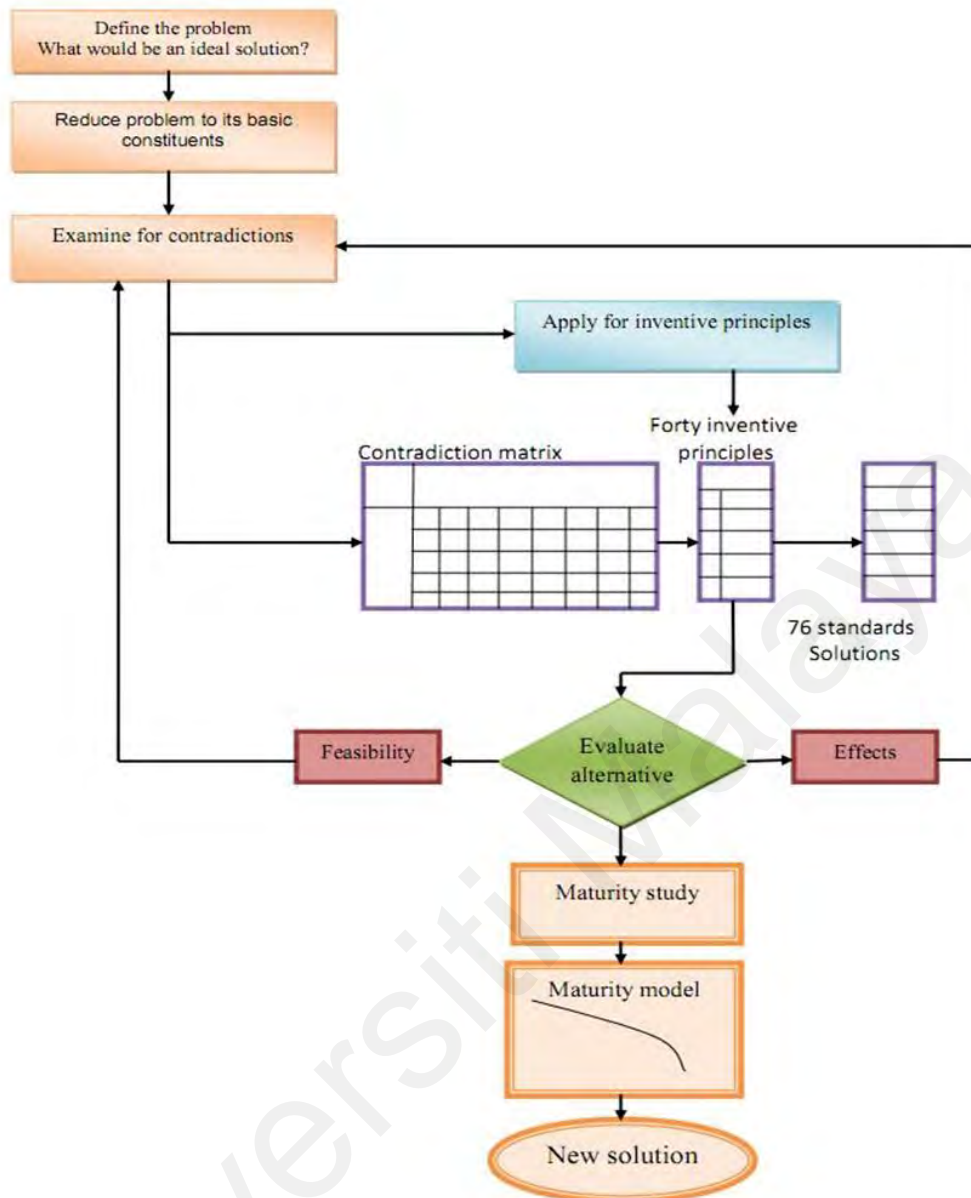
Figure 2-4: TRIZ Process

As can be seen, TRIZ consists of several tools and methodologies. In this research, we just implemented Substance-Field analysis in order to precise the problem and generate new concepts.

CHAPTER 3: METHODOLOGY

In this chapter of the dissertation, we introduce the methods used in this research.

3.1   Generating concepts

Before designing a complex system, it is necessary to prepare various concepts. Creating a concept is a process that begins with a list of parameters set by the needs and specifications. Based on the requirements, the generation of the concept helps to determine the types of possible solutions that meet these needs. Creating different concepts is one of the challenges in designing a complex system. Various methods such as brainstorming, reviewing previous designs of similar systems, and dividing the system into its components help to create new concepts. This section provides a creative way to generate new concepts for a complex system. As explained earlier, Triz is a systematic way of thinking creatively to solve problems. Triz has several tools, one of which is called the substance-field tool.

Su-field analysis is a TRIZ analytical tool for modeling problems related to existing technological systems. Su-field Analysis provides a quick and easy model for considering various knowledge base ideas. Su field analysis was first used to describe the problem. In this method, in order to create concepts, different fields were first considered in which the subsystems and components of the system operate. Some of the fields were considered as the main fields that meet the main aims of the system and some of the fields that help the main fields in the operation of the system were called auxiliary fields. Concentric circles were drawn. Internal circles were considered as subsystem fields. The outer circle was divided into several rings because in this system several outputs (energy) are generated simultaneously. By changing the auxiliary and main fields and their position, new concepts can be created.

3.2   Mathematical analysis

Mathematical analysis is performed in chapters 4 and 5. In Chapter 4, the diameter of the concentrated light is calculated according to the rim angle and sunlight tracking errors. After creating the concept of CTPC, mathematical analysis is performed according to Snell's law and the optimal dimensions and angles of CTPC are obtained.

Another mathematical analysis is performed in chapter 5 for round and flat optical fibers. The analysis is based on the incident angle of the ray trajectory direction to the plane normal to the fiber's axis and sequential reflections. Then, the results of mathematical analysis for both fibers are compared. finally, the effect of the ratio between the length of the rectangle of flat fiber to the diameter of the round fiber is analyzed.

3.3   Simulation analysis

In chapter four, the efficiency of the designed coupler with nine CTPCs, the angle of inlet light into the fiber optics, and the intensity of light emitted through the CTPCs were investigated under non-collimate irradiation by a ray tracing method. The 3D model is developed by CATIA software and ray tracing is performed by the Non-sequential model in Zemax software.

After designing a coupler with nine CTPCs, two couplers with 25 compound truncated pyramid and cone (CTPC) parts are designed using CATIA software and both couplers are investigated by Zemax software. The couplers are investigated for the propagated light intensity, the collected power of each CTPC, and the efficiency of the designed coupler, by ray tracing. In the first design simulation, the light rays emitted to the coupler are not parallel, while in the second design, the light radiation is simulated with parallel beams.

In Chapter 5, the raytracing method is used to simulate the response of flat fiber and conventional round fiber with a fused silica core and low refractive index resin clad to a tilted source of light. For both cases of flat fiber and conventional round fiber, the flux, relative transmission, and the loss of the light were investigated at different incident angles, i.e., 0° to 30°, relative to the axis of the fiber.

After simulation of a round and a flat fiber optics, A bundle of round optical fibers and a bundle of RGOF are investigated in chapter 5. Raytracing of light rays in the RGOF and conventional round fiber are conducted. Like the previous simulation, a 3D cad model is designed and then simulated by Zemax software. For both cases of the bundle of flat fiber and bundle of conventional round fiber, the flux, and the loss of the light were investigated. The results of both bundles are compared. Both bundles have the same cross-sectional area and material.

3.4   Experiments

In this research several experiments are conducted on RGOF and round optical fiber. At first, the profile of the output beam of RGOF is investigated experimentally. A supercontinuum white-light laser of NKT Photonics Company was implemented as a source, and a beam profiler of Thorlab Company is employed for detecting the profile of the beam. Two samples of RGOF are tested. The material of the core of one sample is fused silica and the other is borosilicate 3.3 and the material of cladding is XPC 373 low refractive index polymer and Teflon respectively.

The next experiment is performed on both round optical fiber and RGOF to evaluate the results of simulation and mathematical models. Relative transmission of RGOF in angles between 0° to 20° is investigated under the propagation of white light of a xenon lamp. A 740 mm RGOF with dimensions 10mm×0.4mm and a 740 mm round optical

fiber with 1mm diameter is used for investigating the relative transmission of RGOF to angular propagation of focused light and is compared with the result of round fiber optics.

A RGOF with a length of 2.2m is examined for its bending. The fiber without jacket has just a polymer as clad. The fiber is bent on a cylinder with 350 mm diameter and twisted 90° along its longitude axis. A designed and fabricated receiver with round optical fibers is presented with four multi-junction solar cells. Four separated bundles are in contact with multi-junction solar cells. Each rearranged bundle has a square shape in contact with the cells. A small designed part holds the fibers in a square position with dimensions 10mmx10mm.

A 55-Watt xenon lamp at a color temperature of 6000 K and a maximum brightness of 3000-4000 Lm was used in a solar simulator with a spectrum similar to sunlight, particularly in the visible range. The receiver was placed under the propagation of the lamp. The output intensity of the solar simulator at the entrance of the receiver and the output power of the receiver is measured by using a PV system analyzer (PROVA 1011) capable of plotting I-V and P-V curves concurrently. TES 132 data logging solar power meter was used to measure the intensity at the entrance of the receiver. The temperature of the multi-junction solar cell was measured at the back of the heat sink attached to the solar cell.

CHPATER 4: DESIGNING COUPLER

4.1   Introduction

This section introduces a new coupler using the proposed compound truncated pyramid and cone (CTPC) shape. Each CTPC can be connected to the core of one fiber. Therefore, the loss would be reduced, which leads to the reduction of temperature on the tips of the fiber optics. An analytical model was developed to design the components of this structure.

The new design is capable of transmitting sunlight into fiber optics and working as a secondary concentrator. It also reduces the angle of incident light before entering the fiber optics while simultaneously increasing the coupling efficiency by reducing the number of optical components with different mediums. We split the sunlight into nine beams, where each beam hits one CTPC with a small angle of incidence. The designed CTPC facilitates the assembly process of fiber optics and coupler. The design of the coupler is simulated, and the results are presented.

4.2   Coupling design, theory, and methodology

4.2.1   Assembly design

Fig. 4-1 shows a schematic of the proposed coupler for Uncollimated light, dish, and fiber optics. The coupler is attached to the dish and fiber optics. The dish is used as a primary concentrator, and the fiber optics transmit the sunlight. The proposed coupler includes nine CTPCs mounted on a transparent plate. The coupler is placed a few millimeters from the focal point of the dish. Since the refractive index of the plate is higher than that of air, it reduces the refracted angle of light. Considering prototype methodology, two different concepts were developed.
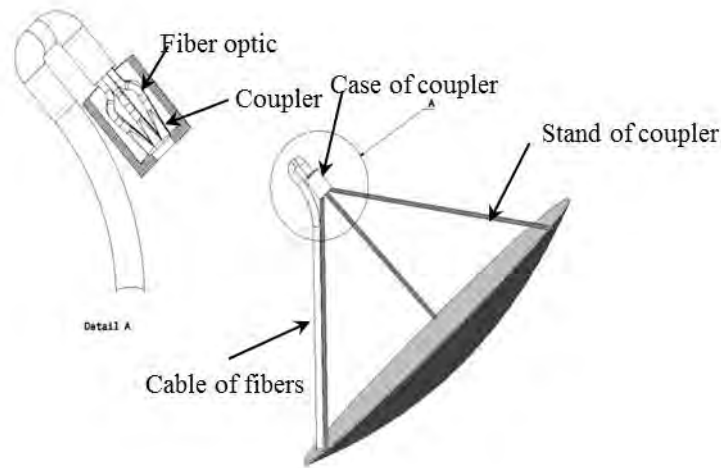
Figure 4-1: Schematic of a parabolic dish, coupler, and fiber optics.

First, a prototyping process with a flat plate as the base of the coupler was assumed. In this case, the bottom of each CTPC was cut to a specific angle. In the second approach, one side of the plate was machined so that it could contain nine square surfaces with different angles. In this case, all the CTPCs were the same, which rendered them more suitable for mass production. As shown in Fig. 4-2(a) and Fig4-3 (a), according to the first concept, the surface of the bottom side of the CTPCs is rectangular in order to accommodate them on the flat plate with no empty space.

The bottom side is also cut with an angle to the symmetrical axis of the CTPCs. This angle tilts the CTPCs as they sit on the plane, which reduces the entrance angle of transmitted light Fig 4-2 (b). The upper side of the CTPCs is carved into a cone shape and extended to form a cylinder. The cylindrical part of the CTPCs could be aligned easily with the fiber optics and spliced to the core of the fiber. The vertical CTPC, shown in red, is located at the center of the plate. Four CTPCs, shown in yellow, are positioned at the side of plate at the same angle, and four more CTPCs, shown in green, are placed at the same angle at the four corners of the flat plate.

In the second concept, the plate is carved into square surfaces with different angles; therefore, the bottom sides of the CTPCs are perpendicular to the symmetrical axis. This structure is shown in Fig4-3(b). As can be seen, unlike the first approach, the plate is not flat and the CTPCs stand on the carved surface with no empty space. However, according to derived simulations, both concepts have the same results.

By using the extra numbers of CTPCs, the total surface area of the cores connected to the coupler increases, and thus the coupler could be used for larger primary concentrators. An investigation into the cost effectiveness of such a system is needed in order to optimize the size of the primary concentrator for different applications.

(a)   (b)
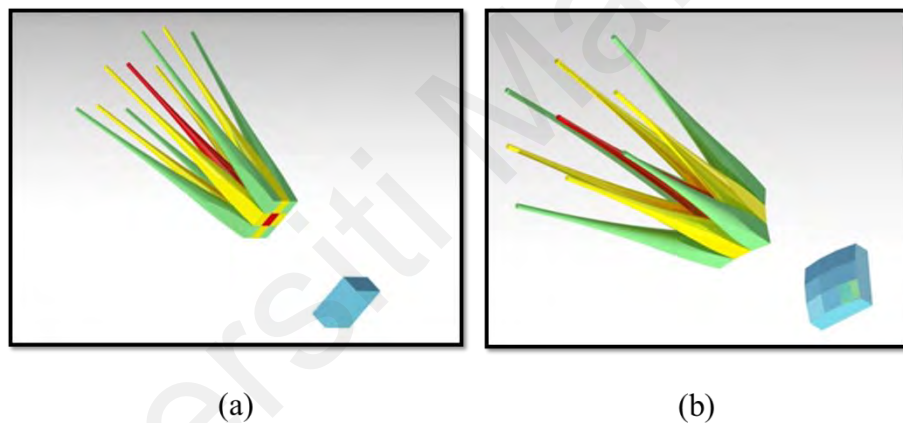
Figure 4- 2: assembly of coupler: (a) concept of flat plate and (b) concept of carved plate.

(a)   (b)
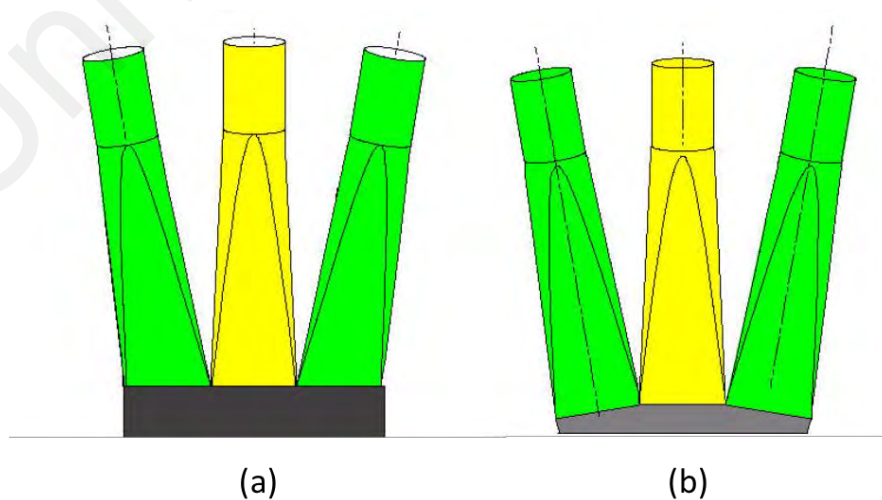
Figure 4-3: CTPCs cross-section: (a) flat design and (b) carved design.

4.2.2   Plate design

The inlet light of coupling comes from the primary concentrator. Fig. 4-4 shows the flux of sun that is illuminated on a dish with an aperture of D. The rim angle is ϕ, the sunlight angle is θs, and the diameter of concentrated light is d. An acceptable precision for θs is 0.27∘, and the occurrence of the probable cumulative errors in the system is given by Δθ. The sources of error in the system are an imperfect surface, the structure, movement, alignment, and the sensors of the sun tracker, etc. The diameter of concentrated light is given by

$$d = \frac{D sin(\theta s + \Delta\theta)}{sin\varphi(cos(\varphi + \theta_S + \Delta\theta))} \tag{4.1}$$

To minimize the diameter of concentrated light, the rim angle is considered to be 45∘. Therefore, we can rewrite Eq. (4.1) as

$$d = \frac{2D \sin(\theta_S + \Delta\theta)}{\cos(\theta_S + \Delta\theta) - \sin(\theta_S + \Delta\theta)} \tag{4.2}$$

Based on the derived diameter and the definition of the geometrical concentration $\left(C = \left(\frac{D}{d}\right)^2\right)$ we have (A. Rabl, 1985):

$$C = \frac{1 - sin2(\theta_S + \Delta\theta)}{4sin^2(\theta_S + \Delta\theta)} \tag{4.3}$$
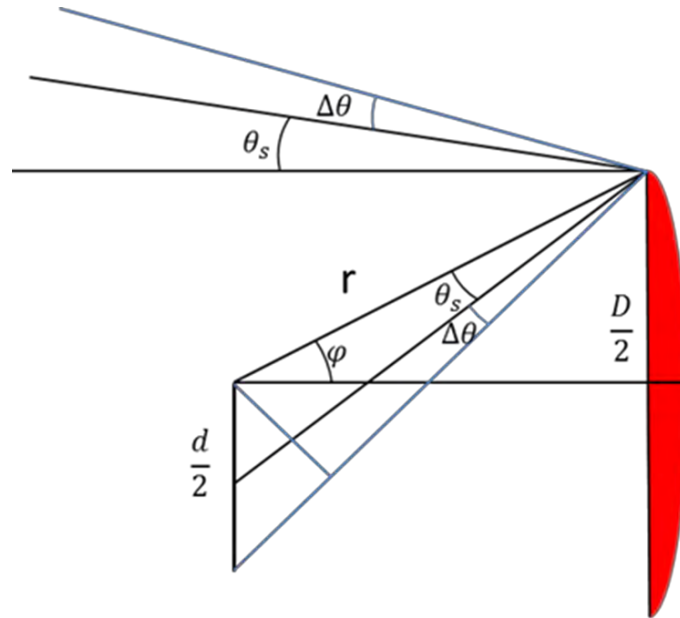
Figure 4-4: Concentrated sun flux by a parabolic dish mirror.

Fig. 4-5 shows a reduction of the geometrical concentration of a parabolic dish as the system error increases from zero to 0.3∘. On the other hand, the diameter of the concentrated light increases significantly with increasing errors, which is illustrated in the same figure. Calculation of the concentrated light diameter leads to computation of the dimensions of the plate, with the assumption that the length of the square plate is equal to the focal point diameter.
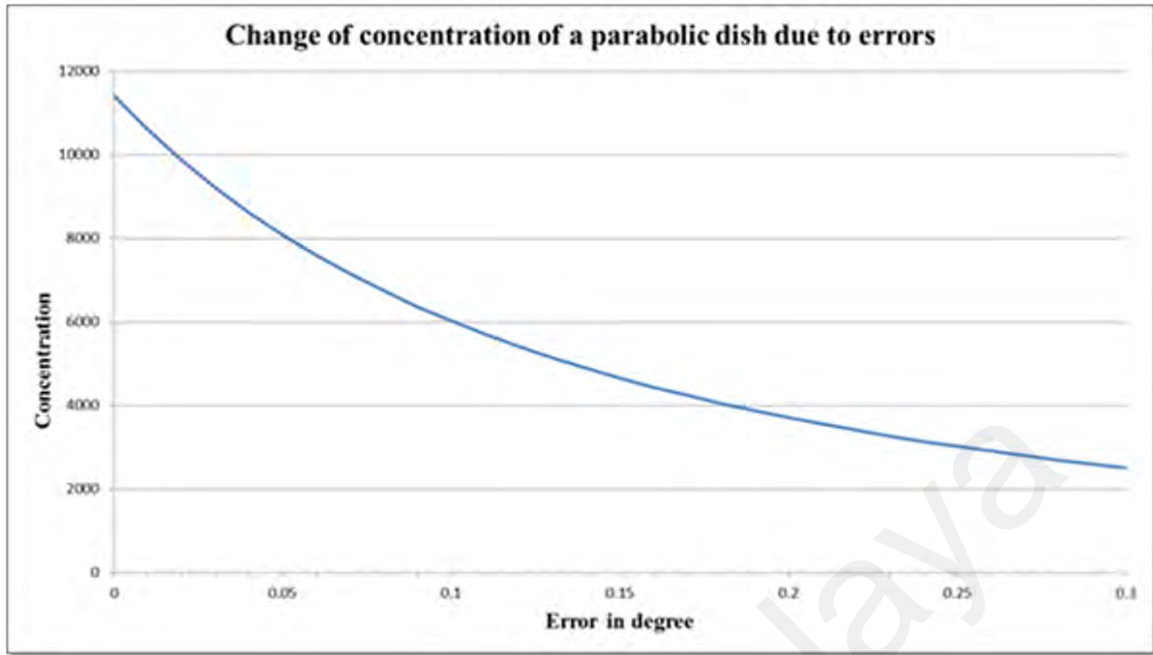
Figure 4-5: Variation of geometrical concentration of a parabolic dish with respect to errors for 45° rim angle.

4.2.3 CTPC design

A key part of the CPVTD system is the coupler of sunlight. The duty of this part is to collect concentrated sunlight and coupling the light with fiber optics. The diameter of concentrated sunlight at the focal point is about 15 mm for a small dish with a 600 mm diameter. Fused silica multimode fiber optics demonstrates low loss compared to other fiber optics for visible and near-infrared wavelength. Fused silica multimode fibers work at a higher temperature than polymer optical fibers and are durable in harsh situations. The drawback is that they cannot bend when they are thick, and they are expensive. However, low-OH fused silica fiber optics with one-millimeter diameter of the core is in the market now. To cover a surface area with 15mm diameter, we need at least 140 of such fiber optics. A bundle of fiber optics could be a solution, but a lot of loss would be in cladding and the gaps between claddings. Another way is to make arrays of very small dishes and every dish implements one fiber optics. By using small dishes, the gaps

between the dishes constitute a loss in the total amount of sunlight captured, and ultimately it is more costly than using a single big dish.

These kinds of problems are known in TRIZ as contradictions. Based on an analysis of contradiction and frothy principles of TRIZ, we designed two new couplers. The couplers collect the concentrated sunlight and divide the beam into narrower beams. Each narrow beam again concentrates by a small truncated pyramid. The truncated pyramid is rounded and gradually formed a cone that continues to form a cylinder at the bottom for ease of alignment with the core of fiber optic. In this way, the beams are coupled to the core of fiber optics and the loss is reduced compared to the loss in a bundle of fiber optics. On the other hand, we can use the big dish.

A truncated cone is a simple shape that is widely used as a coupler located between the first concentrator and the fiber optics/photocells. In comparison with compound parabolic concentrators (CPCs), it shows better performance than cones; however, producing CPCs is more difficult and expensive. Williamson (Williamson, 1952) illustrated a geometrical method of ray tracing in a simple cone, and Witte (Witte, 1965) demonstrated that the same procedure is applicable for skew rays. Mayer (Myer, 1980) implemented the same method for the concentration of collimated paraxial rays in a cone. Here, we develop a new approach for designing CTPCs for couplers connected to fiber optics.
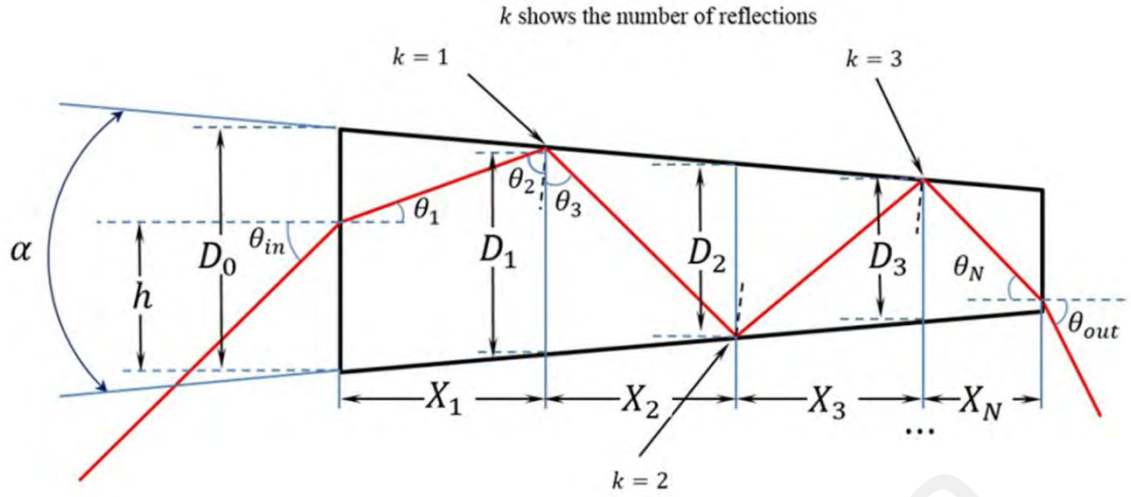
Figure 4-6: CTPC with total internal reflection and the dimensions of reflection points.

The proposed CTPC design can be divided in two parts. The first part involves the calculation of the maximum amount of total reflection based on the variation of the inlet light and CTPC angles. The second part involves the calculation of CTPC dimensions with respect to the amount of total reflection. Fig. 4-6 shows a CTPC and meridian ray with three total internal reflections. Based on Snells law,

$$n_1 \sin \theta_{in} = n_2 \sin \theta_1 \tag{4.4}$$

where, n_1 is the refraction index of the medium of the inlet ray, n_2 is refraction index of CTPC, θ_in is Angleof incident light to forward surface, and θ_1 is refracted angle. To satisfy the total internal reflection condition on the body of CTPC:

$$\theta_2 = \theta_3 \; ; \quad \sin \theta_2 > \frac{n_1}{n_2} \tag{4.5}$$

where the angle of the first incident light to the side wall is θ_2 and θ_3 is the first total reflection on the side wall of the CTPC. At the first incident light to the side wall of CTPC,

$$\theta_2 = \frac{\pi}{2} - \left(\theta_1 + \frac{\alpha}{2}\right) \tag{4.6}$$

where α is the CTPC angle equal to the angle of the pyramid. Substituting (4.6) into (4.5) yields

$$\cos(\theta_1 + \frac{\alpha}{2}) > \frac{n_1}{n_2} \qquad (4.7)$$

For the number of reflections on the side wall, k, with total internal reflections, we have

$$\theta_1 < \cos^{-1}(\frac{n_1}{n_2}) - k\frac{\alpha}{2} \qquad (4.8)$$

Since an optical fiber with a core and cladding is connected to CTPC, in order to prevent reflection on the end of its surface, we use

$$\sin \theta_{out} \leq \sqrt{n_{core}^2 - n_{clad}^2} \qquad (4.9)$$

where n_{core} and n_{clad} are the refractive indexes of core and cladding, respectively. On the other hand, these two fiber parameters can be related to the numerical aperture $\left(NA = \sqrt{n_{core}^2 - n_{clad}^2}\right)$. The output angle of transmitted light from CTPC is indicated by θ_{out}. By using the relationship between the internal angles of designed CTPC in Fig. 4- 6, we can obtain:

$$\theta_N = \theta_1 + k\alpha \qquad (4.10)$$

where θ_N is the incident angle of light to the output surface of CTPC. By applying Snells law for CTPC and optical fiber, we obtain

$$n_2 \sin \theta_N = n_{core} \sin \theta_{out} \qquad (4.11)$$

Substituting (4.11) for (4.10) and using (4.9), we can find θ_1 as

$$\theta_1 \le \sin^{-1}\left(\frac{n_{core}}{n_2}\sqrt{n_{core}^2 - n_{clad}^2}\right) - k\alpha \tag{4.12}$$

Fig. 4-7 compares the variation of θ_1 in terms of the number of total reflections based on two different relations derived from Eqs. (4.8) and (4.12). The assumed refractive indexes are: ($n_1 = 1, n_2 = 1.517, n_{core} = 1.459, n_{clad} = 1.378$).
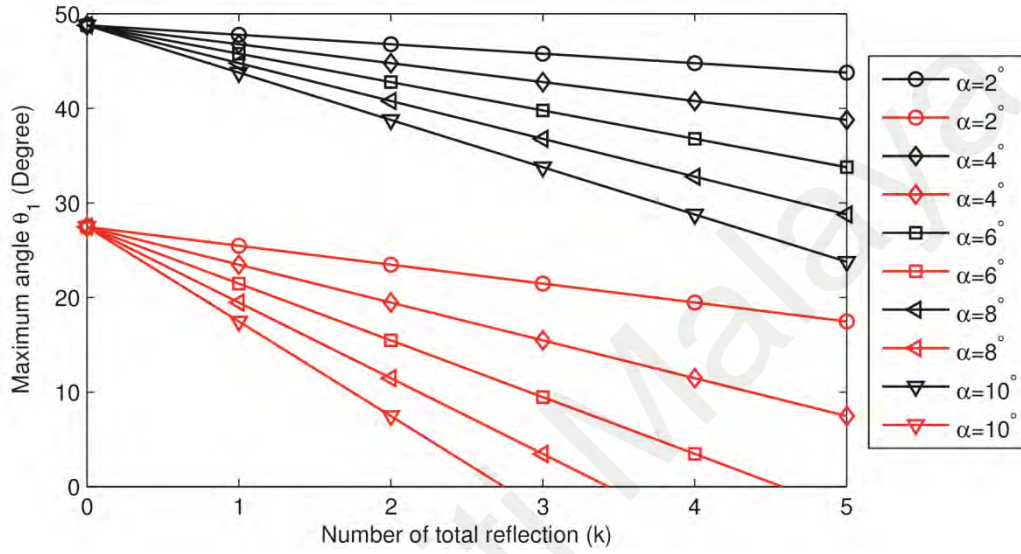
Figure4-7: Maximum angle of θ_1 with respect to the number of total reflections on the body and the end surface (to prevent reflection) for different CTPC angles.

According to Fig. 4.7, there are two different approaches to obtain the maximum value of θ_1 with various angles of CTPC. The upper lines show the mentioned value for the total reflection inside CTPC, whereas the lower lines show the maximum value of θ_1 for preventing reflection at the end of CTPC. Connecting the inlet light angle θ_{in} to θ_1, using Eqs. (4.4) and (4.12), yields

$$\theta_{in} \le \sin^{-1}\left[\frac{n_2 \sin\left(\sin^{-1}\frac{n_{core}}{n_2}\sqrt{n_{core}^2 - n_{clad}^2} - k\alpha\right)}{n_1}\right] \tag{4.13}$$

Fig. 4-8 shows the inlet angle versus the maximum number of total reflections on the body of CTPC. For a specific inlet angle (θ_{in}), the number of total reflection (k) decreases by increasing CTPC angle (α).
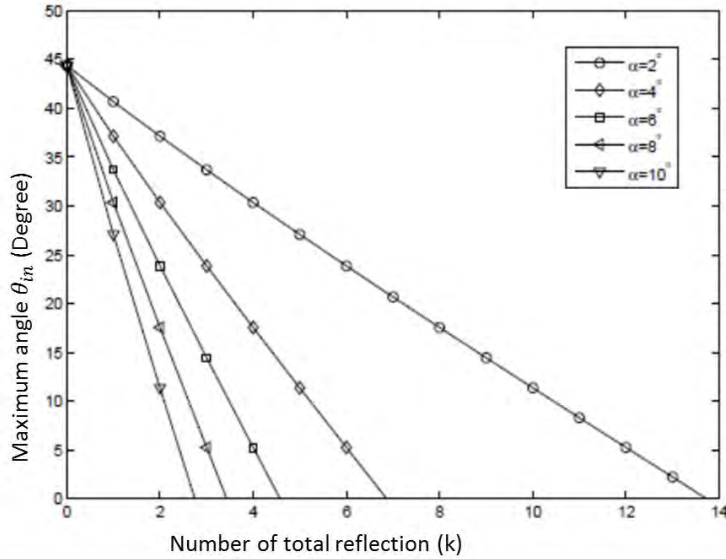
Figure 4-8: Maximum angle of θin with respect to the number of total reflections for different CTPC angles.

To find a relationship between the length of CTPC (L) and the different parameters of the designed CTPC, such as the base lengths for various points of incident light (D_0, D_1, ..., D_{k-1}, D_k) and angle (α), we define φ_k in terms of the refracted angle (θ_1) and the CTPC angle as

$$\varphi_k = \theta_1 + (k-1)\alpha \tag{4.14}$$

where k is the number of reflections and k≥1. On the other hand, using the tangent formula in the right triangle *ABC* yields:

$$\tan \varphi_k = \frac{BC}{AB} = \frac{D_{k-1} - BE}{AB} \tag{4.15}$$

Since the angle $\widehat{BAE}$ is half of the CTPC angle, for the right triangle ABE, we have

$$\tan \frac{\alpha}{2} = \frac{BE}{AB} \tag{4.16}$$

By combining (4.14) and (4.15), using (4.16), and regarding that $AB = X_k$,

$$\tan[\theta_1 + (k-1)\alpha] = \frac{D_{k-1}}{X_k} - \tan \frac{\alpha}{2} \tag{4.17}$$

45

It is clear in Fig. 4-9 for the right triangle MNP that

$$\tan \theta_1 = \frac{D_0 - h - w}{X_1} \qquad (4.18)$$

and that for triangle PMQ,

$$\tan \frac{\alpha}{2} = \frac{w}{X_1} \qquad (4.19)$$
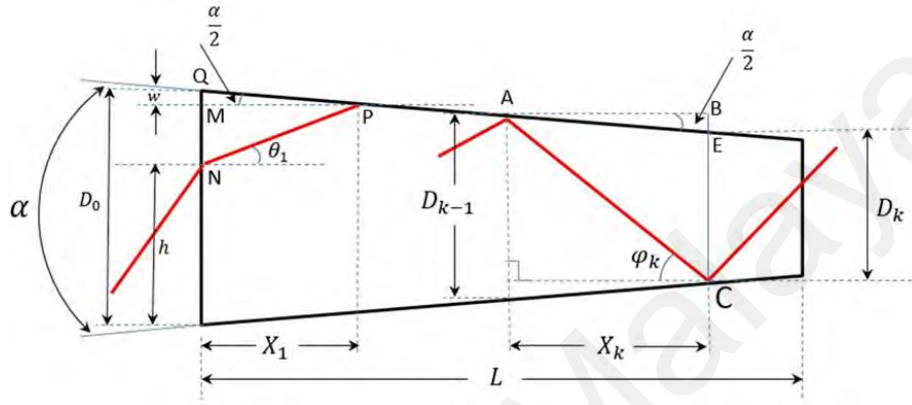
Figure 4-9: Total internal reflection of incident light in a CTPC at K^{th} reflection

By eliminating w between Eqs. (4.18) and (4.19), we get:

$$X_1 = \frac{D_0 - h}{\tan \frac{\alpha}{2} + \tan \theta_1} \qquad (4.20)$$

In the first reflection (see Fig4-6), it is apparent that the first base length (D_1) of CTPC is:

$$D_1 = D_0 - 2X_1 \tan \frac{\alpha}{2} \qquad (4.21)$$

Using a mathematical induction of Eq. (4.21), the distance between reflection points can be derived as follows:

$$X_k = \frac{D_{k-1}}{\tan \frac{\alpha}{2} + \tan(\theta_1 + (k-1)\alpha)} \qquad k \geq 2 \qquad (4.22)$$

where D_{k-1} can be obtained using the following recurrence relation:

$$D_k = D_{k-1} - 2X_k \tan \frac{\alpha}{2} \qquad k \geq 1 \tag{4.23}$$

Finally, integrating the above calculated distances leads us to find the length of CTPC as:

$$L \leq \sum_{k=1}^{N} X_k \tag{4.24}$$

The upper side of CTPC is shaped as a cone (see Fig. 4-3). Therefore, the derived equations are applicable on the cone part as well. The thicker diameter of cone is the chord of square base of the pyramid, which reduces the maximum amount of incident light. The maximum concentration of sunlight in the proposed design is limited by the refractive index (n_{core}) and sunlight angle (θ_s) based on the following equation (Ari Rabl, 1976):

$$C_{max} \leq \frac{n_{core}^2}{\sin^2 \theta_s} \tag{4.25}$$

Therefore, in designing of the coupler, the above limitation of total concentration must be considered.

4.3 Design and simulation of a coupler with nine CTPCs for Uncollimated light

A coupler was designed based on the derived equations of Section 2 to design a plate and CTPC. We assumed 900 W/m2 as the total integrated power intensity of the sun for an AM 1.5 D reference spectrum (ASTMG 173) (Georgios E. Arnaoutakis, Jose Marques-Hueso, Tapas K Mallick, & Bryce S. Richards, 2013). The calculated angle between CTPCs was 9.5°. Geometrical concentration of CTPC was 1.97, and the input power of the coupler was assumed to be 300 W for a dish with a 650 mm aperture diameter. Using CAD modeling software, a 3D model was created to be used in further studies of the experimental model and the fabricating process. Fig. 4-10 shows a CAD prototyping of the proposed coupler.
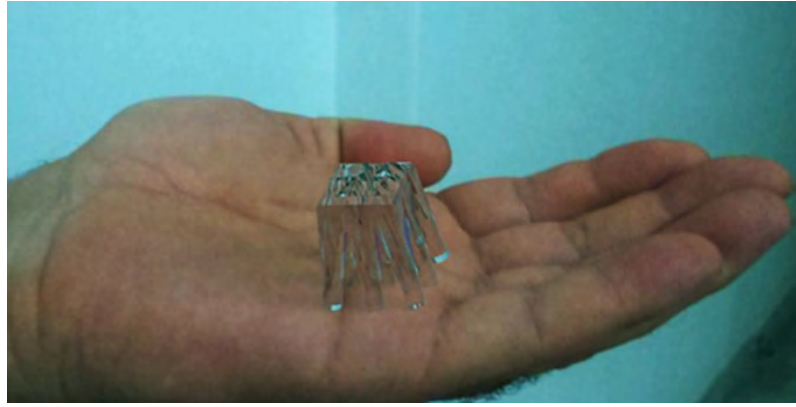
Figure 4-10: CAD prototype of coupler.

The 3D model was developed, using the Non-sequential model for ray tracing in Zemax software. The rim angle of the dish was considered 45°, which concentrated the light directly onto the coupler. Hence, the multipoint sources of light were assumed to propagate the light with five wavelengths from 400 to 800 nm in our simulation. The angle of propagation was 45°, and a detector was located behind the point source, whereas each CTPC had a smaller- diameter detector. The coupler was placed a few millimeters from the focal point, and therefore the rays were divergent. In the simulation, BK7 was considered as a material for coupler. Wave lengths in the simulation were 400, 550, and 700 nm. Fig. 4-11 shows a layout of coupler with a ray tracing format in shaded and 3D models.
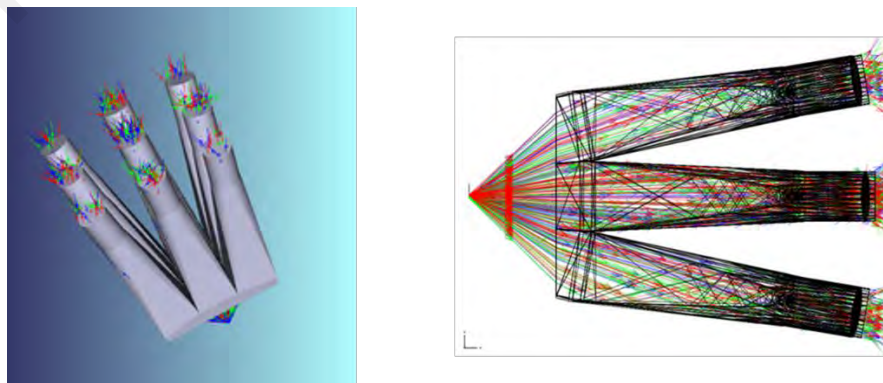
Figure 4-11: Layout of coupler for ray tracing: (a) shaded model and (b) 3D layout.

The efficiency of the designed coupler under non-collimate irradiation, the angle of inlet light into the fiber optics, and the propagated light intensity via the components were investigated by ray tracing. This efficiency was calculated by dividing the total occupied powers by CTPCs to the light source power through the following equation:

$$eff = \frac{\sum_{i=1}^{n} P_i^T}{P_{in}} \tag{4.26}$$

Where PT is the power transmitted by each fiber optic, Pin is the total inlet power of the coupler and n is the number of CTPCs. Fig. 4-12 shows the power transmitted by each CTPC while a 300 W power was applied by multipoint sources. Although there was significant variation between the power transmitted by CTPCs on the corners, sides, and center, the amount of power transmitted by the CTPCs that were positioned on the sides or corners were close to each other.
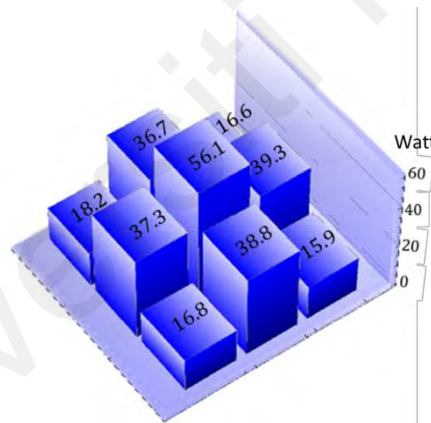
Figure 4-12: Distribution of power amplitudes (in watts) transmitted by CTPCs for a 300 W input.

The efficiency of the designed coupler was 92% in the simulation. Fresnel reflection on the surfaces of the optical components caused a loss of power. In this coupler, Fresnel reflection only occurred on the flat plate surface. Incoherent irradiance of the transmitted light and the distribution of radiant intensity by CTPCs are shown in Fig. 4-13 for a 10 W source power. The maximum intensity of light was exhibited by the centrally placed

CTPC and the least intensity of transmitted light was exhibited by CTPCs positioned on the corners of the plate.
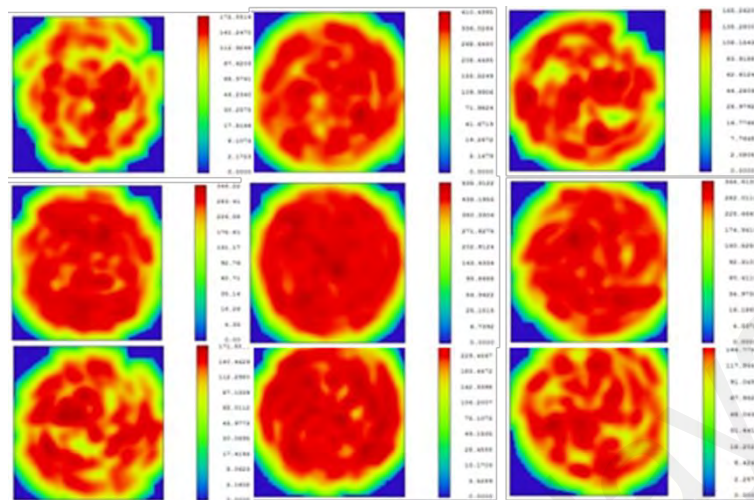
Figure 4-13: Distribution of radiant intensity for CTPCs according to their position.

The angle of inlet light into the fiber optics plays a key role in reducing the light leakage of fiber optics in the transmission of sunlight (Polyanskiy, 2016). Fig. 4-14 compares the angular range and the amplitude of light intensity for CPTCs. The coupler was designed for a fiber with a numerical aperture (NA) of 0.48, which means that the maximum acceptable cone angle of the fiber should be 56∘. The simulated results for angular range demonstrate the validity of the calculations for the designed coupler.
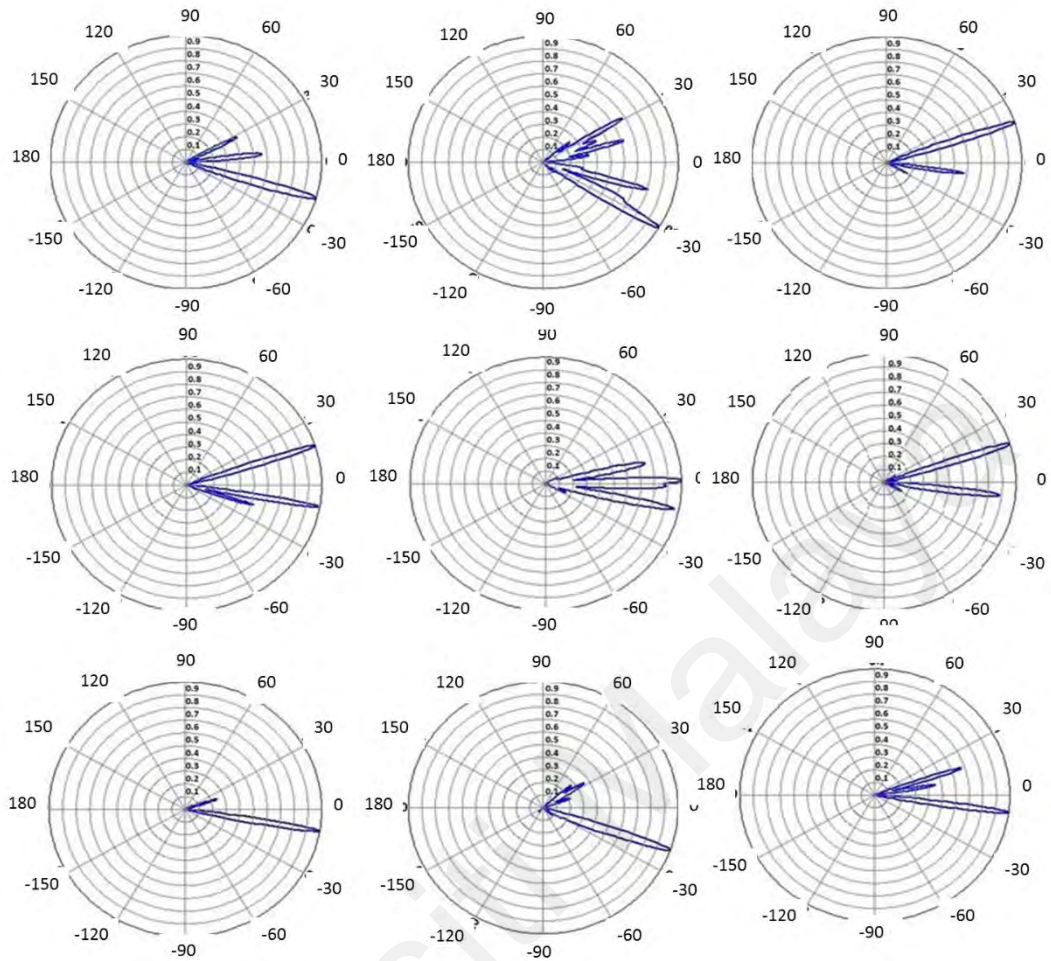
Figure 4-14: Distribution of angular range and amplitude for CTPCs according to their position.

4.4 Design and simulation of two couplers with 25 CTPCs for collimated light and Uncollimated light

Two couplers with 25 compound truncated pyramid and cone (CTPC) parts were designed. We considered the following assumptions:

(a) The material of coupler is pure silica, same material as used in the core of fiber optics, in order to match the refractive indexes.

(b) The diameter of the core is 1000 μm, while the clad is a polymer and numerical aperture of the fiber optic is 0.48.

(c) A 600 mm diameter chromate parabolic dish is used as primary concentrators with 85% efficiency.

(d) The precision of tracker considered ±0.1° and the diameter of cylindrical part of CTPC is equal to the diameter of the core of fiber optic.

(e) The total integrated power intensity of the sun is 900 W/m2 for AM 1.5D reference spectrum (ASTM G 173) (He, Zheng, Li, & Dai, 2009).

The inlet surfaces of both couplers are square in shape; therefore, the diameter of the focal point of the dish is equal to the length of the side of the square. The couplers were designed for two different conditions. First, we considered that a mirror is between the coupler and the dish, so the outcome light is collimated. Second, the light comes toward the coupler directly from the dish so is not collimated. Fig. 4-15 shows both conditions (a) uncollimated light comes from parabolic dish, and (b) collimated light comes from a mirror that is in focal point of parabolic dish. The couplers are placed in a case, and water can flow in the case to reduce the temperature of the couplers.

(a) Uncollimated light   (b) Collimated light
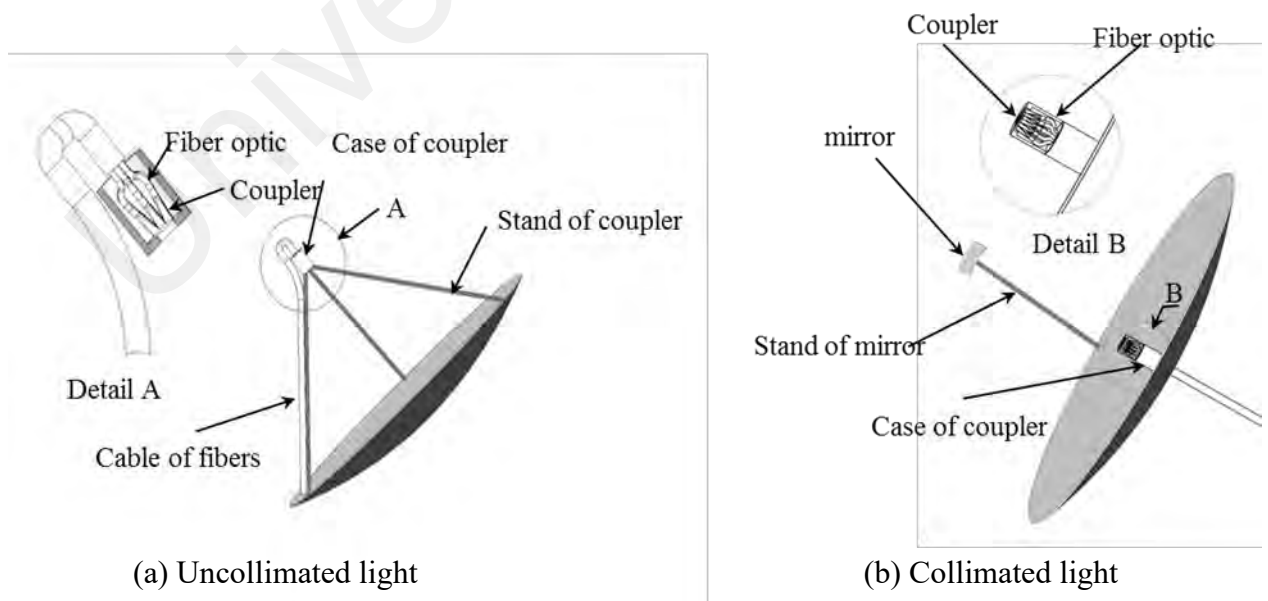
Figure 4-15 : General arrangement of coupler and solar dish for collimated and uncollimated light. (a) uncollimated light (b) collimated light by a mirror.

Both of designed couplers have same functions. The CAD model of first design is shown in Fig. 4-16 (a). The angle between the beams caused the CTPCs are tilted to accommodate the light in a small angle of incident. The angle between CTPCs was calculated by dividing the inlet angle of the sunlight inside the coupler to the number of rows of CTPCs.

The second design is based on the collimated beam. A mirror receives the concentrated light from the dish and reflects toward the coupler. The reflected light is collimated; therefore, the CTPCs need not be tilted. Fig. 4-16(b) shows the CAD model of the second coupler.

(a) Uncollimated light   (b) Collimated light

Figure 4-16 : CAD models of the couplers for uncollimated and collimated light.
(a) Uncollimated and (b) Collimated.

A 3D model for simulation was developed, and a non-sequential model was implemented for ray tracing in Zemax software. For uncollimated condition, the rim angle of the dish is considered to be 45°, which concentrates the light directly onto the coupler. Hence, we assumed that the point sources of light to propagate the light in five wavelengths, from 400 to 2200 nm, in our simulation. Based on the rim angle, the angle of propagation is considered to be 45°, and a detector is located behind the point

source, whereas each CTPC has a separate detector. Because of using the light coming directly from the dish, the rays of sources are not collimated rays. We placed the coupler a few millimeters far from the focal point, and, therefore, the rays are divergent. In the simulation, BK7 is considered as a material for the coupler. For collimate radiation, we add a lens between the point sources and coupler. Therefore, the Fresnel reflection effect of the mirror is considered. Fig. 4-17 shows the layout of the coupler: (a) for uncollimated light and layout of the coupler, and (b) for collimated light with two ray tracing formats.
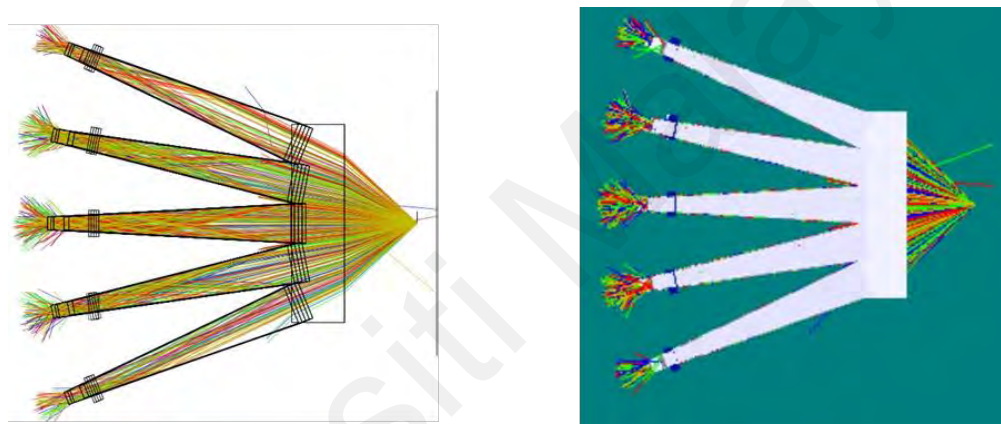
(a) Uncollimated light
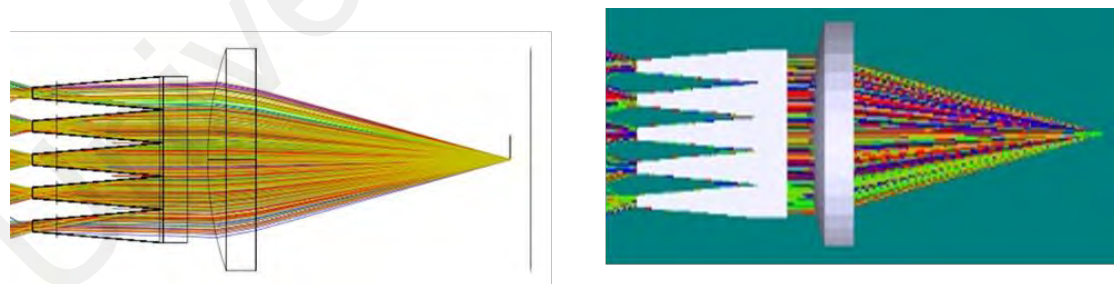
(b) Collimated light

Figure 4-17 : Ray tracing of the couplers for two kinds of radiation. (a) Uncollimated light (b) collimated light by a Plano concave lens.

4.4.1 Simulation results and discussion of the couplers designed for uncollimated and collimated light

We investigated the propagated light intensity, the collected power of each CTPC, and the efficiency of the designed coupler, (A) in uncollimated irradiation and coupler, and (B) in collimate irradiation by ray tracing. Fig. 4-18 shows the distribution of power in CTPCs and with respect to the position of each CTPC for both couplers. The total inlet power is 200 watts. The amplitude of power transmitted by the CTPCs alters from 14.1 to 0.6 watt for coupler A and from 11.2 to 0.4 for coupler B. The power of each ray of the CTPCs increases at the middle and reduces toward the corners. The amplitudes of power for the CTPCs symmetrical to the center are relatively close to each other.
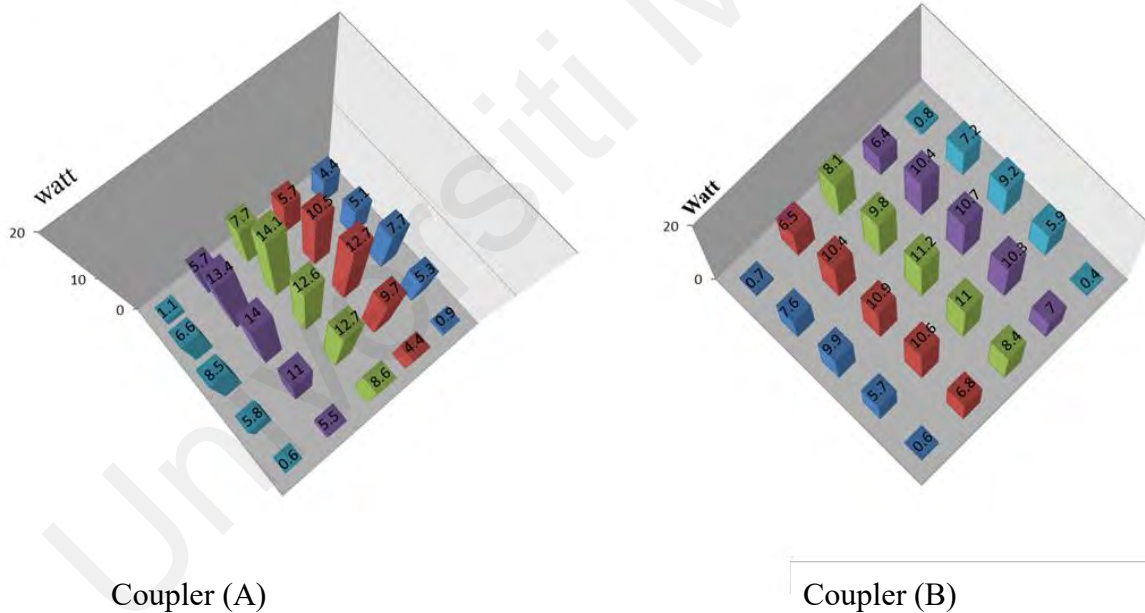
Coupler (A)   Coupler (B)

Figure4-18 : Distribution of power amplitudes (in watts) transmitted by CTPCs according to position of CTPCs in the couplers A and B.

The efficiency of the coupler is defined as the total output power of the coupler to the inlet power. In the designed couplers, the input power is divided into the CTPCs and

each CTPC transmits a portion of power to the core of a fiber optic. So, we calculated the efficiency by dividing the total output power by the inlet power of the coupler through following equation.

The efficiency of the coupler (A) was 97% in the simulation while the efficiency of the couple B was 93%. The effect of Fresnel reflection occurred only on the inlet surface of Coupler A whereas the effect of Fresnel reflection occurred on the inlet surface of coupler B, and the surfaces of the lens. Fig. 4-19 shows the distribution of intensity of light with respect to the position of the CTPCs in the coupler A. The maximum intensity of light is observed in the CTPC near the center of the coupler and the least amount of the intensity is observed in the CTPCs positioned at the corners of the coupler.
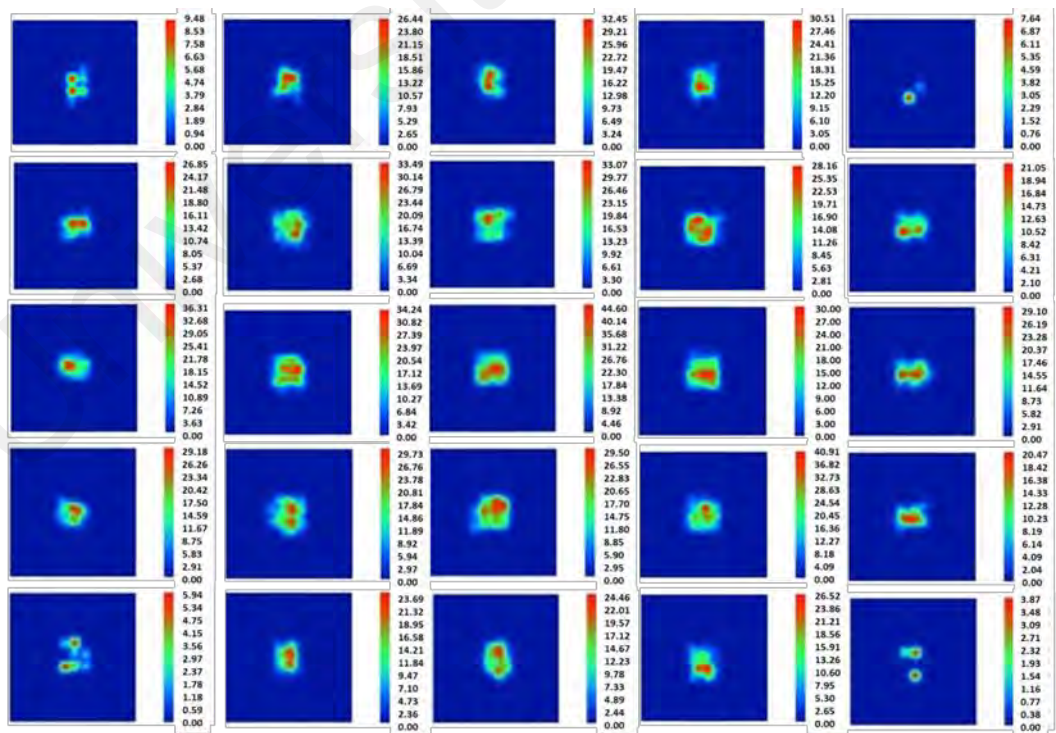
Figure 4-19 : Distribution of radiant intensity for CTPCs according to their position in coupler A.

Fig. 4-20 shows the distribution of intensity of light for the coupler B. The distribution is similar to the coupler A. However, the amplitude of the intensity is higher than coupler A. As can be seen, the propagation of the light in coupler B is more uniform than coupler A.
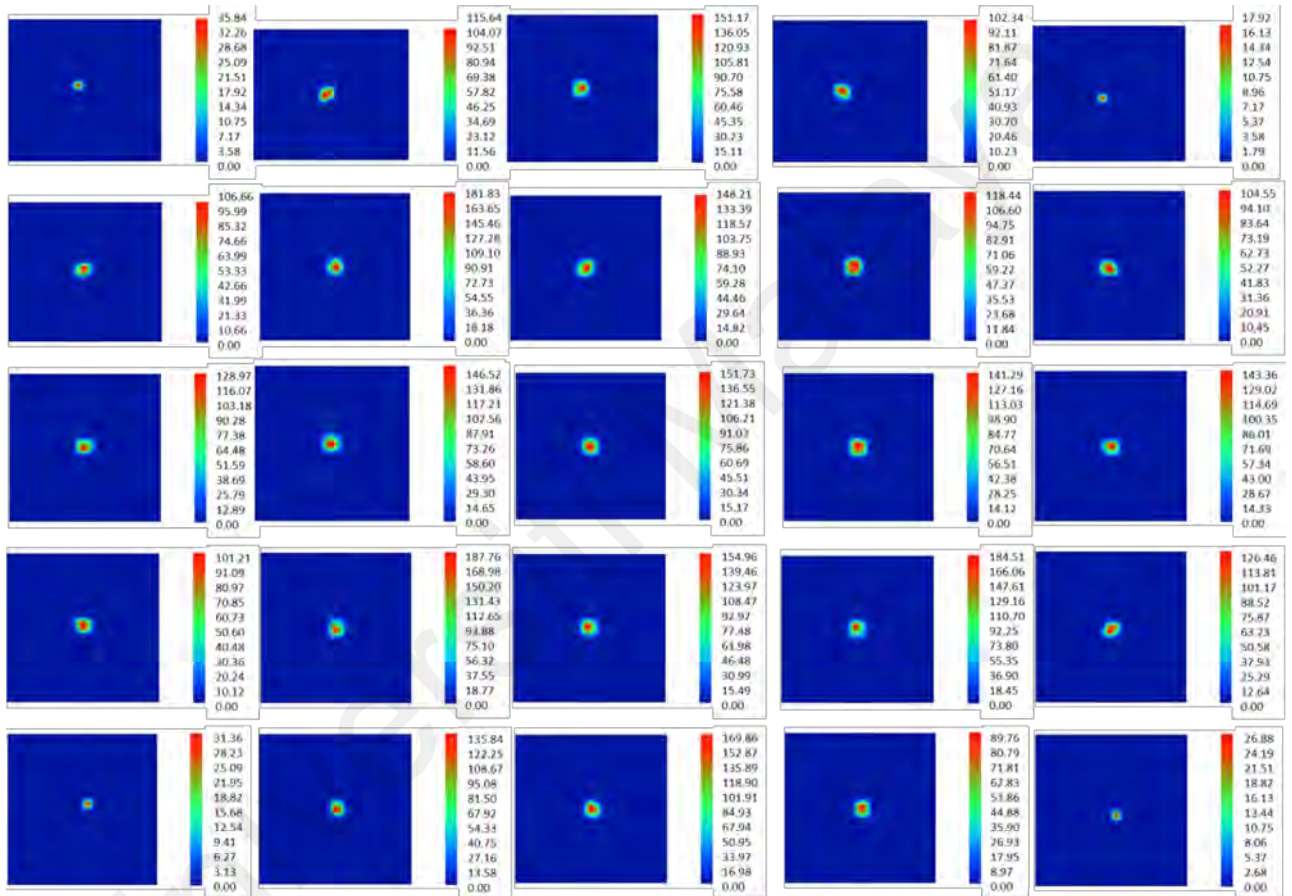
Figure4-20 : Distribution of radiant intensity for CTPCs according to their position in coupler B.

M. Tian et al. studied on a CPC coupler for a CPVTD system (Tian, Yu, Su, Zheng, & Riffat, 2018) . The maximum optical efficiency was 80%. Compared to a CPC coupler, the efficiency of a CTPC coupler with 25 CTPCs is 16% higher than that of a CPC coupler.

CHAPTER 5: RECTANGULAR GLASS OPTICAL FIBER

5.1 Introduction

Optical fibers have been used for transmitting sunlight in Daylighting systems. Glass optical fibers have advantages of higher transmission relative to polymer fibers. Considering the limitation of core diameter in glass optical fiber, the leakage of fiber at a specific angle of propagation increases with the length of glass optical fibers. The high loss of fiber leads to limitations in the number of floors that may use glass optical fiber for daylighting. Glass optical fiber with the rectangular cross-section "sometimes is named flat fiber" provides uniform rectangular beam shape and a top-hat profile at the output. In this paper, a mathematical model of the relative transmission of round optical fiber and a mathematical model of the relative transmission of rectangular optical fiber in different angles are compared. A specific design of rectangular glass optical fiber (RGOF) is presented for use in the receiver of the concentrator photovoltaic and daylighting (CPVD) system. The bundle of RGOF is compared with a bundle of round optical fiber. The RGOF and the bundle of RGOF are simulated using the raytracing method. The mathematical model and simulation of the designed RGOF demonstrate improvement in relative transmission of the designed RGOF and reduction in leakage of the optical fiber. The simulation result shows that a higher flux of sunlight transmits by the bundle of RGOF compare to a bundle of round optical fibers due to the higher coupling efficiency. The results of experiments on relative transmission in different angles for both round optical fiber and RGOF validate the results of simulation and mathematical models. The beam profile of a RGOF is presented. The fabricated RGOF is capable to be bent on a cylinder with a radius of 150mm and to be twisted 90° along with a length of 2.2 m.

In this chapter, we introduce flat fiber as a lighting transmission medium at the receiver of the CPVTD system. Conventional round optical fiber is compared with newly

proposed flat optical fiber as a lighting transmission medium from the concentrated sunlight to the array of solar cells.

This chapter consists of:

1. A brief review of round and flat optical fiber and the discussion of leakage in transmitting sunlight through optical fibers.

2. An analytical approach on leakage of optical the fiber during transmitting sunlight

3. A simulation of a flat fiber and round optical fiber with an equal area of the core under the same conditions.

4. A simulation of two bundles. A bundle of flat fibers and a bundle of round optical fibers. A bundle of 100 conventional round optical fibers with a core diameter of one millimeter each was simulated. The result was compared with the results obtained from a bundle of flat fibers having the same cross-sectional area.

5. we discuss the fabrication of flat fiber, the profile of flat fiber, and the test of flat fiber under a solar simulator.

6. Results of the tests on fabricated flat fiber with soda lime material as core of the fiber and low refractive polymer resin.

5.2 Analytical approach on leakage of optical fiber during transmitting sunlight

The efficiency of a fiber under the propagation of a full spectrum is different from the efficiency of the fiber under a collimated laser beam with a thin bandgap. Manufacturers of optical fibers provide information about the attenuation of fiber at specific wavelengths. However, it does not show the efficiency of the fiber while the source of light propagates a broad spectrum of light. The loss of a fiber with a specific attenuation

varies with the length of the fiber. The light is coupled with the fiber with an angle of 0°. We may consider a source of light beam bigger than the diameter of optical fiber. If the angle of propagation increases up to the acceptance angle, the loss is changed with the cosine of the incident angle. The loss of fiber under the propagation of a wide spectrum with an angle of incidence is less than expected loss. Feuermann measured the leakage of optical fiber under the propagation of a wide spectrum with different angles of propagation and different ratio of the length of fiber to the diameter of the core. For a fiber with a specific numerical aperture and specific angle of propagation, the ratio of the length of fiber to the diameter of the core directly affects the amount of leakage. Fig. 5-1 shows the result of measuring leakage of fiber with a fused silica core and numerical aperture of 0.44(Feuermann et al., 2002).
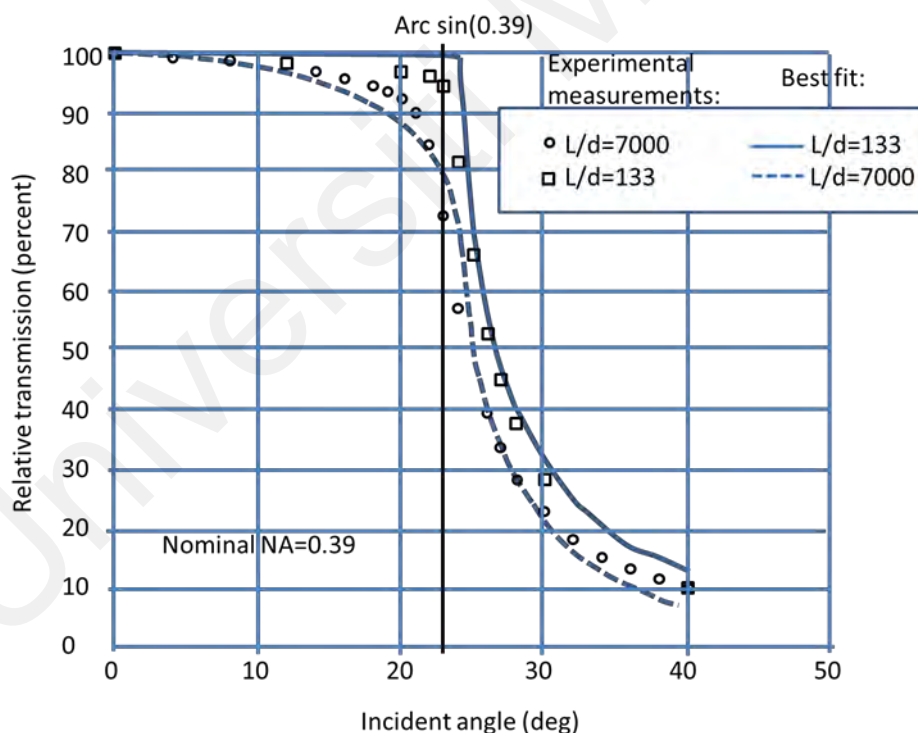
Figure 5-1: Measured angular response of optical fiber with fused silica core under propagation of a wide spectrum (quartz-halogen lamp).

The mechanism of leakage in transmitting of sunlight by optical fiber was studied, and it was found that the reflection of light between core and cladding is not perfect and the number of reflections of light determines the amount of leakage in fiber. The

concentration of sunlight leads to an increase in the angle between the rays of sunlight. The number of reflections increases in such a condition, and the effect of the very small loss due to reflection is noticeable. The number of reflections increases with adding the angle of incident and the ratio of length to the diameter of the fiber.

Although raytracing is a popular method, a mathematical analysis of loss is useful for understanding the behavior of fiber in various conditions and for assessing the accuracy of numerical methods. For mathematical analysis of loss due to the number of reflections between core and cladding, the fibers were exposed to the collimated light of a tilted source. This likely happens while the bundle of fibers is used in the receiver of a CPVD system. The rays have an angle with the axis of the fiber. Fig. 5-2 shows the setup of a collimated light with an angle of incidence relative to the fiber. The average number of reflections for all rays is a variation that affects the relative transmission and determines the loss of the fiber due to the angle of incident.
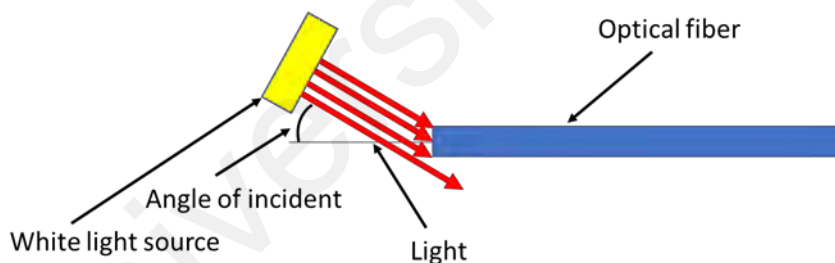
Figure 5-2: setup of the tests for both round and flat fibers with rotating source

Fig. 5-3 (a) shows that the azimuth angle of the rays is 90º and rays skew along the length of the fiber. Fig. 5-3 (b) shows the rays in the rectangular fiber. The rays in round optical fiber skew around the axis of fiber but in rectangular fiber, the rays move in a zigzag form. Fig. 5-3 (c) shows the relation between 2x, dL, θ, and θ_d in a round optical fiber.
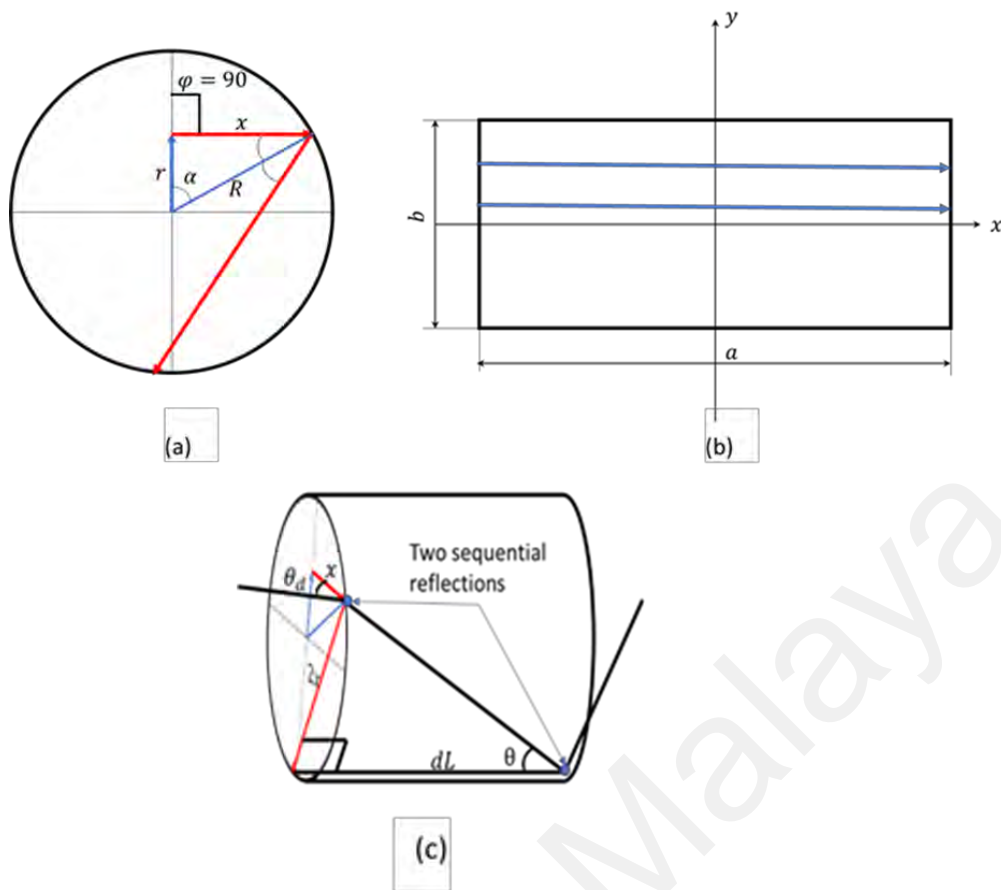
Figure 5-3: (a) incident angle of the ray trajectory direction relative to the plane normal to the round optical fiber's axis; (b) incident angle of the ray trajectory direction relative to the plane normal to the rectangular fiber's axis; (c) trajectory direction relative to the plane to the round optical fiber's axis between two sequential reflections

For the setup of Fig.5-2and based on Fig 5-3(a), in round optical fiber we have

$$\sin \alpha = \frac{x}{R} \qquad (5.1)$$

$$\tan \theta = \frac{2x}{dL} \qquad (5.2)$$

2x is the distance between two sequential reflections in the plane normal to the round optical fiber's axis. Where R is the radius of fiber and dL is the distance between two sequential reflections in the plane including a line parallel to the axis of optical fiber and 2x. θ is the angle between dL and trajectory onto the plane through the dL including 2x.

$$N_i = \frac{L \tan \theta}{d \sin \alpha} \tag{5.3}$$

Where Ni is the number of reflections for a ray in the length of fiber, L is length of optical fiber, d is diameter of the fiber. The total number of reflections of all rays is

$$N_t = \int_0^{N_{max}} N_i = \frac{L}{d} \int_0^{\theta_d} \int_{\alpha_{min}}^{\frac{\pi}{2}} \int_0^R \int_0^{2\pi} \frac{\tan \theta}{\sin \alpha} d_\theta d_\alpha r d_r d_\omega \tag{5.4}$$

where r and ω represent the polar coordinate of interface of fiber

$$N_t = \frac{L \times \pi d}{4} \ln|\cos \theta_d| \times \ln \left| \tan \frac{\alpha_{min}}{2} \right| \tag{5.5}$$

Considering uniform distribution of rays on surface of the interface of fiber we have

$$N_{av} = \frac{L}{d} \ln|\cos \theta_d| \times \ln \left| \tan \frac{\alpha_{min}}{2} \right| \tag{5.6}$$

Where N_{av} is the average number of reflections for all rays. The angle of α min corresponds to the rays with the highest reflection and the lowest acceptable energy. We may consider that rays with a lower angle than α min are ignored. If the diameter of the propagated light is bigger than the diameter of optical fiber then the power of incident light is proportional to the cosine of incident angle. We have

$$\frac{\tau}{\tau_0} = \cos \theta_d \, R_{av}^{N_{av}} \tag{5.7}$$

Where R_{av} is arithmetic average of reflectivity and θ_d is angle of incident relative to axis of optical fiber (Fig. 5.3). τ_0 is transmission of optical fiber at angle 0 degree.

In flat fiber, we do not have skew rays. The direction of rectangular fiber to the propagated light determines zigzag transmitting of light direction. Fig.5-4 (a) shows the effect of the zigzag direction on the number of reflections. Fig. 5-4 (b) shows the relation between the length of rectangle b, dL, and θ in a rectangular optical fiber. Fig. 5-4 (c) shows the

relation between the width of rectangle a, dL, and θ in a rectangular optical fiber. Considering the independent reflections in both sides of rectangle fiber, zigzag movement of the rays, and constant angle of reflection in each trajectory, we analyze rectangular fiber in two dimensions of the rectangle. The average number of reflections on each side should be calculated separately. we have

$$\tan \theta = \frac{b}{dL} \tag{5.8}$$

$$N_i = \frac{L \tan \theta}{a} \tag{5.9}$$

Where a and b are length and width of rectangle.

$$N_t = \frac{L}{a} \tan \theta \int_0^a \int_0^b d_x d_y \tag{5.10}$$

Where dx and dy represent the Cartesian coordinate of interface of fiber

$$N_{av} = \frac{L \tan \theta}{a} \tag{5.11}$$

For another side we have

$$N_t = \text{La} \tan \theta \tag{5.12}$$

$$N_{av} = \frac{L \tan \theta}{b} \tag{5.13}$$

If the diameter of the propagated light is bigger than the wide of rectangle in fiber then the power of incident light is proportional to cosine of incident angle. For one side the relative transmission is

$$\frac{\tau}{\tau_0} = \cos \theta_d \, R_{av}^{\frac{L}{a} \tan \theta_d} \tag{5.14}$$

For another side, the relative transmission is

$$\frac{\tau}{\tau_0} = \cos\theta_d \, R_{av}^{\frac{L}{b}\tan\theta_d} \qquad\qquad (5.15)$$

The direction of rectangular fiber to the propagated light determines zigzag transmitting of light direction. Fig. 5-4 shows the direction of zigzag affects the number of reflections.
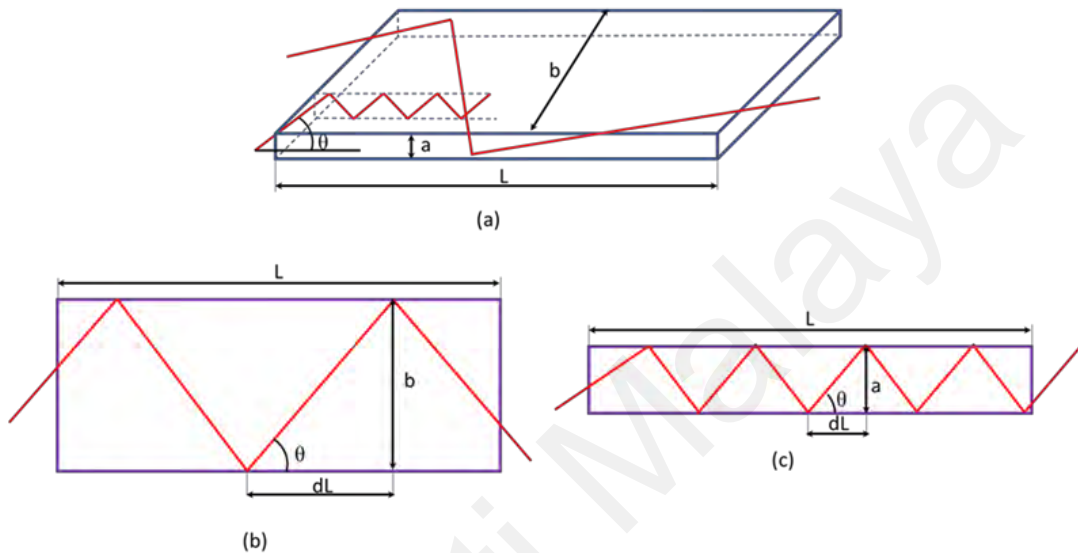
Figure 5-4: (a) incident angle of the ray trajectory directions relative to the plane parallel to the rectangular fiber's axis; (b) trajectory direction relative to the optical fiber's axis parallel to one side of fiber with three sequential reflections; (c) trajectory direction relative to the optical fiber's axis parallel to other side of fiber with several sequential reflections

The designed RGOF is a glass optical fiber with a rectangular shape of core and polymer clad, the ratio of length to width of the rectangle in fiber is more than 5. The width of the rectangle is limited to prevent break-in bending. As an instance, the fabricated RGOF has a thickness of 0.4mm and a minimum bending radius of 150mm.

If the diameter of the propagated light is big enough to cover the surface of the optical fiber and the length of fiber to be short, the cosine of incident angle plays an important role. Fig. 5-5 shows the loss of 100mm length of the round fiber and rectangular fibers. The diameter of the light is big enough and the cosine of the angle of the incident should

be considered. The ratio of the length of the rectangle to the diameter of round fiber affects the relative transmission of rectangular fiber. The effect of loss due to the number of reflections between core and clad is very low and the trends of optical fibers are near to each other and near to cosine of incident angle.

Fig.5-6 shows the relative transmission of fibers with a length of 10000mm. The rectangular fiber with a length of rectangle 10 times of round fiber has lower loss due to the number of reflections between core and clad and shows higher relative transmission than other fibers. The zigzag movement is in a longer trajectory (Fig.5-4). In this figure, the cosine curve indicates a decrease in light intensity without considering the leakage and simply due to the change in the angle of the light source relative to the fiber optic axis.

Figure 5-5: Comparison between round fiber and rectangular fibers. The length of fibers is 100mm and the light covers surface of the fibers. $R_{av} = 0.9999$

If the diameter of the light to be equal to the diameter of the round fiber, a rectangular fiber with the length of rectangle 10 times the diameter of round fiber shows higher relative transmission compare to round fiber. Fig.5.7 shows the relative transmission of a round and a rectangular fiber. The diameter of the round fiber is one millimeter and the length of the rectangle of rectangular fiber is 10mm. the length of both fibers is 10000mm.

The difference between the relative transmission of two fibers increases when the source is more tilted relative to the axis of the fiber.
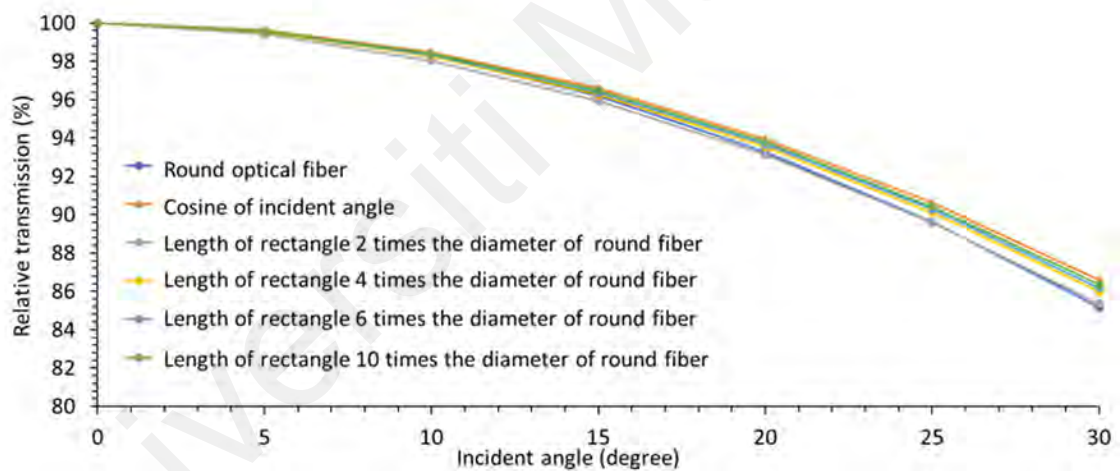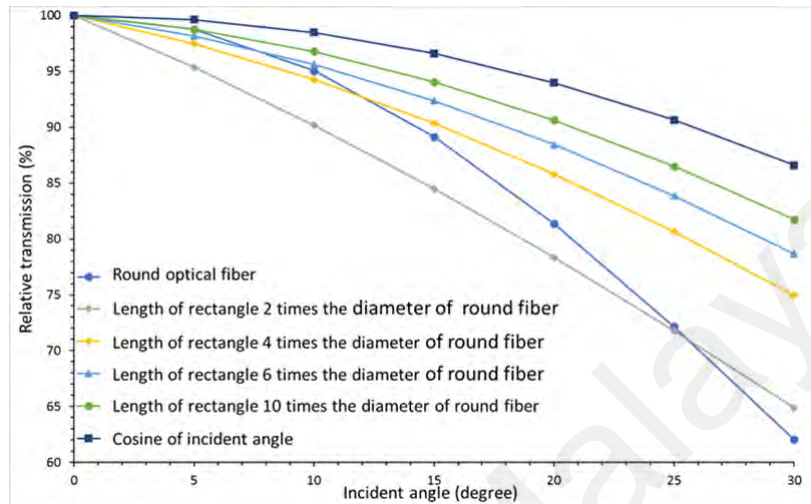

Figure 5-6: Comparison between round fiber and rectangular fibers. The length of fibers is 10000mm and light covers the surface of the fibers. Rav =0.9999
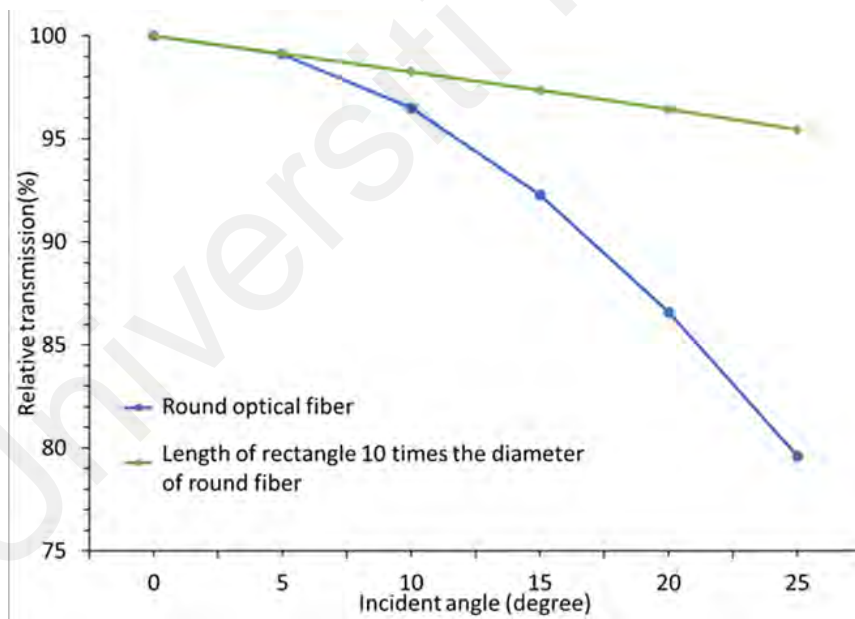

Figure 5-7: Comparison between round fiber and rectangular fibers based on calculation. The length of fibers is 10000mm and diameter of light is smaller than diameter of round fiber. Rav =0.9999

5.3 simulation of a RGOF and comparison with a round optical fiber

The raytracing method is used to simulate the response of flat fiber and conventional round fiber with a fused silica core and low refractive index resin clad to a tilted source of light. For both cases of flat fiber and conventional round fiber, the flux, relative transmission, and the loss of the light were investigated at different incident angles, i.e., 0° to 30°, relative to the axis of the fiber.

Fig.5-8 represent the source file of the model in the background (colored) and the normal solar irradiance of a reference spectrum at standard air mass 1.5 AMd (black and white color). The source file is generated by a black body at a temperature of 5780° K and wavelengths from 400nm to 1600nm. The source has a 2mm diameter and is located with a space of 50 mm from the entrance of the optical fiber. The source file includes 81wavelengths and has reasonable compatibility with the direct normal solar irradiance of a reference spectrum at standard air mass 1.5 AMd that is generated via SMARTS V-2.9.2. ASTM standardizes under the designation G173-03 (2012).

The source with the wavelength range of 400 nm-1600nm contains a significant part of solar irradiance that is used in high concentrator photovoltaic and daylighting systems. Glass optical fibers with fused silica core have a high transmission coefficient in this range.

Fig. 5-9 (a) shows the layout diagram of round optical fiber and Fig. 5-9 (b) shows the layout diagram of RGOF in the simulation. Table 5-1 shows the input data in the simulation for both round optical fiber and RGOF.

The layout of the simulation shows that flat fiber does not have skew rays. The result of the simulation shows that the leakage of round fiber for angles 0°-20° was more than RGOF. Fig. 5-10 shows that for angles 0°-10°, the relative transmission in round fiber is 3% less than RGOF and for angles between 10°- 20° the difference of the relative transmission between the round optical fiber and RGOF increases up to 17% at 20°.

Considering NA=0.39 for the fiber, we may conclude that for an angle less than half of

the acceptance angle round optical fiber shows as low angular loss as a RGOF.
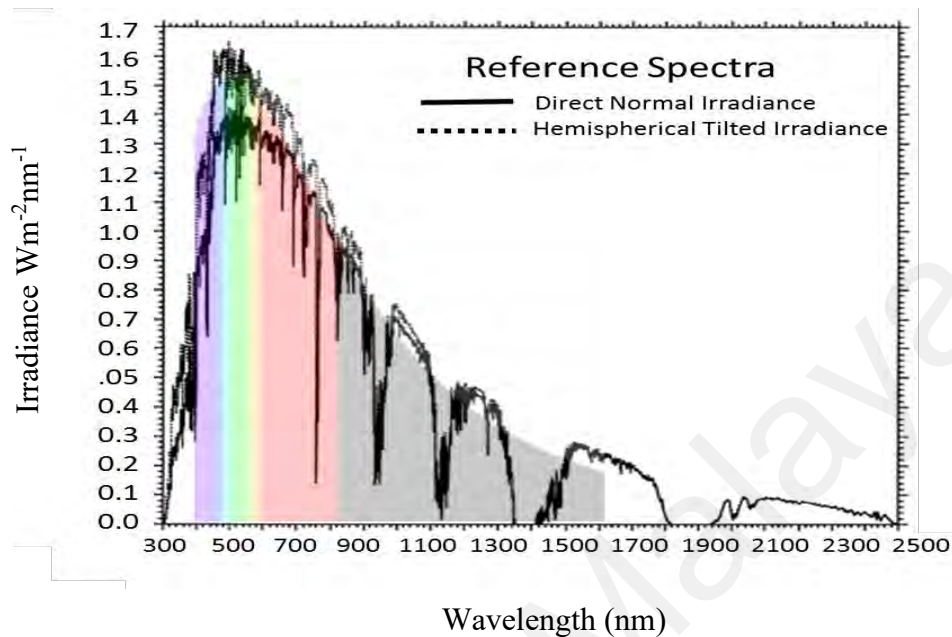
Figure 5-8: comparison between reference terrestrial solar irradiance spectrum (black and white) derived from standard ASTM G173 - 03(2012) and source file model used in simulation-based on 5780º K blackbody from 400-1600nm
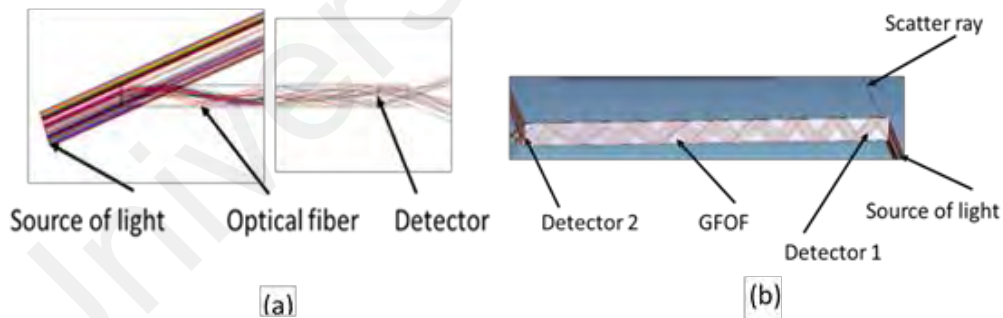
Figure 5-9: (a) layout diagram in simulation of round optical fiber; (b) layout diagram in simulation of RGOF

Table 5-1: input data in simulation for both round optical fiber and RGOF

	In real test	In simulation
Refractive index of core	1.458	1.458
NA	0.37	0.37
Diameter of core	1	1
Diameter of fiber with clad	1.1	1.1
length	1780	1780
Considering Fresnel lens effect	No	No
Buffer diameter	1.4	Without buffer
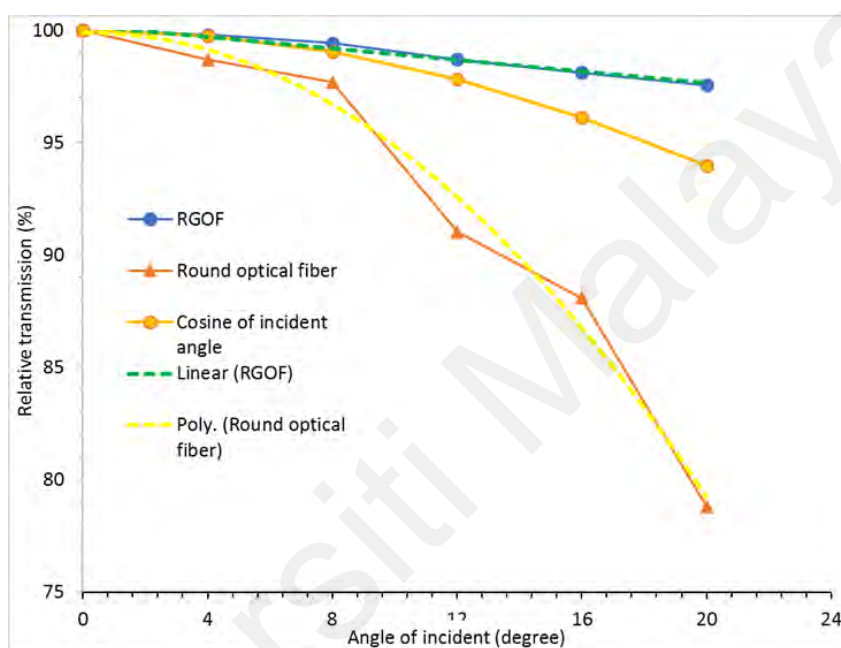
Figure 5-10: simulation of RGOF and round optical fiber with 1000 mm length.

The distribution of light was investigated for both round optical fiber and RGOF. Fig. 5-11 and Fig. 5-12 show the angular response and distribution of round optical fibers and RGOF at the endpoint in angles 0º-25º. The maximum angle of the source with reasonable intensity and uniform output of round optical fiber occurred in 10º that is less than half of the critical angle. Based on the results of the simulation, collimating the light before transmitting the light by optical fibers increases the relative transmissions in angles 0° to 20° significantly.

For angles 0-20, the intensity of light in RGOF was higher than round optical fiber. In angle 25º, the intensity of light dropped dramatically to near zero while in round optical fiber, the skew rays caused a maximum intensity of 4 watts/ steradian. However, the amount of intensity is not considerable.
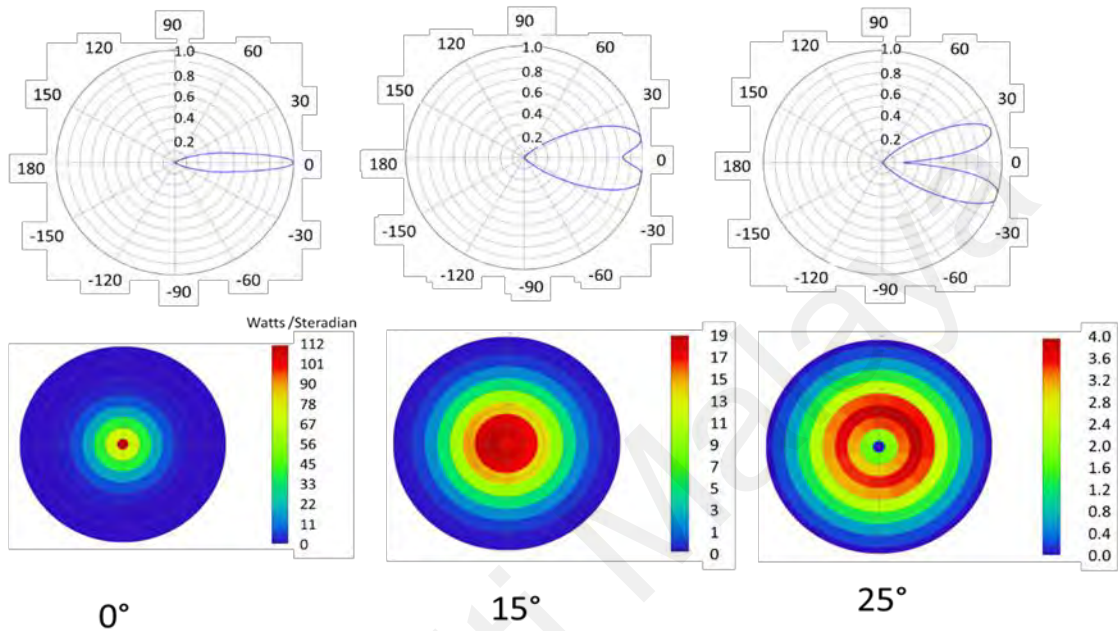
Figure 5-11: the radial intensity of round optical fiber with different angle of a big source. The diameter of source is 2 mm.
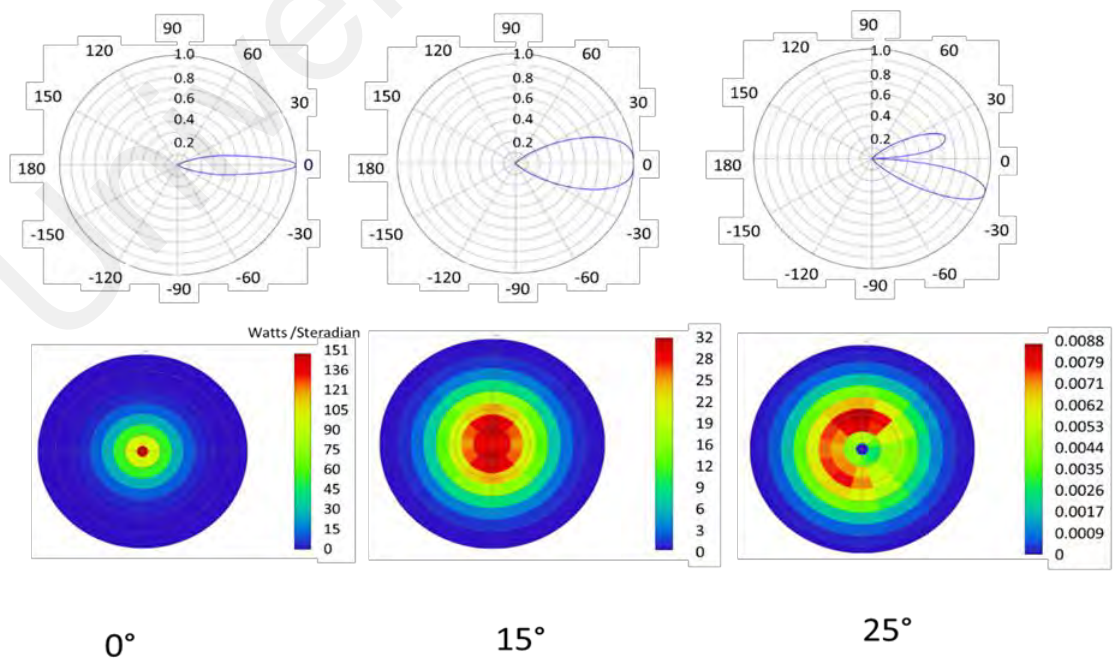
Figure 5-12: the radial intensity of RGOF with different angle of a big source. The diameter of source is 2 mm.

5.4 investigation the effect of gaps in bundle of RGOFs and bundle of round optical fibers

In this section, we assessed the performance of RGOF's bundle and compared it with a bundle of round optical fiber in the same conditions. A bundle of fibers is usually implemented in transmitting a high flux of sunlight. Loss in coupling sunlight to the bundle of optical fibers is considerable. The gap between the fibers in a bundle wastes the energy of sunlight. At the end of the fibers in a bundle, the lack of geometrical matching between a bundle of fibers and a solar cell may cause significant loss in the process of coupling and transmitting sunlight through optical fibers in the receiver of a CPVD.

A bundle of round optical fibers and a bundle of RGOF have been investigated. Raytracing of light rays in the RGOF and conventional round fiber were conducted using Zemax software. The core materials of both fibers were fused silica with a refractive index of 1.458464 at the D-line. The cladding materials of both cases were resin XPC-373 AP clad with a low refractive index of 1.387939 at 852nm. For both cases of RGOF and conventional round fiber, the propagation of light rays was investigated at 0° relative to the central line of the optical fiber. A 1watt light source with wavelengths ranging from 400 nm to 1600 nm based on blackbody radiation at the temperature of 5780 K was applied to illuminate the bundles of optical fibers. The maximum divergence of the light source was 0.27º.

The active area of the photo-detector was square (12 mm × 12 mm) and the thickness of cladding was 25 μm. The area of the bundle of RGOF was 101.6064mm2, and the area of the bundle of round optical fiber was 101.9172 mm2, and the difference between the area of both bundles was 0.3% that is negligible. The power transmission and distribution of light intensity and flux of light were investigated in both cases. Fig. 5-13 shows a row

of 15 units of RGOF with a cross-sectional area of 10.08 mm x 0.67 mm each to form a square bundle of 10.08 mm x 10.08 mm. The light is well mapped with the square shape of the photo-detector in both directions of X and Y. For both cases, we applied the same testing conditions, i.e., light source, photo-detector, length of fibers, material, and cross-sectional area of both bundles. Fig. 5-14(a) shows images of the flux on the surface of the photo-detector for both cases and Fig. 5-14 (b) shows the intensity distribution in X and Y directions. A comparison between the flux distributions in both cases reveals that the transmitted light rays via flat fibers are more uniform than that of round optical fibers.

Bundle of round optical fibers   Bundle of flat optical fibers
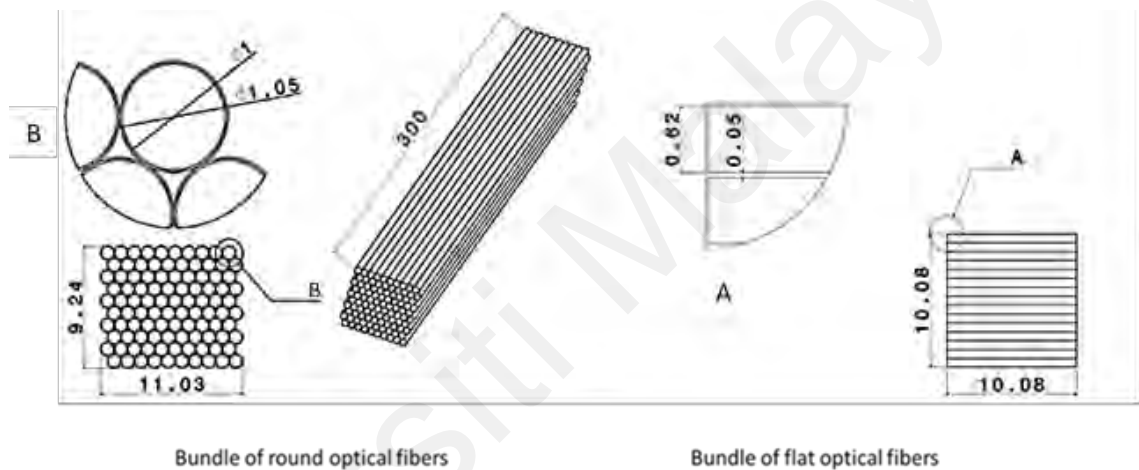
Figure 5-13: Dimensions of a bundle of flat fibers and a bundle of round optical fibers

Fig. 5-15 shows the total powers for both bundles of RGOF and round optical fibers for lengths between 50 mm and 300 mm. The result shows that a bundle of RGOF fibers transmits more power as compared to that bundle of round optical fibers because of lower loss at the entrance of the optical fibers. The area of the cores in the bundle of RGOF is 93.279 mm2 and the area of the cores in the bundle of round optical fibers is 78.539 mm2.
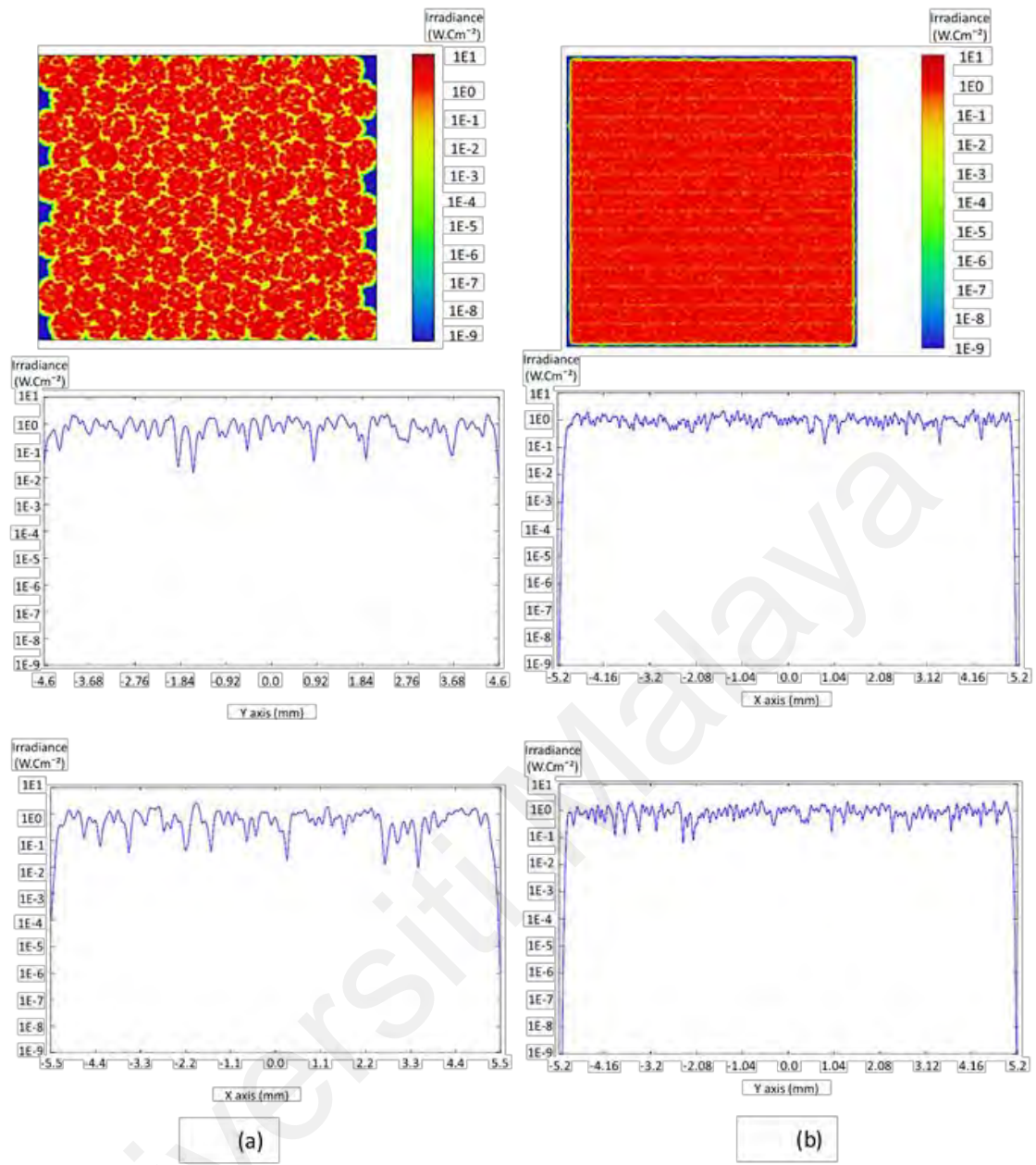
Figure 5-14: (a) incident flux and intensity distribution in bundle of round fibers in X axis and Y axis; (b) incident flux and intensity distribution in bundle of RGOF fibers in X axis and Y axis
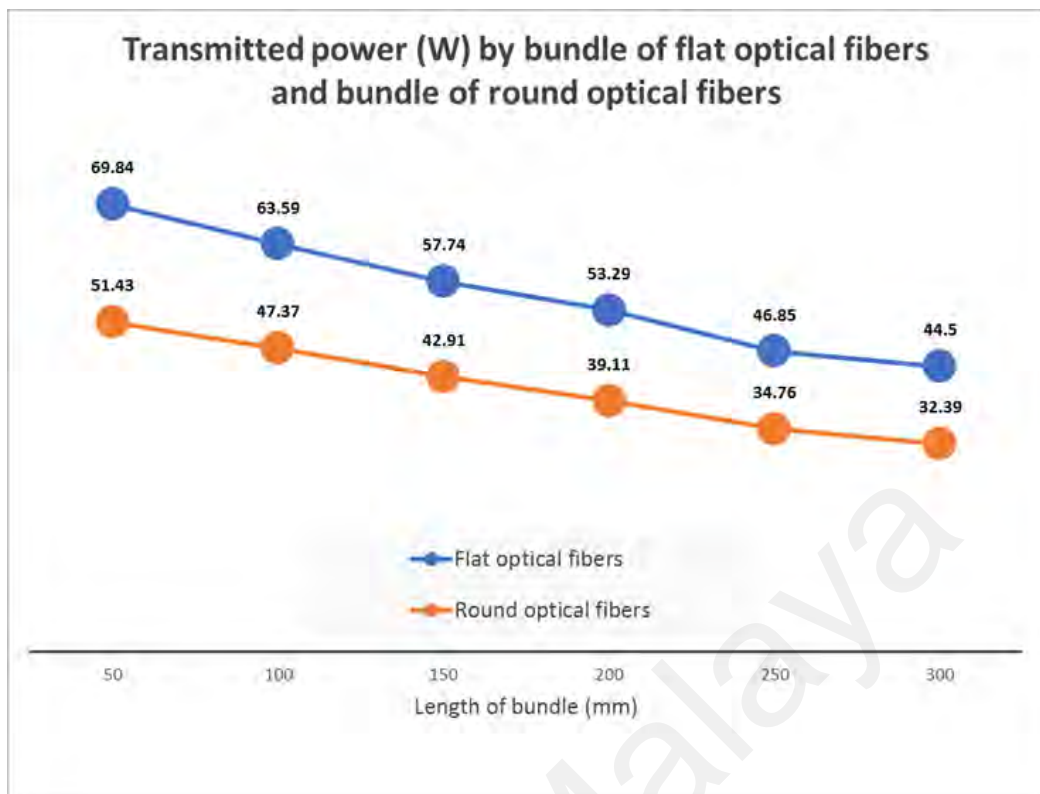
Figure 5-15: comparison between power transmission by bundle of flat fibers and bundle of round fibers

5.5 Experimental investigation of a round optical fiber and a RGOF

The profile of the beam, relative transmission of RGOF for angles between 0° to 25° and collimated white light, focused white light and the laser beam is investigated experimentally. A supercontinuum white-light laser of NKT Photonics Company was implemented as a source, and a beam profiler of Thorlab Company was employed for detecting the profile of the beam. Two samples of RGOF were fabricated. The material of the core of one sample was fused silica and another one was borosilicate 3.3 and the material of cladding was XPC 373 low refractive index polymer and Teflon respectively. Table 5-2 shows the characterizations of the supercontinuum laser.

Table 5-2: characterization of super continuum laser

Spectral coverage (nm)	500-2000
Total power(mW)	200
Total visible power (mW)	40
polarization	unpolarized
Spot size (mm)	1
Output	collimated

Fig. 5-16 shows the experimental setup of the system. The light source propagates the light to one end side of the RGOF, and another end side of the RGOF fiber is positioned in front of the beam profiler.

Fig. 5-17 (a) shows the results of the measured beam profile on the Y-axis. The intensity of light was distributed across the surface of RGOF. The maximum intensity occurred at the center of the fiber. Intensity distributed from zero to 1000 μm along Y-axis. The amplitude of the peak point was 60% of the maximum intensity set in the beam profiler. Fig. 5-17 (b) shows the measurement of the beam profiler along the X-axis.
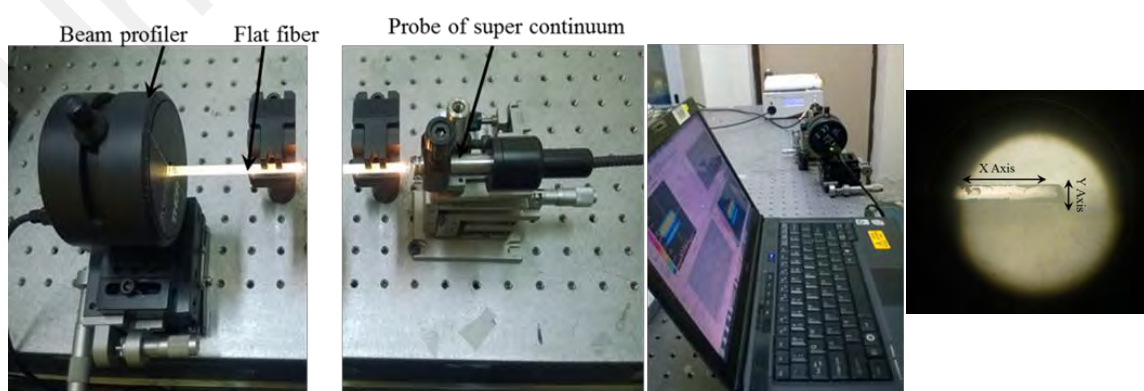
Figure 5-16: Setup of measuring beam profile and the photo of cross section of flat fiber
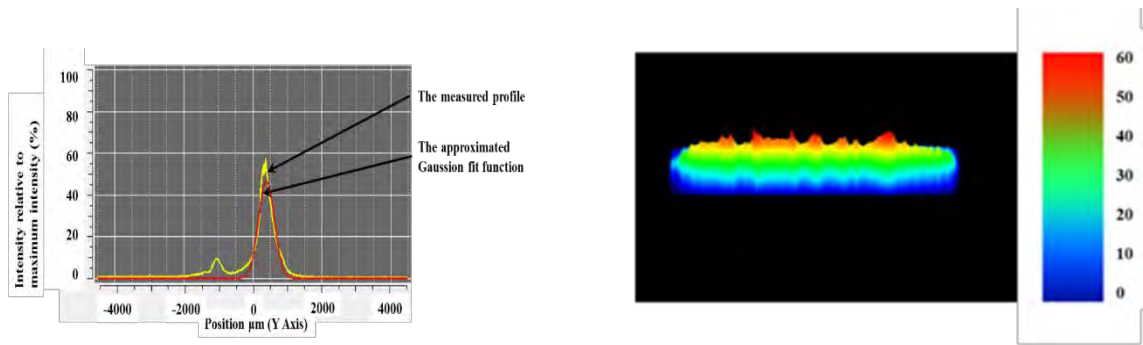
(a)
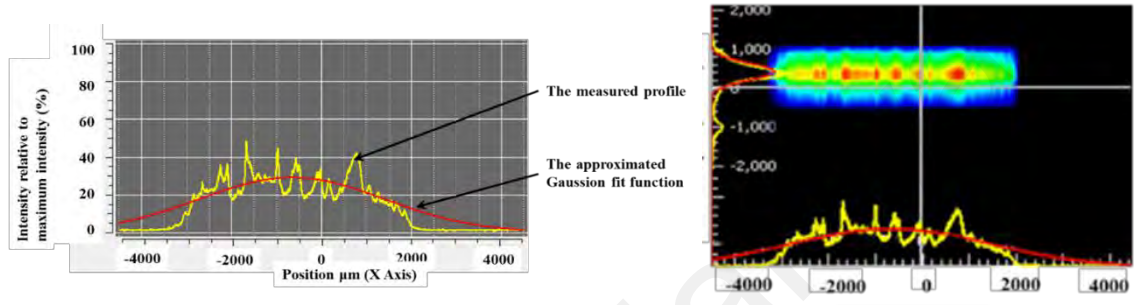
(b)

Figure 5-17: Profiles of the beam of flat fiber in 2-D and amplitude of the intensity in (a) Y-axis and; (b) X-axis.

Relative transmission of RGOF in angles between 0° to 20° was investigated under the propagation of white light of a xenon lamp. Fig. 5-18 (a) shows the setup of the test with a xenon lamp and Fig. 5-18 (b) shows the spectrum of xenon lamp in the test.
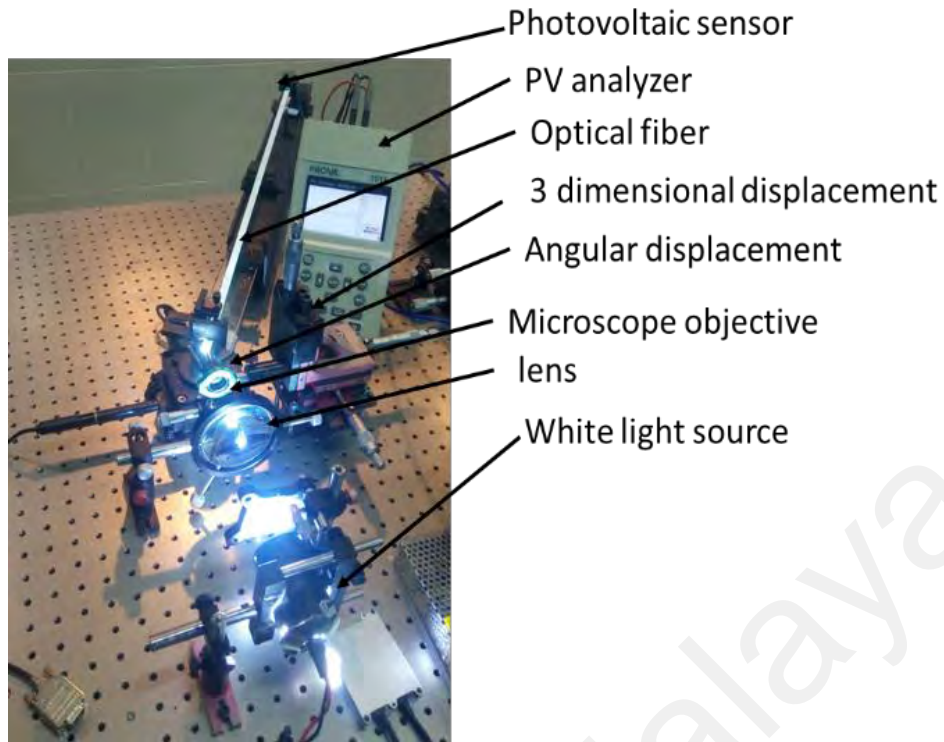
(a)
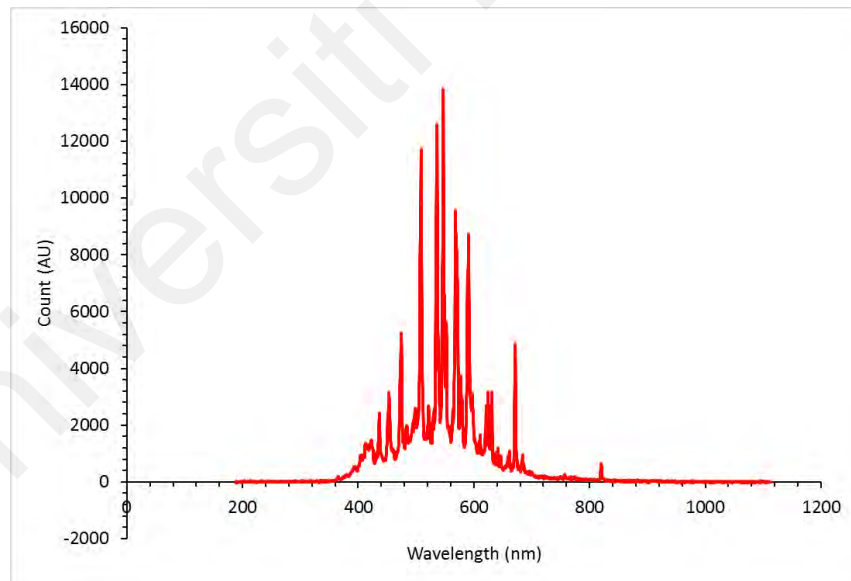
(b)

Figure 5-18: **(a) the setup of the test with xenon lamp; and (b) spectrum of xenon lamp that is extracted by ocean 2002 spectrometer.**

A 740 mm RGOF with dimensions 10mm×0.4mm and a 740 mm round optical fiber

with 1mm diameter were fabricated and used for investigating the relative transmission

of RGOF to angular propagation of focused light. Table 5-3 shows the conditions of the test.

Table 5-3: dimensions of RGOF and round optical fiber and conditions of the test

	RGOF	Round optical fiber
Length of optical fiber	740 mm	740 mm
Dimensions of core	Rectangle: 10mm×0.5mm	Diameter 1mm
Diameter of focused light	1.5mm	1.5mm
Sensor	PV cell	PV cell
Measuring device	PV system analyzer (Prova 1011)	PV system analyzer (Prova 1011)
Light source	Xenon lamp H3 35W 6000 K	Xenon lamp H3 35W 6000 K

Fig. 5-19 shows that round optical fiber follows the cosine of incident light while RGOF has a higher relative transmission. The rectangle cross-section of RGOF has a 10mm length that makes it suitable for a focused light that has a diameter less than 2mm. The result may be used in harnessing the light around the solar cells in the receiver of a CPVD. The light at the middle of the focal plane is uniform enough for multi-junction solar cells and the light around the cells may be transmitted by bundles of RGOF.
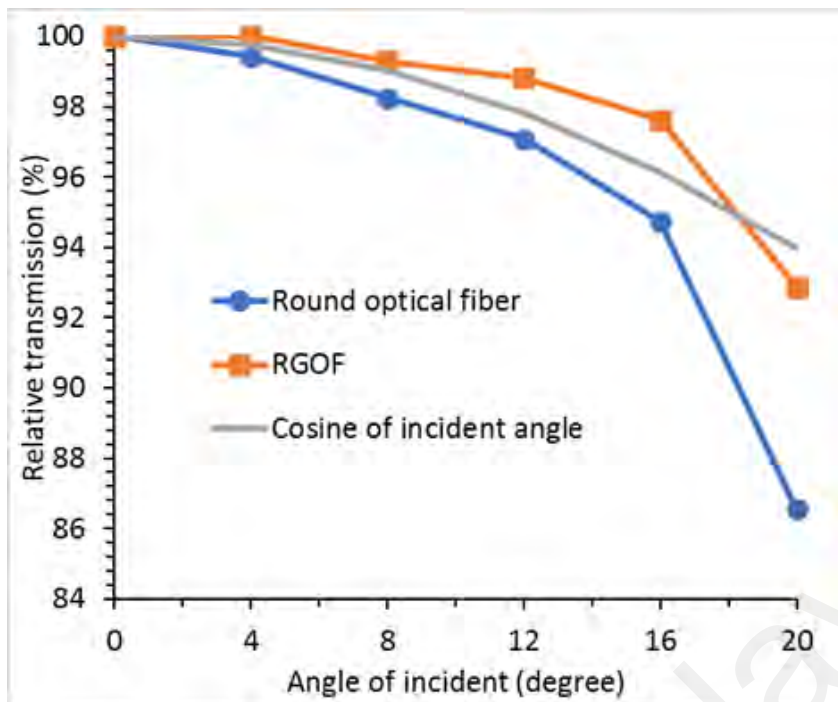
Figure 5-19: comparison between relative transmission of RGOF and round optical fiber in different angles and under propagation of a focused light

The RGOF was examined for its bending. The fabricated fiber has just a polymer as clad. Fig.5-20 demonstrates the bending and twisting of RGOF. The fabricated fiber bent on a cylinder with 350 mm diameter and twisted 90° along its longitude axis with a length of 2.2m. The minimum radius of bending for fabricated RGOF was 150 mm with dimensions 10mm×0.4mm. Low radius may be achieved by an additional coating process.

Figure 5-20: flexibility of flat fiber in bending and twisting

5.6 Design, and fabrication RGOF

Designing an optical fiber must satisfy some criteria for transmitting sunlight through fiber optics. The criteria include power loss per unit meter the length of fiber, geometrical matching with a light source and target, bendability, and uniformity of the light flux distribution in the target plane.

Except for attenuation in optical fiber, power loss in a specified optical fiber for transmitting sunlight may be caused by the coupling sunlight into the tip of the fiber, the gaps between fibers in a bundle, and leakage due to the wide spectrum of sunlight.

Besides, the cost of the fiber is a key factor to be considered. For reducing the fabrication cost of optical fibers, the operational time of the pulling tower machine per one meter of optical fiber excluding setup time and the raw material cost must be reduced.

Based on mentioned criteria I designed a flat fiber with a rectangular core and clad. The proposed advantages for designed fiber are:

1.   A larger cross-sectional area of fiber core can accommodate larger illumination area of light hence requires a smaller number of optical fibers in a bundle as compared to fibers with a smaller cross-sectional area of the core. Reducing the total length of fiber can reduce the operational time of pulling tower machines in mass production but a larger core size will reduce the flexibility of the glass fiber in which the fiber can break easily even light stress is applied on it especially during the bending process.

2.   flat fiber may provide excellent flexibility in one direction as well as allow the fiber to be twisted in a specific length.

3.   The long length of one side in flat fiber makes it suitable for coupling high flux of sunlight and transmitting optical power with lower leakage.

4.   Flat fibers with a larger cross-sectional area may simply reduce the gap spacing among fibers significantly when they are assembled into bundles of fibers.

5.   The rectangular shape of the bundle of flat fibers has the advantage to match well with the rectangular dimension of multi-junction solar cells with maximum packing factor.

We have fabricated the flat fiber from a rectangular preform directly and embraced it with a low refractive index polymer. Two main parameters in pulling tower are feed rate of the preform and the speed of pulling. In our experiment, the feed rate was 20mm/min and the speed of pulling was 0.75 m/min. The main problem in the fabrication process of flat fiber is fiber twisting during the pulling process and alignment of the fiber in the coating process. A simple mechanism was designed and fabricated to prevent fiber

from twisting. Fig. 5-21 shows the CAD model of the designed component and fabricated component in assembly with the cup of resin. Figs. 5-22 (a), (b), and (c) show the pictures of the rectangular preform that was used for fabricating flat fiber, a bundle of flat fiber, and the preform in pulling tower. Fig. 5-23 shows how the RGOF was pulled down from the furnace and rolled on the drum.
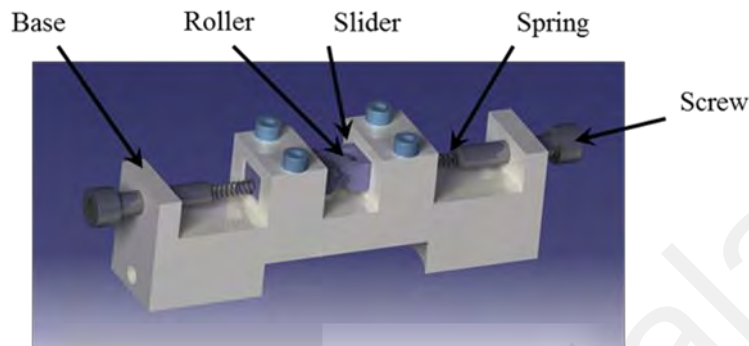
Figure 5-21: CAD model of the mechanism to prevent twisting flat fiber during coating process
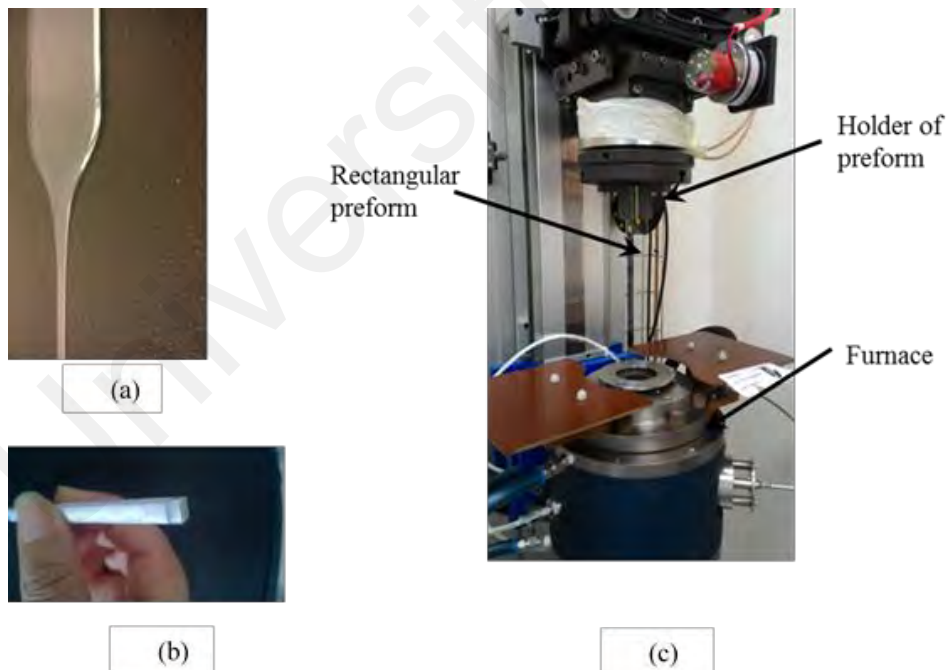
Figure 5-22: (a) Rectangular preform, (b)arrangement of flat fibers to form a bundle of flat fibers and(c) position of preform in pulling tower.
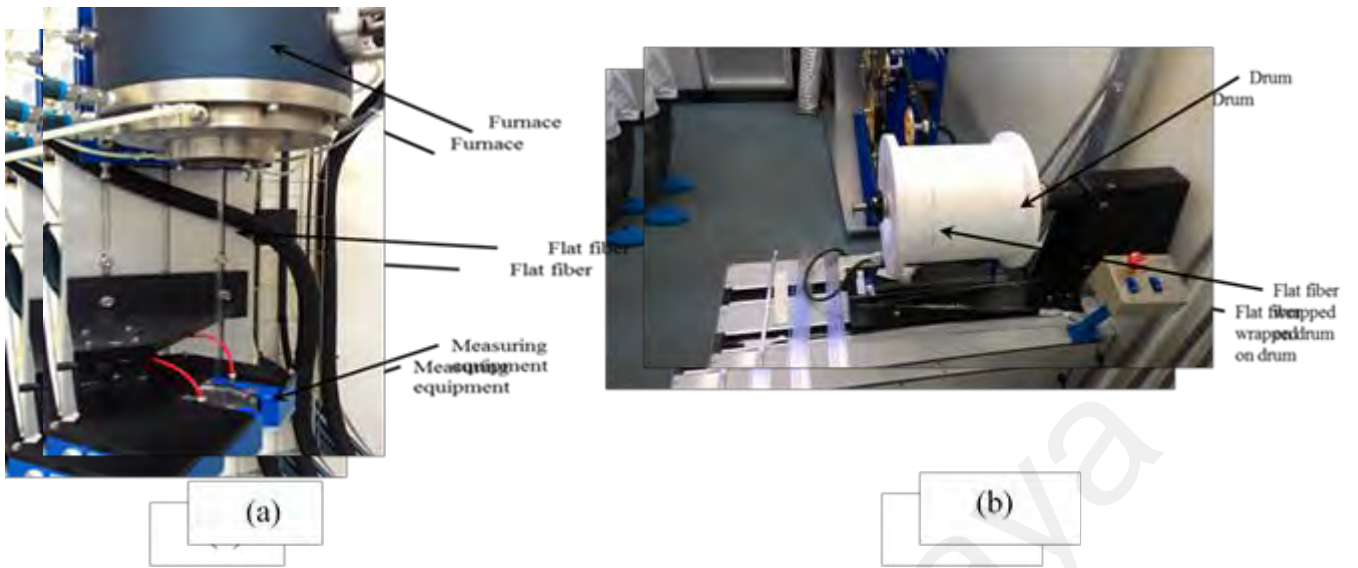
Figure 5-23: (a) flat fiber after pulling out from furnace, and (b) rolling of flat fiber on drum after pulling process

CHAPTER 6: DESIGNING CPVTD RECEIVER

6.1 Introduction

In this chapter, we discuss following issues:

1. TRIZ method for generating concepts of receiver

2. Design and fabrication of a receiver for CPVTD

3. Test of receiver

6.2 TRIZ method for generating concepts of receiver

A stationary PV module system is the simplest system that includes a PV module, inverter, cable, and control system. PV module system is a power system designed to convert usable solar energy to electricity by means of photovoltaics. Both the desired objective (Electricity) and the component that cause the objective are named substance. Two substances interact through the field. Fig.6-1 shows the substance-field (Su-field) model of a simple stationary PV module system. The stationary PV system (substance 1) causes electric current (substance 2) through the function of converting the energy of photons to electricity. The interaction between the substances occurs in the photovoltaic field.
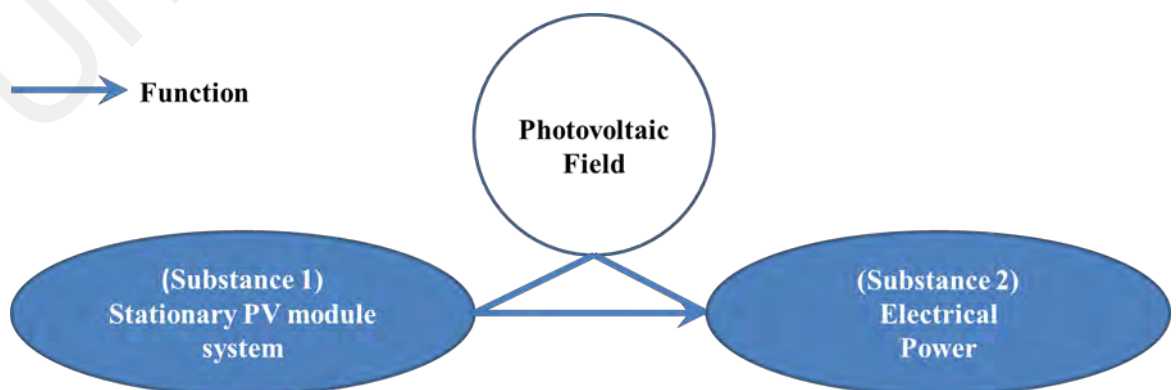
Figure 6-1: Su-field model of a stationary solar PV power system

A photovoltaic system with a concentrator and sun tracker system has a higher level of efficiency due to the tracking of the sun and the possibility of converting a wider band spectrum of solar energy to electricity. The mechanical and optical components affect the efficiency of the main useful function of the system. The functions of subsystems that improve directly the main useful function of the system are considered auxiliary functions.

A subsystem serves its main function in the auxiliary field, but the main useful function of the system is in the main field. The illustration of a CPV system is shown in Fig.6-2 whereas the mechanical and optical are auxiliary fields (red color circles) and are shown inside the main field of photovoltaics. However, the auxiliary fields impose more complexity and costs to the system. The heat generated by the facing solar cells to concentrated sunlight is a harmful function and is eliminated by a heat sink. So, heat energy is wasted in CPV system.
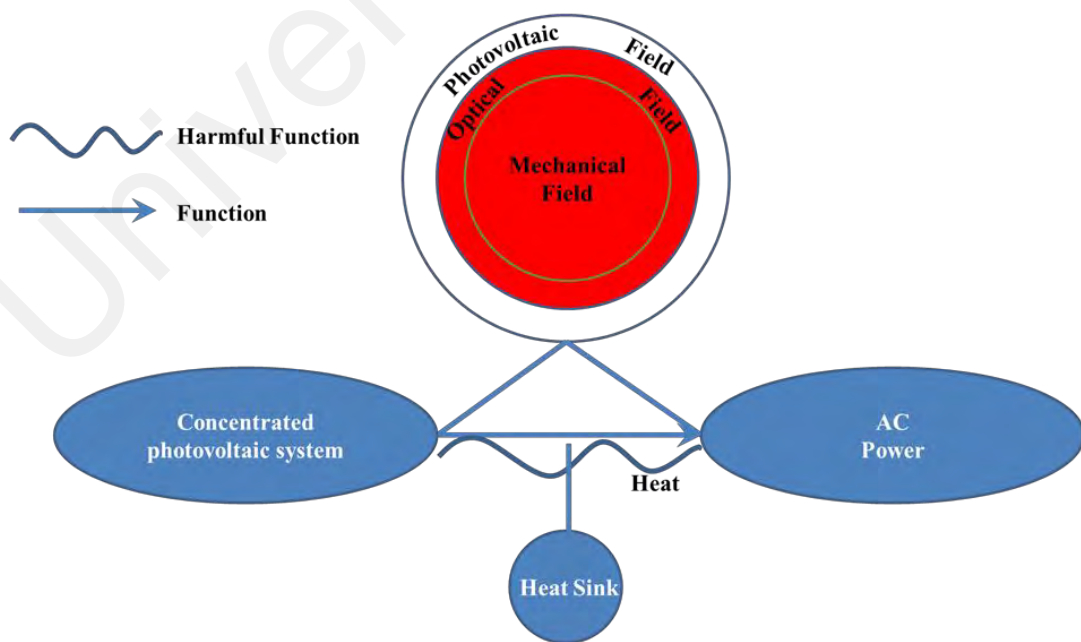
Figure 6-2: Su-field model of a solar CPV power system

For a CPVT system, we may have two different Su-field models. Fig 6-3 (a) shows a model that has two main fields that use concentrated light of optical components. In this model, the light is split and one part may be used for generating electricity and one part may be used for heating water. Fig. 5-3 (b) shows another concept extracted from the Su-field model. In this concept photovoltaic field is the main field for generating electricity and is an auxiliary for the thermal field. In this concept, all sunlight is used for generating electricity and wasted heat will be used for heating water. In the second concept, the photovoltaic components should tolerate higher temperatures if the temperature of the water should be high.

We have two distinct main fields, so each field implements the tools that are completely different. The functions of tracking the sun and concentrating sunlight are the functions of subsystems and account as the auxiliary fields that serve both main useful functions of the CPVT system.

Based on the Su-field model Adding a new main function entitled cold daylighting to CPVT is possible but the field of the lighting function adds to the main fields. Cold lighting is another main field that must be added to the main fields. The advantage of using auxiliary fields for various main functions improves efficiency in the cost of complexity.
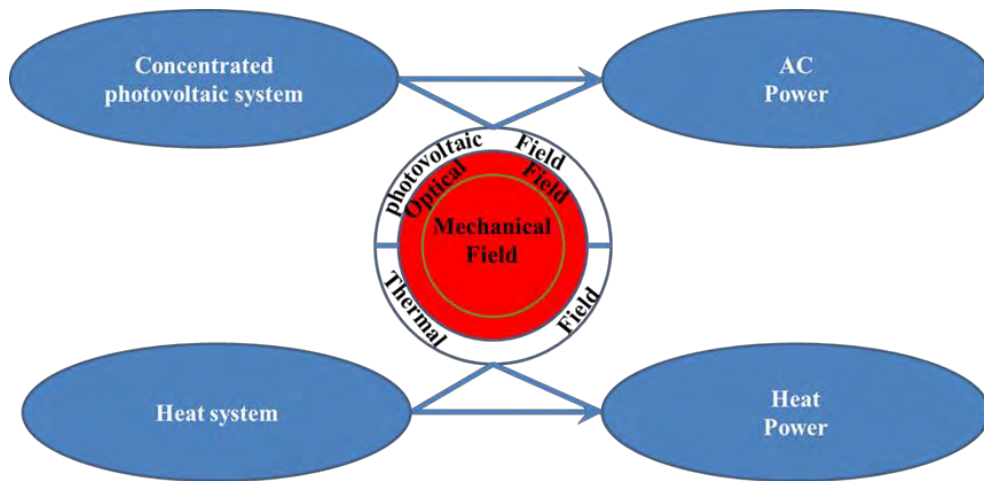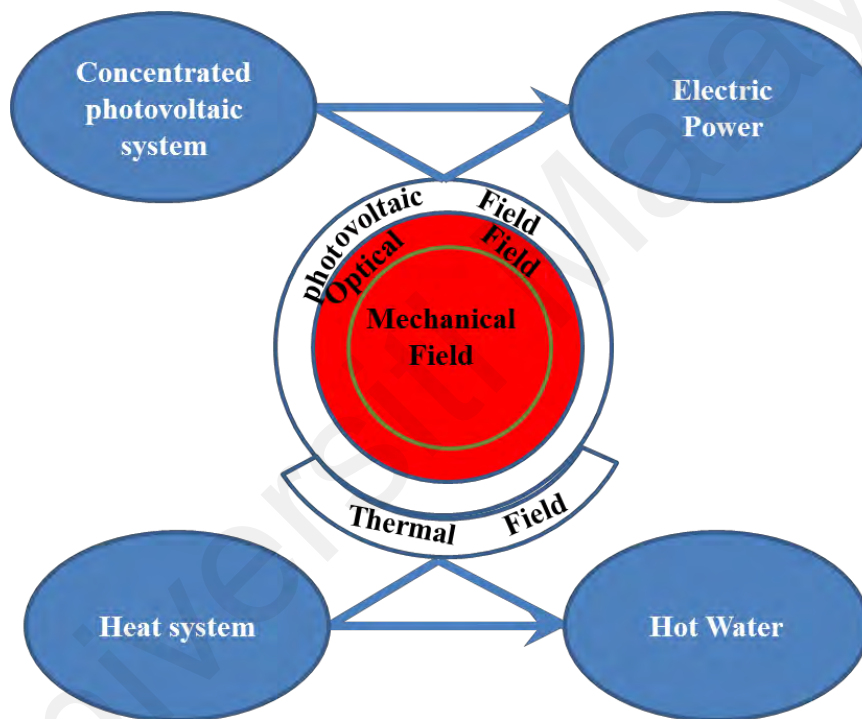
Figure 6-3: (a) Su-field model with separate main fields of thermal and photovoltaic; (b) photovoltaic field is auxiliary field for thermal field

Three concepts of CPVTD system entitled concept one, concept two and concept three are presented.

Concept one converts the energy of sunlight to heat, electricity, and cold separately from the optical field. Three components of PV cells, heat collector, and light coupler use concentrated sunlight directly from optical components. The light coupler is a medium that matches sunlight with optical fiber (Fig. 6-3 (a)).

Concept two uses the photonics field as an auxiliary field for photovoltaic and thermal. In the second concept, the photovoltaic field is auxiliary to the thermal field. In the second concept, concentrated sunlight is coupled to optical fiber then the light can be split by separating fibers. The waste heat of photovoltaic is used for heating water (Fig. 6-3 (b)).

Concept three uses a photovoltaic field as an auxiliary field. In concept three, the heat of the photovoltaic process is used for heating water (Fig. 6-3 (c)).

The third concept uses waste energy of converting sunlight to electricity by photovoltaic module. The module of photovoltaic can use a wide spectrum of sunlight for generating electricity. Sunlight can be split for use in both functions of generating electricity and cold light simply by separating optical fibers. The third concept uses optical fiber as a medium between optical component and the photovoltaic module. The third concept is chosen for designing the receiver.

6.3   Modeling a receiver for CPVTD with bundle of RGOF

In the first step of designing, the block diagram was generated to show the elements of the system and their position. Fig. 6-5 shows the diagram. The dish accommodates multi-junction solar cells, fiber optics, the heat collector, and a coupler. The other parts including battery, inverter, switches, pump, valves, and the tank of hot water place beside the dish.

(a)

(b)

(c)
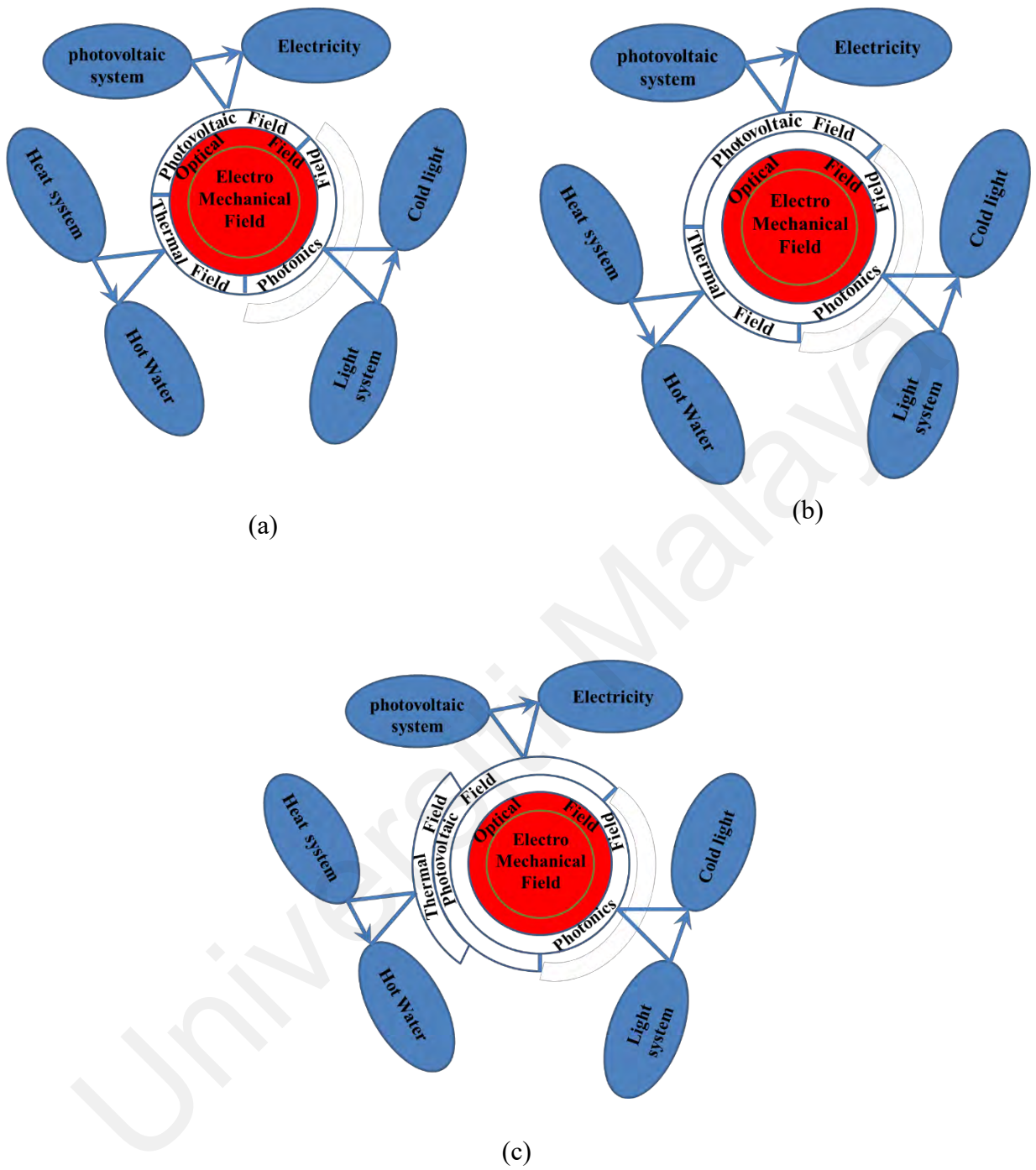
Figure 6-4: three concepts for generating electricity, hot water, and cold light simultaneously
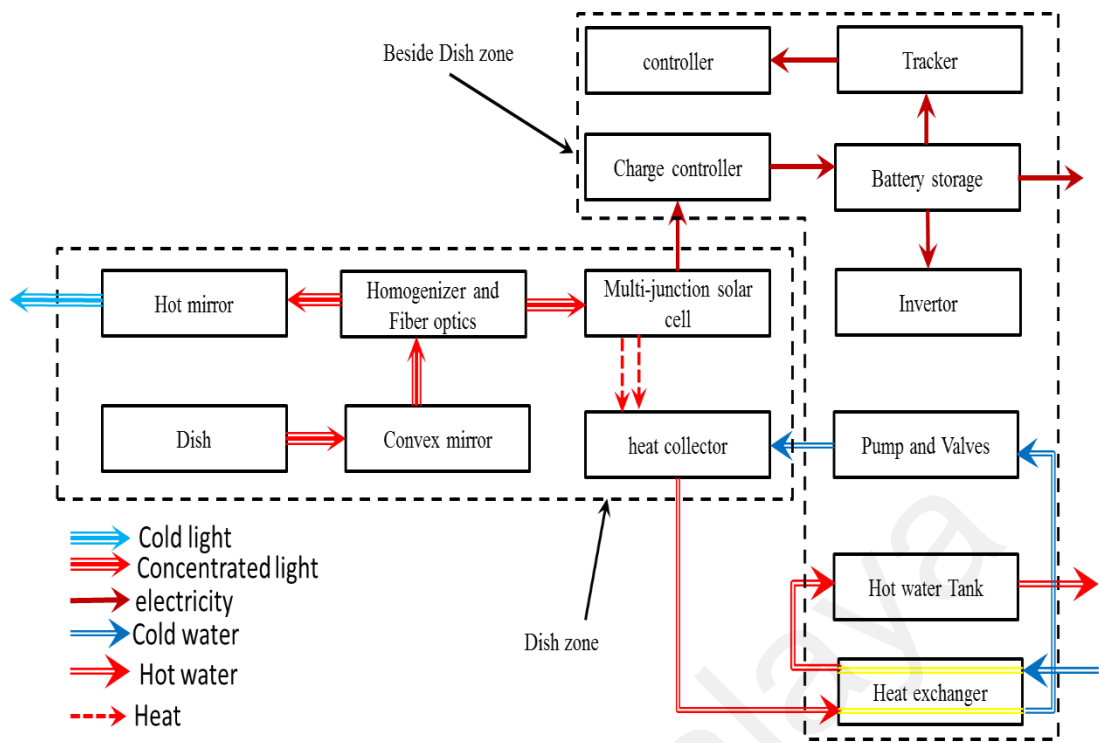
Figure 6-5: block diagram of main components and their positions relation to dish

The scope of the research doesn't include battery, heat exchanger, tank, pump, inverter, and charge controller. A model based on components in the dish zone is designed.

6.3.1 Imaging dish concentrator and convex mirror

A parabolic dish is an old imaging concentrator. Coupling concentrated sunlight through a parabolic dish with optical fiber through the truncated pyramid and cone was studied in our previous work. In this chapter, we modeled the system with a parabolic dish as a primary concentrator that its characterizations are illustrated in table 6-1. Regarding the simple method of fabricating dish on a scale of less than one-meter diameter by spin forming and pressing method, high concentration ratio at the focal plane in a dish, and same uniformity of light in high concentration ratio with non-imaging dish concentrator and imaging concentrator, the parabolic dish concentrator is chosen for the proposed model.

The concentration of dish considering angle between sun rays and errors due to tracker and fabrication is computed by:

$$C = \frac{1 - \sin 2(\theta_s + \Delta\theta)}{4 \sin^2(\theta_s + \Delta\theta)} \qquad (6.1)$$

Where θ_s is the angle between sun rays and $\Delta\theta$ is total errors including the error of tracker and fabrication. In our model, we considered 0.1º error of tracker, 0.27º sun rays' angle, and 0.3º error in fabrication. Based on our experiments in previous works.

Table 6-1: characterizations of dish

Dimeter of dish	0.83m	Aperture of the dish	0.541m2
Focal point length	0.501m	Concentration ratio considering 0.27º angle of rays of sun, 0.3º error of tracker and fabrication	2661
Coat of dish for reflection	aluminum	Concentration ratio considering 11mm distance between focal pale and apex of convex mirror	632.6
Dept of dish	85.941mm	Dimeter of focal plane	16.089 mm
Rim angle	45º	Aperture of the dish	

6.3.2 Convex mirror and homogenizer

A convex parabolic mirror is placed in front of the primary concentrator. Dimension of convex mirror can be computed as:

$$\tan \varphi = \frac{d}{2(f-h)} \qquad (6.2)$$

$$f = \frac{d^2}{16h} \qquad (6.3)$$

from equation (1) and (2) we have:

$$h = \frac{d}{4 \tan \varphi} \left(\sqrt{1 + tan_\varphi^2} - 1 \right) \qquad\qquad (6.4)$$

where h is dept, d is diameter, and φ is rim angle of the convex mirror. Based on the above formula table 6-2 shows the dimension of the convex mirror. The apex of the convex mirror is placed at a distance in front of the focal the point of the dish. The diameter of light in focal point of parabolic concentrator considering total errors is computed by:

$$d_p = \frac{D \sin(\theta_s + \Delta\theta)}{\sin \varphi_p \cos(\varphi_p + \theta_s + \Delta\theta)} \qquad\qquad (6.5)$$

In the above equation D is the diameter of the dish, θ_s is the angle between rays of the sun, φ_p is the rim angle of the dish and $\Delta\theta$ is the total expected error in tracker and fabrication. The diameter of the light on the surface of convex mirror d_L is simply calculated by:

$$d = d_p + 2\,(L - h) \tan(\varphi_p) \qquad\qquad (6.6)$$

Where L is the distance between the apex of the convex mirror and focal point of the parabolic mirror and h is the dept of a convex mirror, d_p is the diameter of light in the focal point of parabolic concentrator without convex mirror. Fig. 6-6 shows a parabolic dish, a convex mirror, the focal plane of both mirrors, and the area of the focal plane with and without a convex mirror.
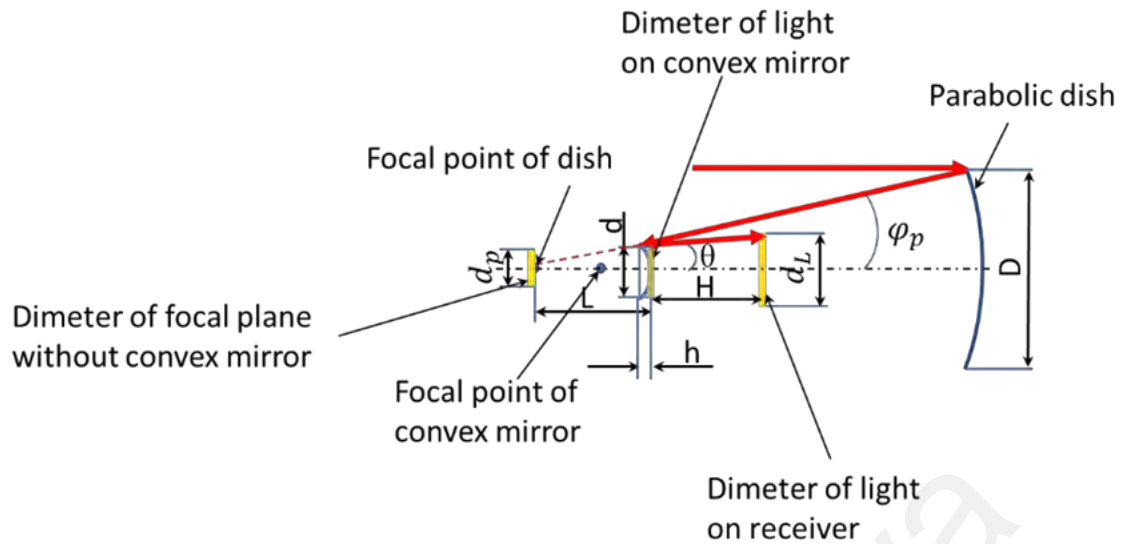
Figure 6-6: parabolic dish, convex mirror, the focal point of both mirrors, and the surface of light with and without convex mirror.

Table 6-2: characterizations of convex mirror and homogenizer

Convex mirror		Homogenizer	
Rim angle (φ_m)	45º	length	20mm
Dept (h_m)	3.733 (mm)	shape	square
Diameter	36 (mm)	size	10.5mm×10.5mm
Focal length	21.7 (mm)	distance between focal point of dish and apex of convex mirror	11mm
Diameter of light on apex of convex mirror	32.996 (mm)	Distance between homogenizer and focal point	40 mm

The dimension of homogenizer, dish convex mirror, and distance of the components to focal point computed and simulated by raytracing method. Fig. 6-7. Shows the schematic of the model for reflecting, homogenizing, separating, and filtering sunlight for generating power by cells and providing cold light. The dish is not included.
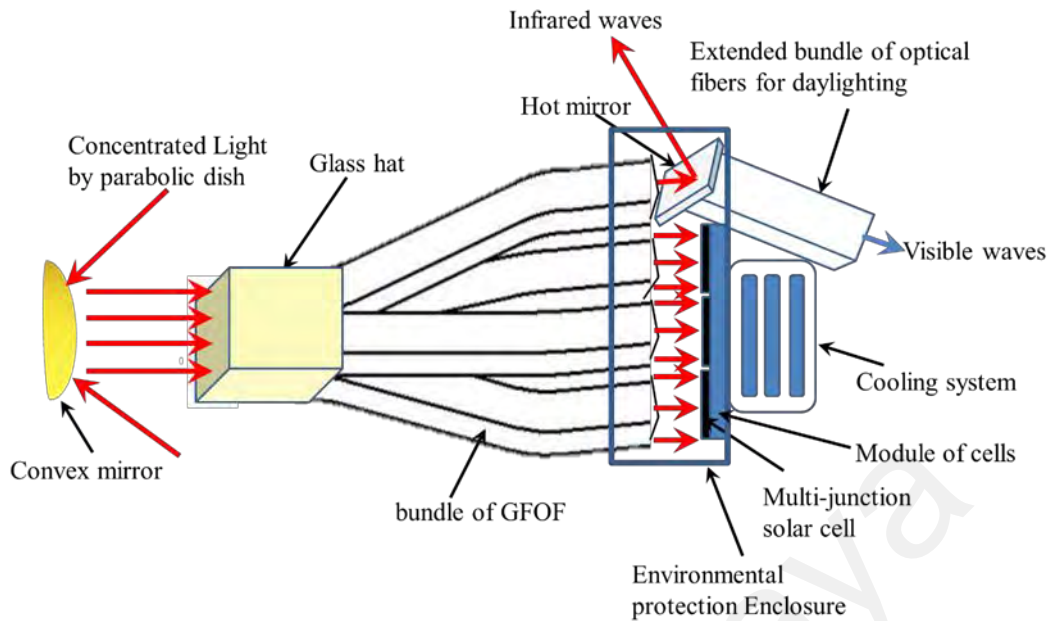
Figure 6-7: the model of the system including the receiver and convex mirror

The concentrated rays create a focal plane instead of a focal point and the convex mirror reduces the angle between the rays but increases the diameter of concentrated light. The area of the concentrated light increases to 8.55 cm2 and the overall concentration decreases to 632 suns. The role of the convex mirror is to reflect the rays toward the center of the dish where the receiver is safe, and the length of the fiber reduces. The material of substrate and coat of convex mirror is important for reflecting wavelengths in the range of 400nm to 1600nm. Borosilicate 3.3 chose for substrate and silver as the coat of convex mirror on the substrate. Borosilicate glass is a durable material with high resistance to heat stress with a low thermal expansion coefficient of $3 \times 10-6$ K-1 at 20 °C.

6.3.3 Solar cell

Multi-junction solar cell III-V GaInP/GaInAs/Ge has shown higher efficiency and is less sensitive to the rise of temperature than silicon cells. Fig. 6-8 (a) shows the schematic of a multi-junction solar module. The module includes a cell, diode, and the base plate. The base plate transfer heat to the heat sink. The geometry of heat sink and base plate affect heat transfer.

Fig. 6-8 (b) shows a dense array of multijunction solar cells that are compacted on a base plate. The fewer distance between cells causes the higher temperature of cells and a high-efficiency forced-cool system is required. The matching light profile and the geometry of solar cells optimize the performance of the power generation by the cell. Characterizations of multi-junction III-V GaInP/GaInAs/Ge are shown in table 6-3.

Table 6-3: characterizations of multi-junction cell and module used in the model

Type of cell	III-V 3C42 version MC/Glass	Recommended glue for homogenizer	Silicon glue
Material of cell	GaInP/GaInAs/Ge	Anti-reflection coating	TiO_x/AlO_x
Dimension of cell	10mm×10mm	Dimension of module	29.6mm×31.6mm
Efficiency at 25º and AMD1.5 and 1000 suns	40.2	Board material	Sandwich of two copper with Al2O3 in the middle
Refractive index of top layer GaInP at 600nm	3.60636	Thickness of materials in board	Al2O3 0.5mm, copper each side 0.15mm
Maximum permission temperature	110º	By-pass diode	2×10 A
Power reduction in higher temperature than 25º	-0.106 mwk-1	Fill factor at 500 suns	88.8%

Many works have been carried to study the matching the focused sunlight with the square shape of multi-junction solar cells. In our designed receiver, we used multi-junction modules that are shown in Fig.6-8 (a) to reduce the temperature at the surface of cells in the focal plane and maximize heat transfer by a bigger space between cells. The bundle of RGOF is bent with a radius of 150 cm to provide more space between multi-junction solar cells. A heatsink is considered behind the cells for transferring heat to the environment. The heat may be collected in a subsystem too.
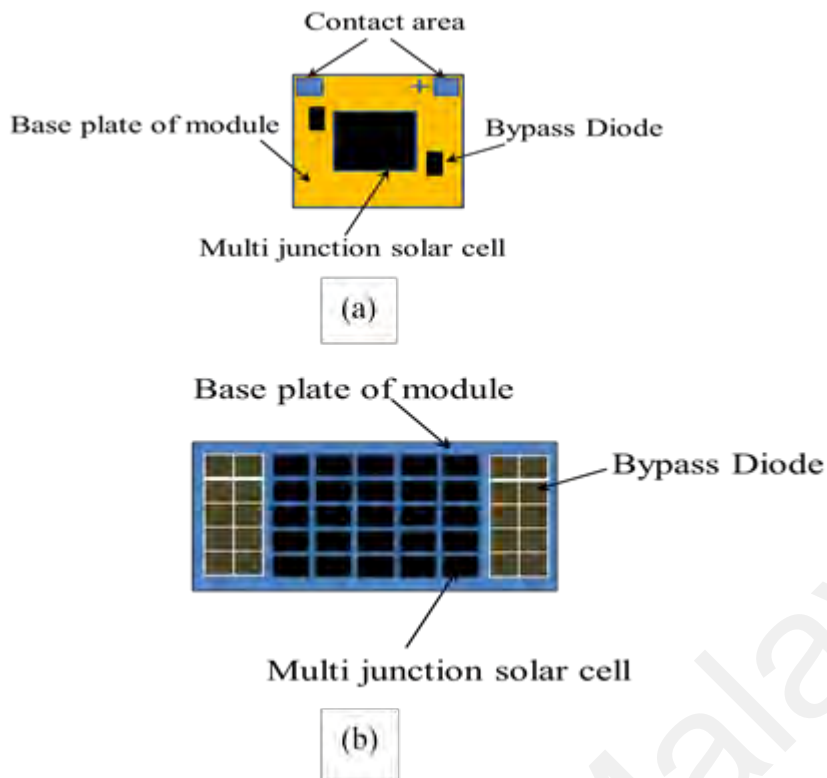
Figure 6-8: (a) Schematic of a multi-junction module; (b) dense array of multi-junction solar cells in a module

6.3.4 Bundle of RGOF

Rectangular core fibers in the market have round clad. The core is made of fused silica for its Broadband UV to NIR Transmittance while clad maybe glass or low refractive polymer. Fig. 6-9 shows the attenuation of a square core in the market in different wavelengths. The core of the fiber is fused silica and cladding is a hard polymer.
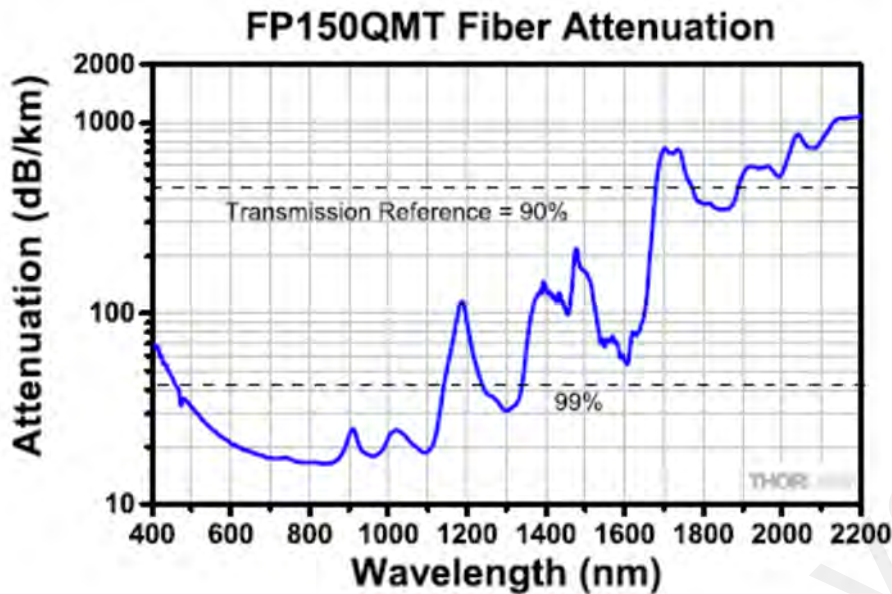
Figure 6-9: attenuation of a square core fiber of a typical square core optical fiber in the market (derived from Thorlabs website)

As mentioned in chapter 5, the efficiency of a fiber under the propagation of a specified spectrum is different from the efficiency of fiber under a collimated laser with a thin bandgap. Manufacturers of optical fibers provide information about the attenuation of fiber in a different wavelength, but it does not show the efficiency of the fiber while the source of light propagates a wide spectrum of light. The loss of fiber under the propagation of a wide spectrum with an angle of incident is not only dependent on the length and attenuation coefficient but also is dependent on the numerical aperture of fiber, the diameter of the fiber, and angle of incidence.

The shape of most multi-junction solar cells in the market is approximately square, and the bundle of rectangular optical fiber is well-matched with the shape of the cell. Rectangular clad instead of round clad provides a lower gap between the fibers in the bundle and reduces the loss of coupling. Fused silica core is more efficient than polymer core. The rectangular core transmits a high flux of sunlight and reduces the leakage of light due to a bigger equivalent diameter with lower thickness. Round glass optical fiber

has the limitation of diameter because of breaking in bending. Rectangular fibers improve the limitation by a big wide and small thickness. The durability of rectangular core optical fiber in bending and heat cycle test shows that rectangular fiber can tolerate in ten million times bending with 150mm radius.it also showed a good result in the heat cycle test in 5º-60 º.

In our model, we used a rectangular core and clad as a medium between the glass hat and solar cells. A bundle of RGOF is extended for transmitting sunlight to the target. The core material was fused silica with a refractive index of 1.458464 at the D-line. On the other hand, the cladding material was resin XPC-373 AP clad with a low refractive index of 1.387939 at 852nm.

6.3.5 Glass hat (homogenizer)

The fiber inlet temperature increases due to exposing the entrance surface of the fiber to high intensity of sunlight. For protecting the bundle of RGOF a glass hat of fused silica is placed at the inlet of the bundle. The glass hat homogenizes the incident light too. Dimension of the glass hat overlap bundle of RGOF. Solar absorptance of fused silica is 0.03 and emissivity is 0.93. the temperature on the entrance surface of the glass hat without considering convection heat transfer and sky temperature is determined by (Lienhard, 2011):

$$T^4 = \left(\frac{\epsilon \times P_i}{\alpha \times \sigma \times A}\right) \qquad (6.7)$$

Where σ (Stefan Boltzmann constant) $=5.67 \times 10^{-8}$, α is solar absorptance, ε is emissivity, A is the area of glass hat, and P_i is the power of light while entering the glass hat. The temperature of the fiber inlet is calculated at 635º. This temperature in real would be less than 635^{oc} considering convection, conduction, and sky temperature. However, fused silica is a durable material at this temperature.

6.3.6 hot mirror

A hot mirror is an optical spectral filtering device. A hot mirror passes visible light and reflects near-infrared (NIR) light. A hot mirror with a reflection of NIR at 45º and fused silica substrate material was chosen. Fig. 6-10 (derived from manufacturer company website) shows the reflectivity and transmission of the chosen hot mirror. The absorption of the mirror is less than 2% and thickness is 5mm. the diameter is 25mm that is more than the diameter of the bundle of RGOF.
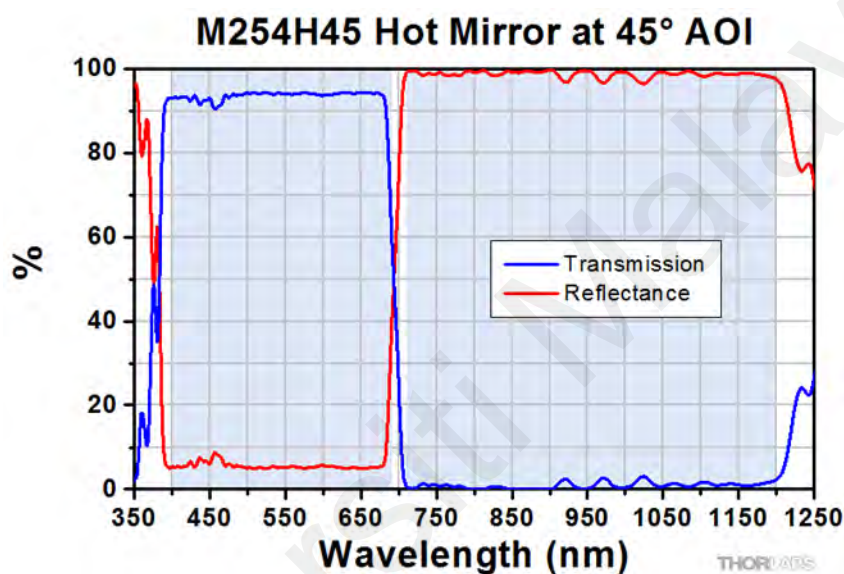
Figure 6-10: transmission and reflectance of hot mirror with 45º angle of incidence for the range wavelengths from 350nm to 1250nm (derived from manufacturer company website)

6.3.7 Method of simulations

The raytracing method is used for optical simulation. Table 6-4 shows the parameters of the simulation. A 3D cad model of a parabolic mirror, convex mirror, homogenizer, and four bundles of RGOF were provided. The Zemax software version 13 was used for optical simulation. After downloading cad models in the zemax cad file, parameters of the software were set based on table 6-4.

Table 6-4: parameters of simulation by raytracing method

parameter	explanation	quantity	unit
Non-sequential	Type of system		
Temperature	Environment	20	ºC
pressure	Environment	1	ATM
Source radial maximum angle 0.29º	Blackbody 5780ºK	81 waves 400-1600	# nm
Detector (absorber)	Rectangle pixels	21x21 1000x1000	mm #
Homogenizer	Rectangular volume	21 x21 x20	mm
Analysis rays	Maximum permittable	10,000,000	#
Material of core Material of clad Material of coat Material of homogenizer	Fused silica Low refractive polymer Ag for mirrors Fused silica	n=1.458 n=1.37 n=1.458	
Position of source Position of parabolic mirror Position of homogenizer and receiver Position of convex mirror	X,Y,Z	0,0,-20 0,0,501 0,0,40 0,0,11	mm

6.3.8   Performance of the model

Total power of the source is 688.9 watt from a source radial with dimension 0.83mx0.83m that provide an intensity of 1000 Wm^{-1} for our system. Fig. 6-11 (a) shows the distribution of intensity at the focal plane of the parabolic mirror in angular, radial, and irradiance image of distribution. The concentrated reflected power in the focal plane is 536 watts and is 77.8% of the power source. Fig. 6-11 (b) shows the length of the focal plane in the X and Y axis i.e. 19.2 mm while the detector is a square shape with a side length of 12mm.
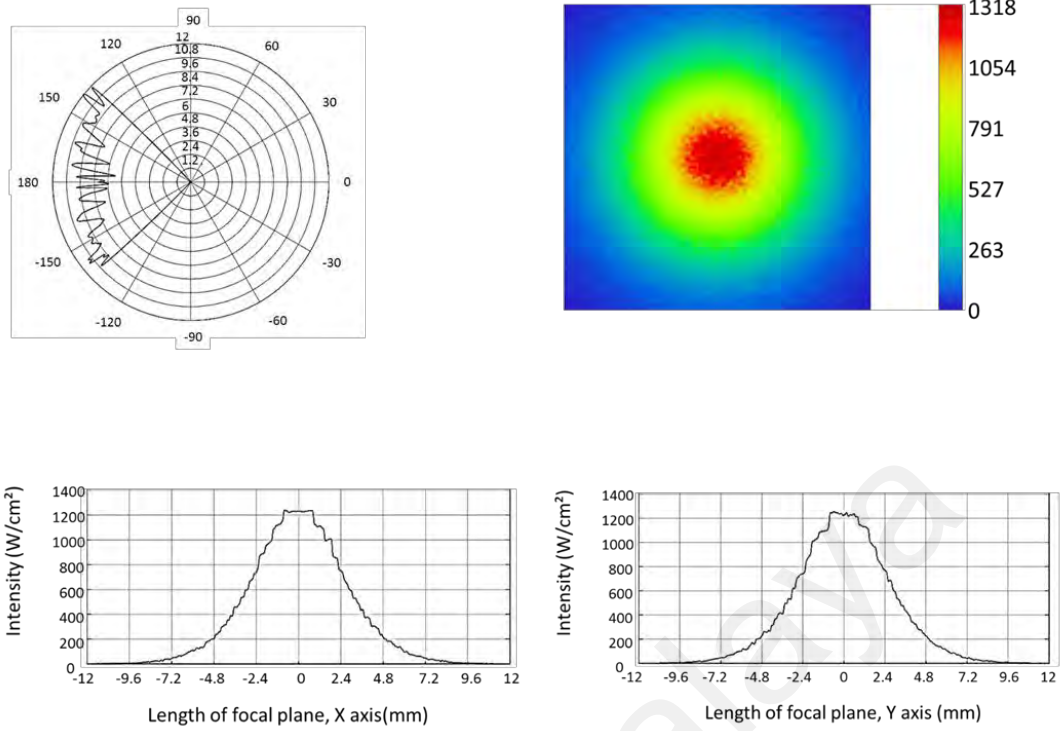
Figure 6-11: (a) angular and radial distribution of the concentrated light on focal plane of Parabolic dish and image of the irradiance distribution; (b) intensity of concentrated light in X and Y axes

The diameter of the convex mirror is equal to the diameter of the focal plane. A clearance considered and a diameter of 36mm is determined for the convex mirror. The rim angle of the dish and convex mirror is equal to the rim angle of the dish. position of the convex mirror changes the output its power. The raytracing was conducted to find the best position of the convex mirror. Theoretically, if the focal point of the convex mirror and parabolic dish overlaps the result is collimated rays. The output rays should overlap the bundle of RGOF and maximize the output power. The distance between the focal point of the dish and the convex mirror causes the uncollimated rays (Fig.6-12). The angle of the rays to the focal line (τ) is calculated by:

$$\tau = \tan^{-1}\left(\frac{d_L - d}{2H}\right) \tag{6.8}$$

Substituting (6) for (8) we find τ as

$$\tau = \tan^{-1}\left[\frac{d_L - (d_P + 2(L-h))\tan\varphi}{2H}\right] \tag{6.9}$$

Where H is the distance between the inlet of the glass hat and the apex of the convex mirror. Fig.6-13 shows the result of raytracing for finding the ratio of output power to input power and percent of shading by glass hat on the focal plane of parabolic dish for a distance between 10mm to 70mm. Since an optical fiber with a core and cladding is connected to a homogenizer, in order to transmit the light by RGOF and prevent the reflection at the outlet surface of the glass hat we use the following equation.

$$\tau \leq \sin^{-1}\left(\sqrt{n_{core}^2 - n_{clad}^2}\right) \tag{6.10}$$

Where n_{core} is the refractive index of the core and n_{clad} is the refractive index of the cladding. The best position for the convex mirror is also dependent on the position of the receiver. A tradeoff between percent of shadow and output power shows that 34mm distance is a reasonable choice for a distance of glass hat.

Using dL=10.5, dP=19.2, L=10.8, h=3.7, φ=45, and H=34 we calculate τ=15° that is less than the numerical aperture of the fiber. Table 6-5 shows the output transmitted light power by components and the efficiency of each part in the model. The output light power for generating electricity and cold light is 389 watts that shows 56% efficiency before generating electricity and cold light.
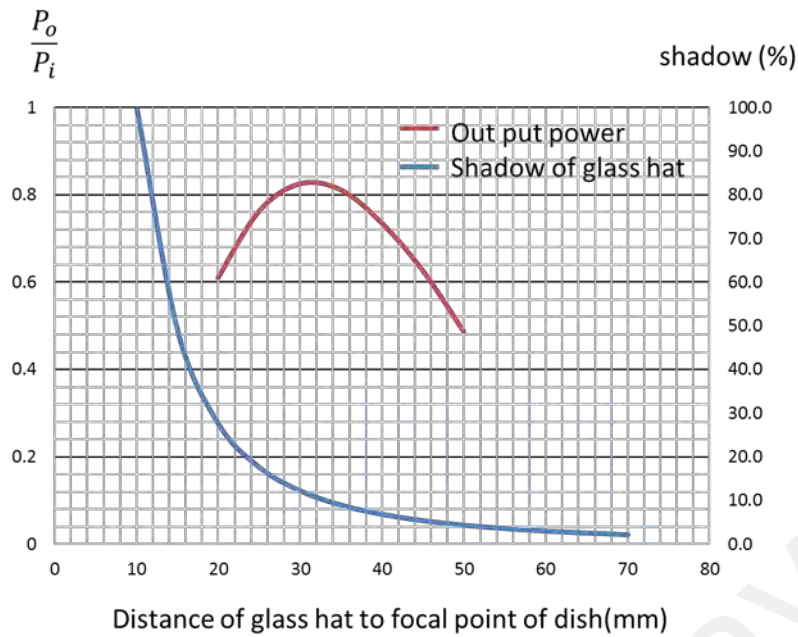
Figure 6-12: percentage of blocked beams by glass hat of receiver on focal plane of dish for distances between 10 mm to 70mm and ratio of output power to input power

Table 6-5: output of the model and components

Intensity 1000 W/m^2 sunlight on a dish with 0.83m diameter (Input power on dish 688.9 watt)				
Component	Input (watt)	Output (watt)	Efficiency (%)	description
Dish with aluminum coating	688.9	536	77.8	0.27º angle of sun, 0.1º inaccuracy of suntracker
Glass hat and convex mirror	536	405	75.6	20mm✗20mm✗20mm fused silica glass (extinction coefficient 4.548x10^{-7})
RGOF	405	389	0.96	Fused silica core n=1.458 with low refractive polymer clad n=1.37
Multi-junction solar cell	289.4	113.2	39.12	Considering 75% of light, 50^{oc} for cell, and -0.106%/K reduction of output due to increased temperature from 25º
Hot mirror	99.6	43.8	90	Commercial mirror in market. Filtered visible light has 44% of input energy
Extended optical fiber for transmitting light for indoor	43.8	32.4	74	10m bundle of RGOF, loss is calculated 30dB/km based on rectangular optical fiber in the market (fig.8)
Total efficiency (power and cold light)	688.9	145.6	21.1	Total fficiency concidering 50^{oc} temperature of cell and 10m optical fiber

Fig. 6-13 shows the layout of the simulation and Fig.6-14 shows the intensity distribution in the X-axis and Y-axis and the image of irradiance distribution in glass hat and four bundles of RGOF. The irradiance of light at the center of the focal plane is higher than the corner then each bundle of RGOF shows a difference of intensity in one axis. On another axis, the intensity of light is relatively uniform. The output power of the bundles is near to each other. The average is 97.575 and the variance is 1.65.

A possible problem in high-temperature climate for a solar cell is the increasing temperature of the cell and the possibility of damaging the cell beyond the maximum limit of temperature for the cell. Using RGOF as a medium in the receiver provides the opportunity of limiting the intensity of sunlight by controlling the space between the cell and bundle of optical fiber. In a normal position, the distance is zero. While the temperature reaches the maximum limited temperature of the cell, the control system will change the distance and reduce the temperature of the cell. When the temperature decreases below the maximum limited temperature, the control system reduces the distance to zero. This model of the receiver may be used in concentrated photovoltaic (CPV) systems for the safety of the cells.
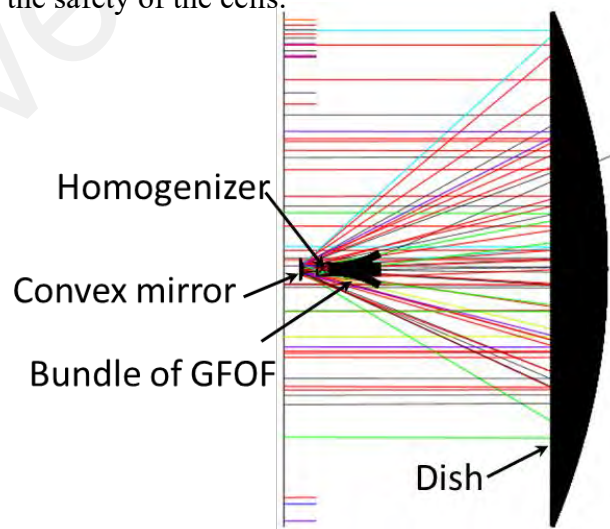

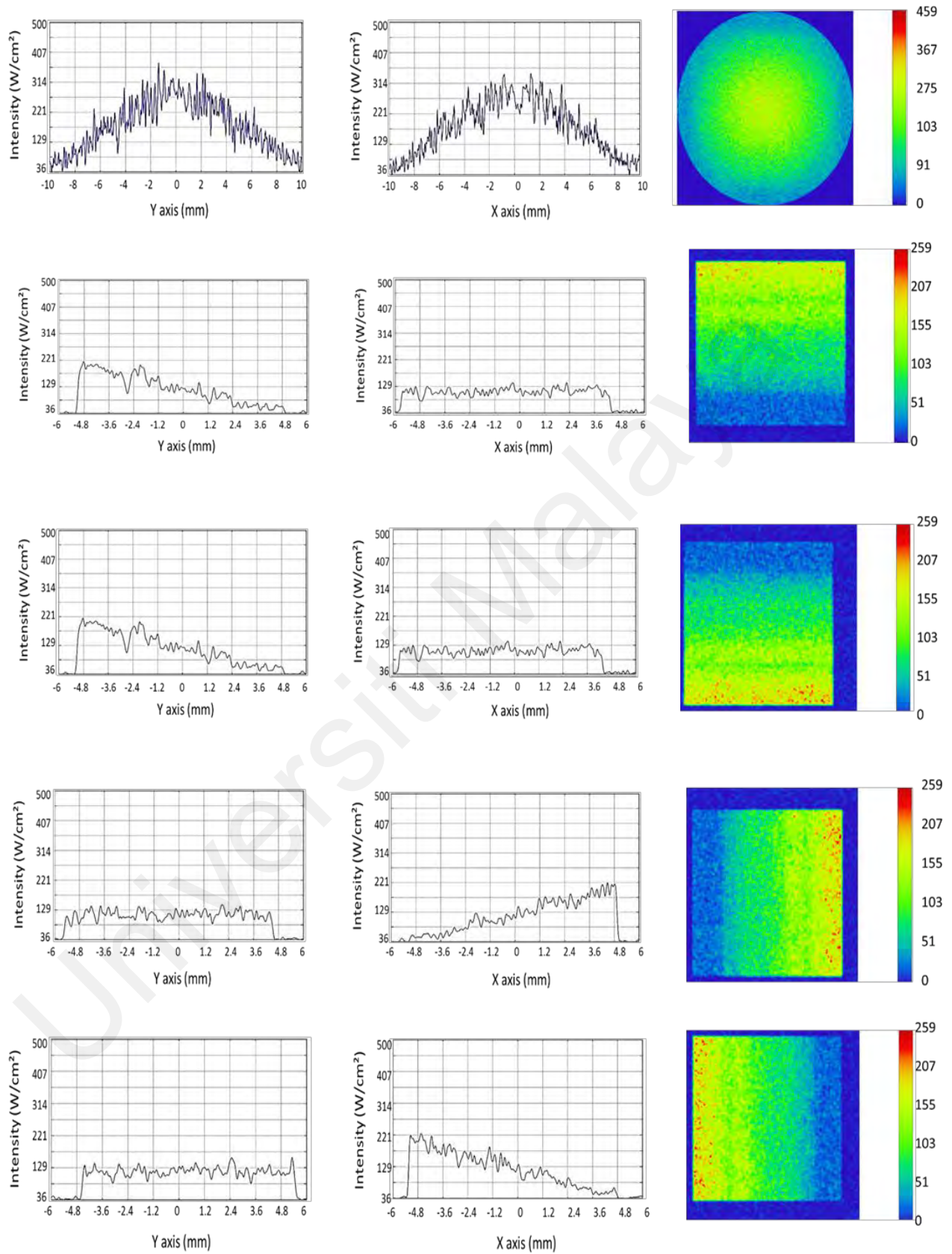**Figure 6-13: layout of simulating dish, convex mirror, homogenizer, and bundles of RGOF**

Figure 6-14: intensity distribution and pattern of the light in; (a)entrance of the light to glass hat ; (b), (c), (d), and (e) at the end sides of four RGOF bundles

6.4 Modeling receiver with bundle of round optical fiber

The fiber has 1mm diameter with a fused silica core and low refractive resin. The numerical aperture is 0.5 and 400 fiber each 300mm length was used for fabricating the receiver. The 3D CAD model of round optical fibers was made for use in optical simulation. Fig. 6-15 shows the CAD model and simulation layout.
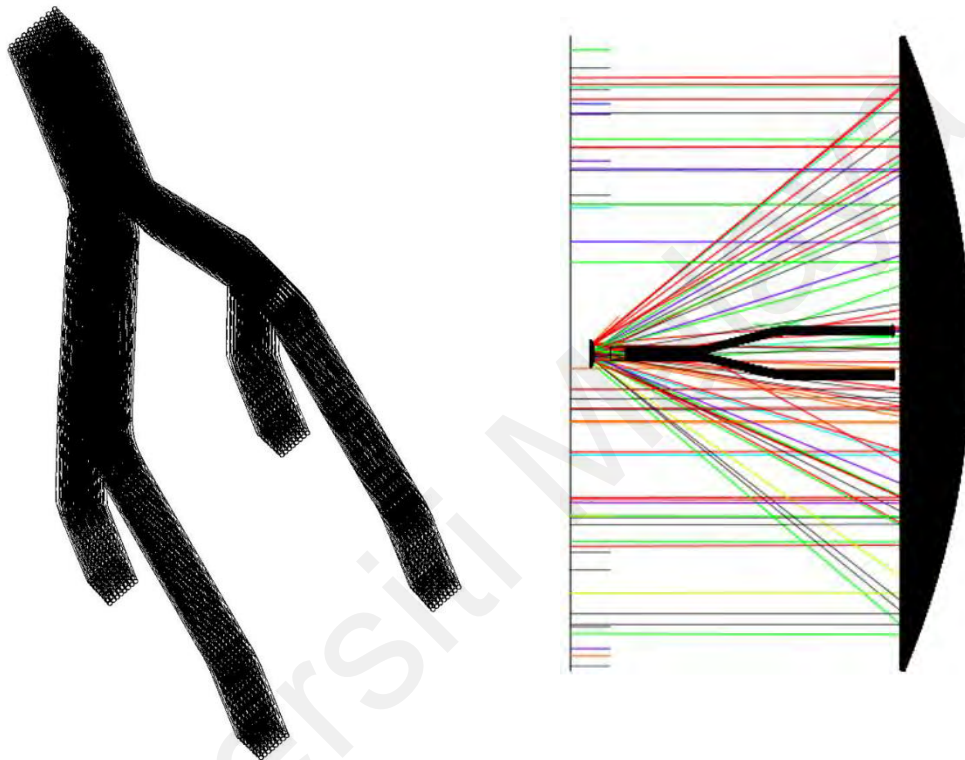
Figure 6-15: CAD model and simulation layout of modle with round optical fibers

In the simulation of the model with round optical fibers, we added the length of fibers to reduce the shading of the receiver. All other parameters in the simulation of the model with RGOF and model with round optical fibers are the same. Fig. 6-16 (a) shows the output power in watts and peak irradiance in Wm^{-2} of each bundle and Fig. 6-16 (b) shows the distribution of intensity in four bundles of round optical fibers. Like a bundle of RGOF, the fibers near the center of concentrated light have higher intensity. It may be possible that the intensity to be more uniform by the contribution of these fibers in the bundle. This is an advantage of round fibers to RGOF. However, for contributing fibers, we need longer fibers. The power of the source like before was 688.9 watts. The total

output power of four round optical fibers is 330 watts with an efficiency of 81.4%. The output of RGOF is 389 watts with an efficiency of 96%. This excess efficiency is due to lower loss in coupling light to the optical fibers. 14.6% higher efficiency due to the coupling process is an advantage of RGOF relative to round optical fibers.
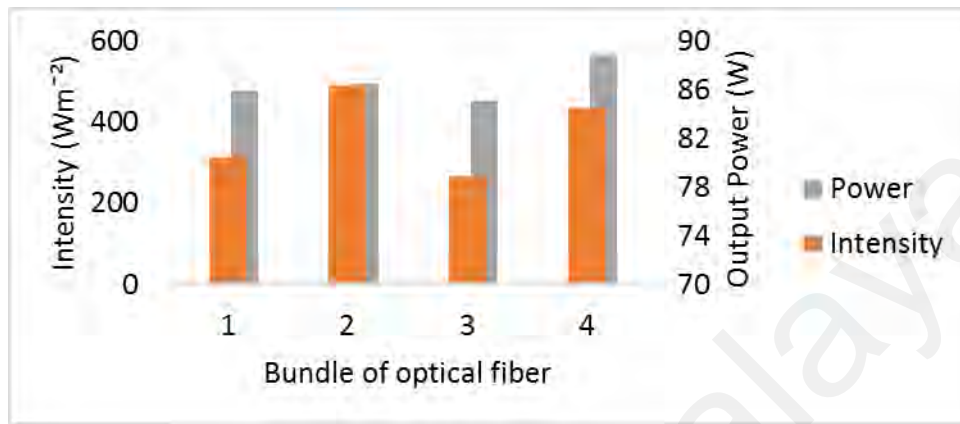
(a)
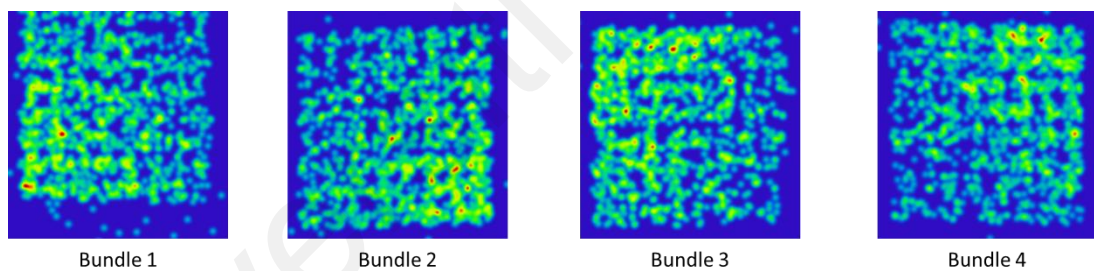
(b)

Figure 6-16: (a) output power and peak irradiance of each bundle of round optical fiber; (b) intensity distribution in bundles

6.5 Designing, fabricating and test of a receiver with round optical fibers

Unfortunately, we didn't have enough RGOF for fabricating a receiver with flat fiber and a receiver with round optical fibers was designed and fabricated. After generating concepts, modeling, and simulation of the system including, dish, convex mirror, homogenizer, and optical fiber we designed the components using CATIA software. Fig.

6-15 shows the CATIA prototyping. Based on modeling, we designed the receiver with four multi-junction solar cells. The model of the receiver used bundles of RGOF.

Bundling round glass fiber was the first issue we approached. The bundle of optical fiber is a collection of fibers that are arranged with fewer gaps between the fibers. Arranging the fibers with hexagonal shape has been demonstrated theoretically and experimentally that results less gap in arrangement of optical fibers. Fig. 6-17 shows the bundle of conventional round optical fibers that is assembled and arranged of fibers.
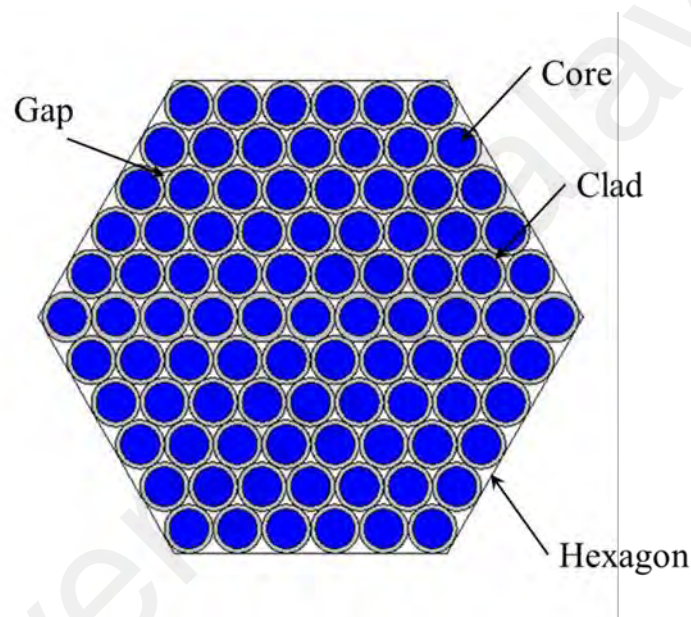
Figure 6-17: bundling optical fiber with the lowest gap between fibers

The arrange of solar cell was studied in designing the receiver. Two concepts were generated. First concept is a dense array of multi junction cells in a row. The second concept is to set the cells in two rows. The first concept has longer length in one direction. So, the length of the optical fibers for the cells far from the center is longer than the optical fibers for the cells near the center. This results more loss for them and the current of the cells farther of the center reduces. The variation of current of solar cells decreases the total efficiency. Fig. 6-18 shows both concepts. In bigger scale with multiple rows, the

method of wiring is important. However, in bigger scale the rows should be arranged to make a square shape too.
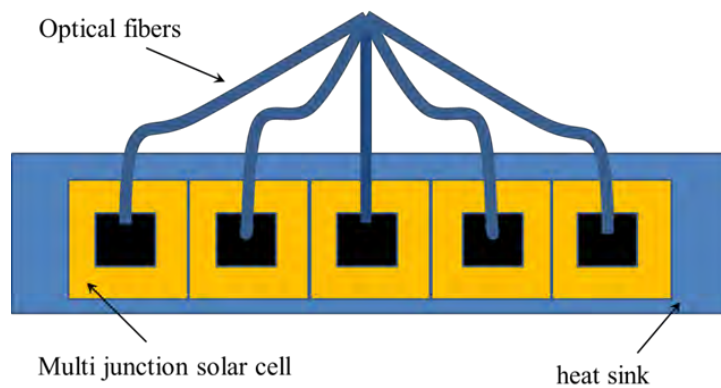
(a)
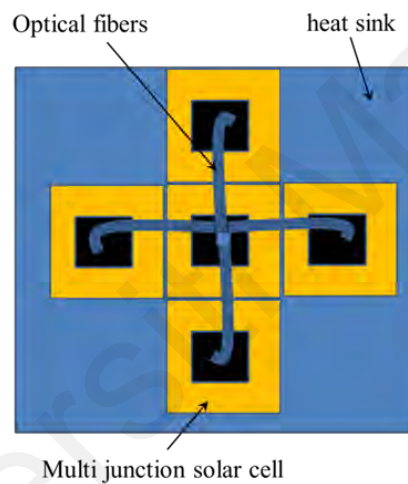
(b)

Figure 6-18: Concepts of arrangement for solar cells (a) in a raw, (b) in rectangular arrangement

The CAD prototype may give a good view of the system and reveals the potential problems. Fig. 6-19 depicted a system including a stand, a tracker, a dish, a convex mirror, and a receiver.

Figure 6-19: CAD prototype of the system

The bundle of the optical fiber in contact with multi-junction solar cells should be separated into four bundles. Each bundle should be rearranged and have a square shape in contact with the cells. a small part designed to hold the fibers in square position with dimension 10mm×10mm. Fig. 6-20 shows the picture of the part. The part has a hole for
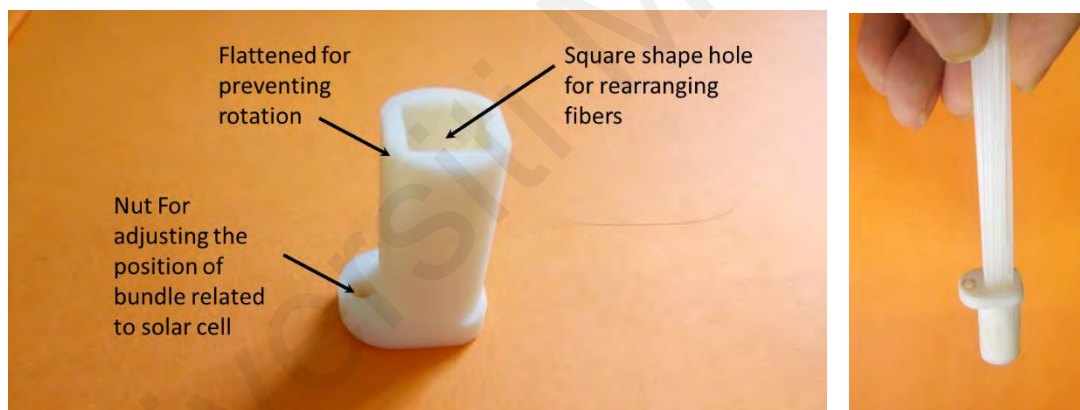
Figure 6-20: holder of optical fibers for rearranging the fiber in square shape

A chamber is needed to protect the solar cells and the fibers. The chamber was designed with four cavities each cavity accommodates the holder and the bundle of optical fiber. Two holes were considered for the check of the light in the test. Fig. 6-21 shows the chamber, holder, and bundle of optical fibers.
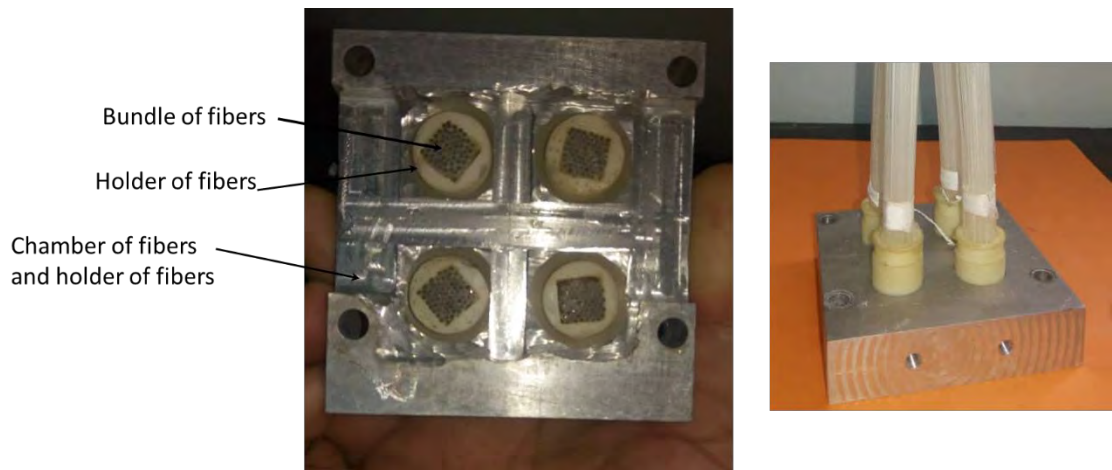
Figure 6-21: chamber of four bundles of optical fiber

A plate with four cavities designed for holding solar cells. the material of the plate is copper, and the plate is in contact with the heat collector. Fig. 6-22 shows the plate with four multi-junction cells.
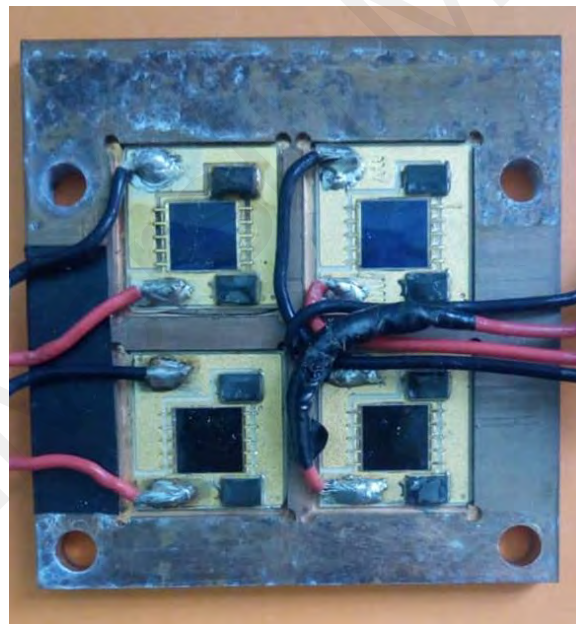
Figure 6-22: copper plate for accommodating four cells

A 55-Watt xenon lamp at a color temperature of 6000 K and a maximum brightness of 3000-4000 Lm was used in a solar simulator with a spectrum similar to sunlight, particularly in the visible range. The receiver was placed under the propagation of the lamp. The output intensity of the solar simulator at the entrance of the receiver and the output power of the receiver is measured by using a PV system analyzer (PROVA 1011)

capable of plotting I-V and P-V curves concurrently. TES 132 data logging solar power meter was used to measure the intensity of the solar simulator at the entrance of the receiver. The temperature of the multi-junction solar cell was measured at the back of the heat sink attached to the solar cell. Fig. 6-23 shows the experimental setup.
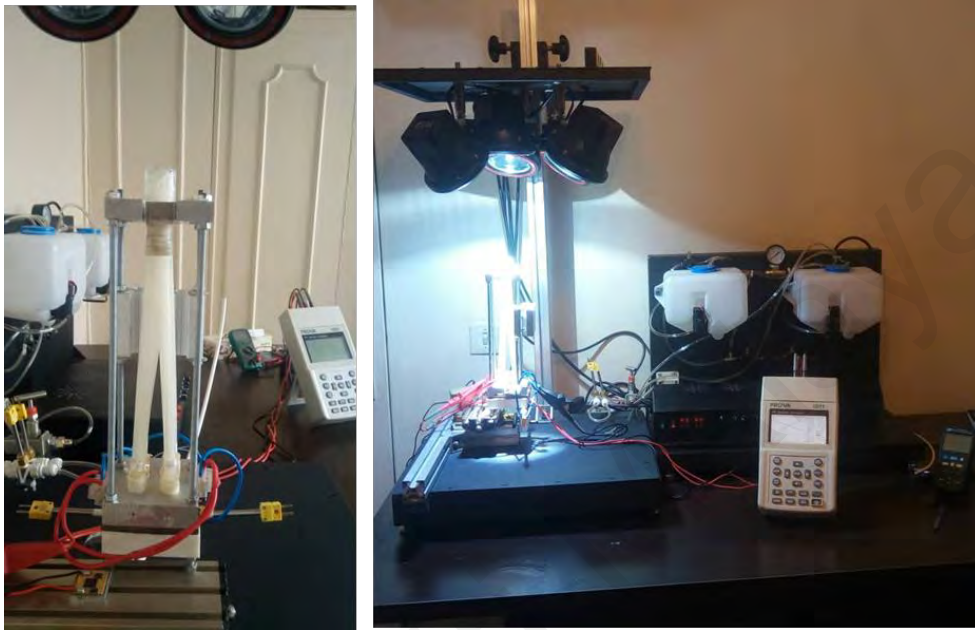
Figure 6-23: receiver under the test by solar simulator

Fig. 6-24 shows normalized output power of the receiver's cell to a cell under standard condition (intensity of 1000 Wm^{-2} in 1.5 AMd, under 1000 suns concentration, and 25° temperature) in a range of sunlight intensity from 600 Wm^{-2} to 1800Wm^{-2}.
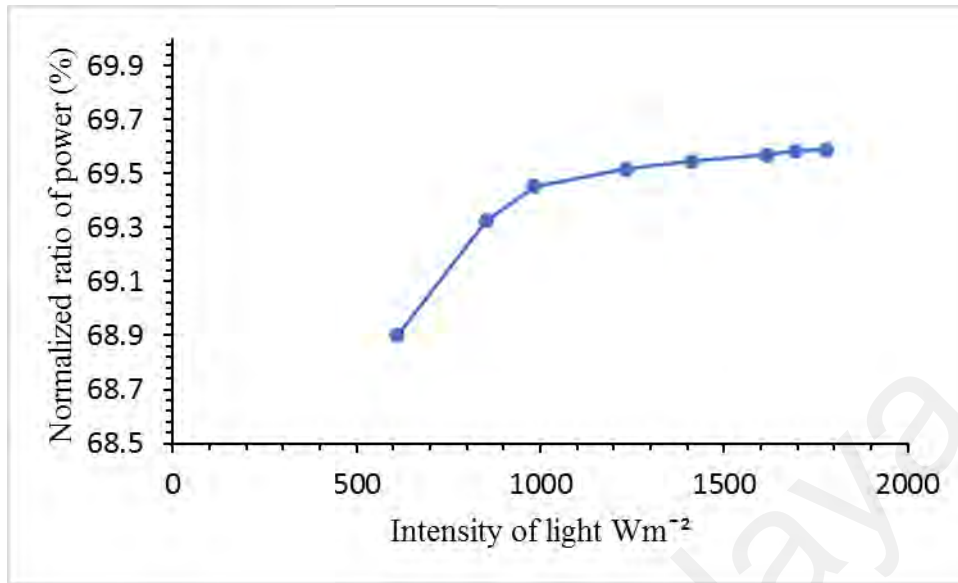
Figure 6-24: normalized ratio of total output power of the cell in receiver to the power of the cell under standard test (intensity of 1000 Wm⁻² in 1.5 AMd, under 1000 suns concentration, and 25º temperature)

For normalization, the bellow equation was used.

$$(\frac{P_{normalized}}{P_{cell\ at\ 1000\ suns}}) = \frac{25000P_o}{(40-0.106(T-298.15))I_o}$$ (6.11)

Where P_o is total output of the receiver, I_o is the intensity of light during the experiment, and T is the temperature of the cell. Based on the results of the experiment, it seems that the efficiency of the receiver is increased in higher intensity. This may be happened because of the temperature of the cell, higher uniformity of light in higher intensity of light.

CHAPTER 7: CONCLUSION

CPVTD is a complex system that may use for generating all kinds of energy from sunlight in a residential or commercial building. Although a complex system has lower reliability, more functionality may make it more convenient especially for people who live in a dry and hot climate. In this case, people don't use sunlight for lighting because of the heat of sunlight or when the window is in the opposite direction to the sunlight.

In this research, we focused on optical, photonics, and multi-junction solar cell as the main components of the system. We implemented the Su-field method for generating concepts. We studied the flat fiber using a mathematical model and ray-tracing simulation method and compared it with conventional round optical fibers. We fabricated a sample of RGOF from soda-lime material. The fabrication method was discussed in detail.

Coupling sunlight is to optical fiber was studied and a new coupler introduced and investigated. The new coupler could capture more flux of sunlight in fiber and reduce the amount of fiber for lighting by conventional round optical fiber.

A new model based on our findings of flat fiber, the generated concepts, and the literature review was introduced and investigated. The model uses a dish, a convex mirror, a homogenizer, a bundle of RGOF, a hot mirror, and four multi-junction solar cell. The heat is collected from a heat collector from a heat sink that is positioned at the back of the multi-junction solar cells.

A receiver with round optical fiber was designed and fabricated and tested. the result of the test shows that the multi-junction cells received uniform intensity of sunlight. It also revealed that the rays of light must be less angular. Further study may be done on coupler and RGOF. RGOF with a fused silica core and polymer clad material with hard polymer

coating can be studied in the future. Step grading clad of RGOF may show a better result for transmitting sunlight.

REFERENCES

Africa, T. W. (1975). Archimedes through the Looking Glass. *The Classical World, 68*(5), 305-308. doi:10.2307/4348211

Ahmad, S., Shafie, S., & Kadir, M. Z. A. A. (2012). *A High Power Generation, Low Power Consumption Solar Tracker*. Paper presented at the International Conference on Power and Energy (PECon), Kota Kinabalu Sabah, Malaysia.

Akisawa, A., Hiramatsu, M., & Ozaki, K. (2012). Design of dome-shaped non-imaging Fresnel lenses taking chromatic aberration into account. *Solar Energy, 86*, 877-885. doi:10.1016/j.solener.2011.12.017

Altshuller, G., Fedoseev, U., & Shulyak, L. (1998). *40 principles, TRIZ keys to technical innovation*. Worcester, Mass.: Technical Innovation Center.

Amara, S. (2011). *Novel and Ancient Technologies for Heating and Cooling Buildings* (Doctoral), Luleå University of Technology (LTU), SE-97187 Luleå, Sweden.

Ambran, S., Holmes, C., Gates, J. C., Webb, A. S., Carpenter, L. G., Adikan, F. R. M., . . . Sahu, J. K. (2012). Fabrication of a Multimode Interference Device in a Low-Loss Flat-Fiber Platform Using Physical Micromachining Technique. *Journal of Lightwave Technology, 30*(17), 2870-2875. doi:10.1109/JLT.2012.2199465

Arnaoutakis, G. E., Marques-Hueso, J., Mallick, T. K., & Richards, B. S. (2013). Coupling of sunlight into optical fibres and spectral dependence for solar energy applications. *Solar Energy, 93* 235–243.

Arnaoutakis, G. E., Marques-Hueso, J., Mallick, T. K., & Richards, B. S. (2013). Coupling of sunlight into optical fibres and spectral dependence for solar energy applications. *Solar Energy, 93*(0), 235-243. doi:http://dx.doi.org/10.1016/j.solener.2013.04.008

Ataei, E., Afshari, R., Pourmina, M. A., & Karimian, M. R. (2011). *Design and Construction of a Fuzzy Logic Dual Axis Solar Tracker Based on DSP* Paper presented at the 2nd International Conference on Control, Instrumentation and Automation (ICCIA).

Baig, H., Sellami, N., Chemisana, D., Rosell, J., & Mallick, T. K. (2014). Performance analysis of a dielectric based 3D building integrated concentrating photovoltaic system. *Solar Energy, 103*, 525-540.

Blomster, O., & Blomqvist, M. (2007). *Square formed fiber optics for high power applications.* Paper presented at the Proc. 4th Int. WLT-Conf. Lasers Manuf.

Burhan, M., Shahzad, M. W., & Ng, K. C. (2019). *Compact CPV—Sustainable Approach for Efficient Solar Energy Capture with Hybrid Concentrated Photovoltaic Thermal (CPVT) System and Hydrogen Production*, Cham.

Canavarro, D., Chaves, J., & Pereira, M. C. (2013). *New optical designs for large parabolic troughs*. Paper presented at the Energy Procedia.

Cariou, J. M., Dugas, J., & Martin, L. (1982). Transport of solar energy with optical fibers. *Solar Energy, 29*, 397–406.

Cau, G., & Cocco, D. (2014). *Comparison of medium-size concentrating solar power plants based on parabolic trough and linear Fresnel collectors* Paper presented at the Energy Procedia.

Christo, F. C. (2012). Numerical modelling of wind and dust patterns around a full-scale paraboloidal solar dish. *Renewable Energy, 39*, 356-366.

Dan, D., & Arvizu, E. (2013). *Global Dynamics in the Energy Landscape*. Paper presented at the Renewable Energy: Capturing the Potential World Future Energy Summit, Abu Dhabi.

Dugas, J., Sotom, M., Martin, L., & Cariou, J.-M. (1987). Accurate characterization of the transmittivity of large-diameter multimode optical fibers. *Applied Optics, 26*(19), 4198-4208.

Engin, M., & Engin, D. (2012). *Sun Tracker Control Strategy for Improved Reliability and Performance* Paper presented at the 5th European DSP Education and Research Conference.

Feuermann, D., & Gordon, J. M. (1999). Solar fiber-optic mini-dishes: A new approach to the efficient collection of sunlight. *Solar Energy, 65*(3), 159–170.

Feuermann, D., Gordon, J. M., & Huleihil, M. (2002). Light leakage in optical fibers: experimental results, modeling and the consequences for solar concentrators. *Solar Energy, 72*(3), 195-204. doi:http://dx.doi.org/10.1016/S0038-092X(01)00100-1

Firat, C., & Beyene, A. (2012). Comparison of direct and indirect PV power output using filters, lens, and fiber transport. *Energy, 41*(1), 271-277. doi:http://doi.org/10.1016/j.energy.2011.06.062

Hallas, J. M. (2011). *Automated Micro-Tracking Planar Solar Concentrators.* (Master of Science), University of California,Sandiego

Han, H. J., Riffat, S. B., Lim, S. H., & Oh, S. J. (2013). Fiber optic solar lighting: Functional competitiveness and potential. *Solar Energy, 94*, 86-101. doi:http://doi.org/10.1016/j.solener.2013.04.010

He, K., Zheng, H., Li, Z., & Dai, J. (2009). Design and investigation of a novel concentrator used in solar fiber lamp. *Solar Energy, 83*(11), 2086-2091.

Hipple, J. (2005). The Integration of TRIZ with Other Ideation Tools and Processes as well as with Psychological Assessment Tools. *Creativity and Innovation Management, 14*(1), 22-33. doi:10.1111/j.1476-8691.2005.00322.x

Hu, J., & Yachi, T. (2012). *An intelligent photosensitive tracker for concentrating PV system* Paper presented at the International Conference on Measurement, Information and Control (MIC).

IEA, I. E. A. (2012). Key World Energy Statistics. France SOREGRAPH.

Jeong, B.-H., Park, J.-H., Kim, S.-D., & Kang, J.-H. (2013). *Performance Evaluation of Dual Axis Solar Tracking System with Photo Diodes* Paper presented at the International Conference on Electrical Machines and Systems, Oct. 26-29, 2013, Busan, Korea

Kaiyan, H., Hongfei, Z., Zhengliang, L., Taotao, & Jing, D. (2009). Design and investigation of a novel concentrator used in solar fiber lamp. *Solar Energy, 83*, 2086-2091.

Kandilli, C., & Ulgen, K. (2009). Review and modelling the systems of transmission concentrated solar energy via optical fibres. *Renewable and Sustainable Energy Reviews, 13*, 67–84.

Kandilli, C., Ulgen, K., & Hepbasli, A. (2008). Exergetic assessment of transmission concentrated solar energy systems via optical fibres for building applications. *Energy and Buildings, 40*, 1505-1512.

Khanna, S., Singh, S., & Kedare, S. B. (2013). *Effect of angle of incidence of sun rays on the bending of absorber tube of solar parabolic trough concentrator*. Paper presented at the Energy Procedia, Germany.

Konishi, K., Kanie, T., Takahashi, K., Shimakawa, O., Mitose, Y., Sasaki, T., . . . Inoue, A. (2010). Development of rectangular core optical fiber cable for high power laser. *SEI Technical Rev., 71*, 109-112.

Kribus, A., Zik, O., & Karni, J. (2000a). Optical Fibers and Solar Power Generation. *Solar Energy, 68* (5), 405–416.

Kribus, A., Zik, O., & Karni, J. (2000b). Optical fibers and solar power generation. *Solar Energy, 68*(5), 405-416.

Kulkarni, A., Kshirsagar, T., Laturia, A., & Ghare, P. H. (2013). *An Intelligent Solar Tracker for Photovoltaic Panels*. Paper presented at the Texas Instruments India Educators' Conference

Leutz, R., Suzuki, A., Akisawa, A., & Kashiwagi, T. (1999). Design of a non imaging Fresnel lens for solar concentrators. *Solar Energy, 65*(6), 379-387.

Li, L., & Dubowsky, S. (2011). A new design approach for solar concentrating parabolic dish based on optimized flexible petals. *Mechanism and Machine Theory, 46*(10), 1536-1548. doi:http://dx.doi.org/10.1016/j.mechmachtheory.2011.04.012

Liang, D., Monteiro, L. F., Teixeira, M. R., Monteiro, M. L. F., & M.Collares-Pereira. (1998). Fiber-optic solar energy transmission and concentration. *Solar Energy Materials and Solar Cells, 54*, 323-331.

Lienhard, J. H. (2011). *A heat transfer textbook*: Dover Publications.

Lovegrove, K., Burgess, G., & Pye, J. (2011). A new 500 m2 paraboloidal dish solar concentrator. *Solar Energy, 85*(4), 620-626.

Luque, A., & Andreev, V. (2007). *Concentrator photovoltaics*: Springer.

Makarova, Y. A., & Kharitonov, A. V. (1972). *Distribution in the solar of spectrum energy in the solar spectrum and the solar constant* (N. T. TRANSLATION & N. T. F-803, Trans.): Nauka Publishing House.

Mann, D. (2002). *Axiomatic design and TRIZ: compatibilities and contradictions.* Paper presented at the 2nd International Conference on Axiomatic Design.

Marcatili, E. A. (1969). Dielectric rectangular waveguide and directional coupler for integrated optics. *Bell System Technical Journal, 48*(7), 2071-2102.

Marcotte, P., & Manning, K. (2013). *Development of an advanced large-aperture parabolic trough collector*. Paper presented at the Energy Procedia.

Matsuzaki, I., Abe, K., & Fujita, K. (2013). PMMA lens with high efficiency and reliability. *AIP Conference Proceedings, 1556*(1), 71-74. doi:doi:http://dx.doi.org/10.1063/1.4822202

Mittelman, G., Kribus, A., & Dayan, A. (2007). Solar cooling with concentrating photovoltaic/thermal (CPVT) systems. *Energy Conversion and Management, 48*(9), 2481-2490. doi:http://dx.doi.org/10.1016/j.enconman.2007.04.004

Mousavi Maleki, S. A., Hizam, H., & Gomes, C. (2017). Estimation of Hourly, Daily and Monthly Global Solar Radiation on Inclined Surfaces: Models Re-Visited. *Energies*, 134.

Myer, J. (1980). Collimated radiation in conical light guides. *APPLIED OPTICS, 19*(18), 3121-3123.

N.L.Christian, & Passauer, L. K. (1989). *Fiber Optic Component Design, Fabrication, Testing, Operation, Reliability and Maintainability*: Noyes Data Corporation.

Nakamura, T., Comaskey, B., & Bell, M. (2002). *Development of Optical Components for Space-Based Solar Power System for ISRU and Regenerative Life Support*. Paper presented at the 40th AIAA Aerospace Sciences Meeting and Exhibit

Núñez, R., Antón, I., & Sala, G. (2013). Hybrid lighting-CPV, a new efficient concept mixing illumination with CPV. *Optics Express, 21*(4), 4864-4874.

Pless, S., & Torcellini, P. (2010). *Net-Zero Energy Buildings: A Classification System Based on Renewable Energy Supply Options*. USA: National Renewable Energy Laboratory Retrieved from www.nrel.gov

Polyanskiy, M. N. (2016). Refractive index database.

Rabl, A. (1976). Comparison of solar concentrators. *Solar Energy, 18*(2), 93-111. doi:http://dx.doi.org/10.1016/0038-092X(76)90043-8

Rabl, A. (1985). *Active Solar Collectors and Their Applications*: Oxford University Press, USA.

Radosavljević, J., & Đorđević, A. (2001). Defining of the Intensity of Solar Radiation on Horizontal and oblique surface on Earth *Facta Universitatis, 2*(1), 77-86.

Rahou, M., Andrews, J., & Rosengarten, G. (2013). *Direct transfer of solar radiation to high temperature applications*.

Saleh, B. E. A., & Teich, M. C. (1991). *Fundamentals of Photonics* (Vol. 8): John Wiley & Sons, Inc.

Santhakumari, M., & Sagar, N. (2019). A review of the environmental factors degrading the performance of silicon wafer-based photovoltaic modules: Failure detection methods and essential mitigation techniques. *Renewable and Sustainable Energy Reviews, 110*, 83-100.

Sapia, C. (2013). Daylighting in buildings: Developments of sunlight addressing by optical fiber. *Solar Energy, 89*, 113-121. doi:http://doi.org/10.1016/j.solener.2012.12.003

Senior, J. M., & Jamro, M. Y. (2009). *Optical fiber communications: principles and practice*: Pearson Education.

Slooff, L. H., Bende, E. E., Burgers, A. R., Budel, T., Pravettoni, M., Kenny, R. P., . . . Büchtemann, A. (2008). A luminescent solar concentrator with 7.1% power conversion efficiency. *phys. stat. sol., 2*(6), 257-259.

smith, s. (2014). PV trackers. Retrieved from http://solarprofessional.com/articles/products-equipment/racking/pv-trackers

Stine, W. B., & Geyer, M. (2001). Power From The Sun: Power from the sun.net. Retrieved from http://www.powerfromthesun.net/book.html.

Tenaga, e. c. o. S. (2014). *National Energy Balance 2012*. Malaysia: Suruhanjaya Tenaga (Energy Commission).

Tenaga, e. c. o. S. (2019). *National Energy Balance 2018*. Malaysia: Suruhanjaya Tenaga (Energy Commission)

Retrieved from https://www.st.gov.my/web/download/listing/151.

Mousavi Maleki, S. A., Hizam, H., & Gomes, C. (2017). Estimation of Hourly, Daily and Monthly Global Solar Radiation on Inclined Surfaces: Models Re-Visited. *Energies*, 134.

Tian, M., Yu, X., Su, Y., Zheng, H., & Riffat, S. (2018). A study on incorporation of transpired solar collector in a novel multifunctional PV/Thermal/Daylighting (PV/T/D) panel. *Solar Energy*, 90-99.

Tyagi, V. V., Rahimb, N. A. A., Rahimb, N. A., & Selvaraj, J. A. L. (2013). Progress in solar PV technology: Research and achievement. *Renewable and Sustainable Energy Reviews, 20*, 443-461.

Ullah, I., & Shin, S.-Y. (2012). Development of optical fiber-based daylighting system with uniform illumination. *Journal of the Optical Society of Korea, 16*(3), 247-255.

Ullah, I., & Shin, S. (2014). Highly concentrated optical fiber-based daylighting systems for multi-floor office buildings. *Energy and Buildings, 72*, 246-261. doi:http://dx.doi.org/10.1016/j.enbuild.2013.12.031

Wang, N., Li, N., & Yu, H. (2010, 25-27 June 2010). *The design of TRIZ expert system inference engine.* Paper presented at the Computer Design and Applications (ICCDA), 2010 International Conference on.

Webb, A. (2002). TRIZ: an inventive approach to invention. *Engineering Management Journal, 12*(3), 117-124.

William, G., & Patrick, C. (2003). Passive Solar Lighting Using Fiber Optics. *Journal of Industrial Technology, 19*(1), 1-7.

Williamson, D. E. (1952). Cone channel condenser optics. *Josa, 42*(10), 712-715.

Winston, R., & Ning, E. (1996). USA Patent No. US Patent.

Witte, W. (1965). Cone channel optics. *infrared Physics, 5*(4), 179-185.

Xia, X.-L., Dai, G.-L., & Shuai, Y. (2012). Experimental and numerical investigation on solar concentrating characteristics of a sixteen-dish concentrator. *Internation Journal of Hydrogen Energy, 37*, 18694-18703.

Xiaofang, S., & Wencheng, G. (2010). *A Sun Spot Center Orientation Method Based on Ellipse Fitting in the Application of CPV Solar Tracker* Paper presented at the International Conference on Intelligent System Design and Engineering Application.

Xie, W. T., Dai, Y. J., Wang, R. Z., & Sumathy, K. (2011). Concentrated solar energy applications using Fresnel lenses: A review. *Renewable and Sustainable Energy Reviews, 15*, 2588–2606. doi:10.1016/j.rser.2011.03.031

Xu, N., Ji, J., Sun, W., Huang, W., & Jin, Z. (2015). Electrical and Thermal Performance Analysis for a Highly Concentrating Photovoltaic/Thermal System. *International Journal of Photoenergy, 2015*, 10. doi:10.1155/2015/537538

Yamashina, H., Ito, T., & Kawada, H. (2002). Innovative product development process by integrating QFD and TRIZ. *International Journal of Production Research, 40*(5), 1031-1050. doi:10.1080/00207540110098490

Yu, X., Su, Y., Zheng, H., & Riffat, S. (2014). A study on use of miniature dielectric compound parabolic concentrator (dCPC) for daylighting control application. *Building and Environment, 74*, 75-85.

LIST OF PUBLICATIONS AND PAPERS PRESENTED

1) Afshin Aslian, Barmak Honarvar Shakibaei Asli, Tan Chin Joo, Faisal Rafiq Mahamd Adikan, Alireza Toloei, Design and analysis of an optical coupler for concentrated solar light using optical fibers in residential buildings, International Journal of Photoenergy

2) Aslian, A., Chong, K.-K., Tavassoli, S. H., Tan, C.-J., & Hazave, O. B. (2020). Rectangular Glass Optical Fiber for Transmitting Sunlight in a Hybrid Concentrator Photovoltaic and Daylighting System. International Journal of Photoenergy.

3) A. Aslian, C.J.Tan, Kok Keong Chong, Theoretical analysis of multi energy generation in a solar energy system, International Conference on Clean Energy and Technology (CEAT) 2016